Unravelling polymetamorphism in east Antarctica using evidence from the Cape Denison Moraines, Terre Adélie Craton, and Gawler Craton, South Australia

Thesis submitted in accordance with the requirements of the University of Adelaide for an Honours Degree in Geology

Megan Alice Williams

November 2015

THE UNIVERSITY of ADELAIDE

UNRAVELLING POLYMETAMORPHISM IN EAST ANTARCTICA USING EVIDENCE FROM THE CAPE DENISON MORAINES, TERRE ADÉLIE CRATON, AND GAWLER CRATON, SOUTH AUSTRALIA

RUNNING TITLE: POLYMETAMORPHISM IN EAST ANTARCTICA

ABSTRACT

Polymetamorphic signatures in rocks can be difficult to deconvolve, especially where events have similar metamorphic grade. In situ and erratic samples from the Terre Adélie Craton, Antarctica, and in situ samples from the formerly contiguous Gawler Craton, South Australia, are examined to deconvolve microstructural, pressure–temperature and geochronological evidence of terrane-scale polymetamorphism. In situ monazite U–Pb geochronology shows that coastal and erratic samples record c. 1700 Ma and c. 2420 Ma ages, consistent with known ages of the Kimban and Sleafordian events, respectively. In situ samples from the Antarctic coast record exclusively c. 2420 Ma ages whereas most erratic samples from the glacial moraines at Cape Denison record only c. 1700 Ma ages. Phase equilibria forward modelling for the c. 2000 Ma Redbanks Charnockite uniquely constrains peak metamorphic conditions of the c. 1700 Ma Kimban Orogeny to 5.0–7.2 kbar and 700–860 ºC. Peak metamorphic conditions of the c. 2420 Ma event are ~5–8.7 kbar and 690–1000 ºC, as constrained by in situ samples from the Terre Adélie coast. As the peak pressure–temperature conditions for the two events are similar and the record of polymetamorphism is cryptic and spatially variable in the rock record, Antarctic samples that only record Kimban ages are interpreted as reflecting either a record of complete overprinting of the older (c. 2420 Ma) event, or that the rocks are younger than the c. 2420 Ma event. In such a situation polymetamorphism at a terrane scale may only be detected by differences in geochronological data. This study serves to highlight the careful approach required when investigating polymetamorphic terranes and argues that a spatially variable record of overprinting metamorphism is possibly related to locations of retrogression occurring either in the waning/exhumation stages of the earlier event or between events.

KEYWORDS

polymetamorphism; Antarctica; Mawson Craton; high-grade metamorphism; U–Pb geochronology; pseudosection; Cape Denison

TABLE OF CONTENTS

LIST OF FIGURES AND TABLES

INTRODUCTION

Recognising and unravelling the expression of multiple overprinting metamorphic events ('polymetamorphism') is an enduring topic of research effort within metamorphic geology (e.g. Zwart 1962, Holdaway et al. 1982, Hand et al. 1992, Diener et al. 2008, Morrissey et al. in press). Old terranes are likely to have experienced multiple orogenic cycles, and thus understanding the expression of these events can help us to understand complex terrane histories (e.g. Harley 1989, Zirkler et al. 2012). Historically, mineral overprinting relationships and complex reaction microstructures used for pressure–temperature (*P*–*T*) analysis were attributed to single-cycle metamorphism where no evidence was found—or available—to the contrary. However, this sample-scale approach often causes the number of events in polymetamorphic terranes to be misinterpreted as it assumes that the sample contains all crucial information required for the interpretation at the terrane scale (Hand et al. 1992, White and Powell 2002). More recently, high precision U–Pb monazite and/or zircon geochronology has allowed resolution of polymetamorphic histories of metamorphic terranes with greater ease (e.g. Goncalves et al. 2004, Kelly and Harley 2005, Zirkler et al. 2012). Recent work by Morrissey et al. (in press) has examined the problem of apparently spatially 'patchy' reworking and polymetamorphism in the Rayner Complex of east Antarctica, where widespread ice cover inhibits efforts to unravel the geological *P*–*T*–*time* history.

This study investigates another part of east Antarctic crust, in Terre Adélie–King George V Land, hereafter referred to as the Terre Adélie Craton (Ménot et al. 1999), which, together with its Australian correlative, the Gawler Craton, forms the Mawson

Craton, also known as the 'Mawson Continent' and 'Mawson Block' (Figure 1; Fanning et al. 1996, Payne et al. 2009). The studied region of the Mawson Craton preserves an intriguing record of polymetamorphism, and thus allows for an appraisal of how and why polymetamorphism may be cryptically recorded and recognised in granulite facies metamorphic rocks. This study utilises, amongst others, samples collected during the Australasian Antarctic Expedition 1911–14, led by Sir Douglas Mawson, with the collection of in situ LA–ICP–MS monazite U–Pb geochronology and calculation of metamorphic phase equilibria forward models used together to explore the time-integrated metamorphic history of the interior of the east Antarctic continent. This study aims to (a) constrain the timing and conditions of metamorphic events recorded in sub-ice bedrock samples of the Terre Adélie Craton; (b) compare the timing and conditions of metamorphic events in the continental interior of Terre Adélie, as sampled by the moraines at Cape Denison, with those recorded in coastal outcrops both in Terre Adélie and in the southern Gawler Craton; and (c) appraise the nature and expression of polymetamorphism recorded in the Mawson Craton.

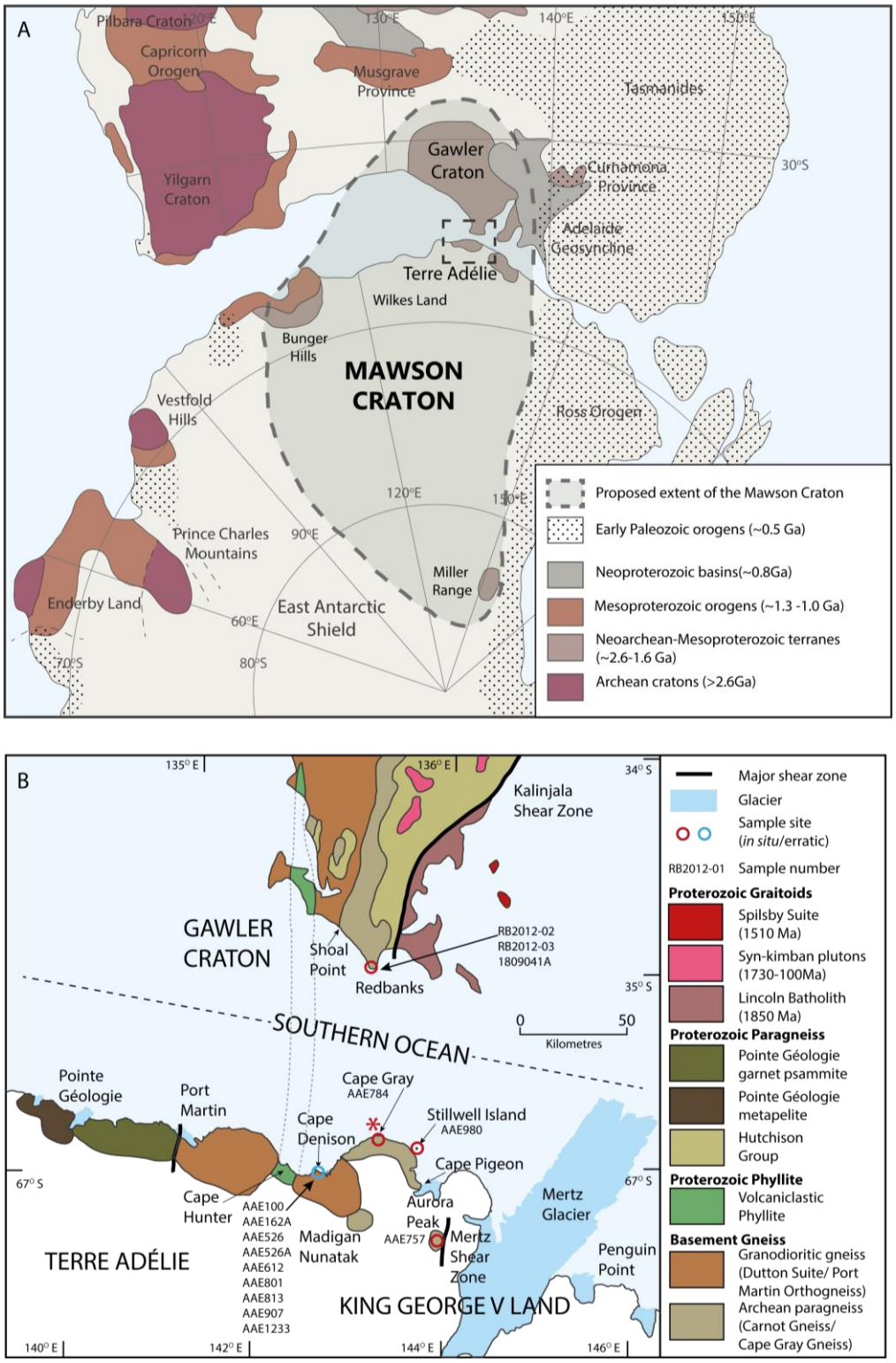

Figure 1: Reconstruction of the Mawson Craton. (a) Reconstruction of Australia and Antarctica (after Reid and Hand 2012). The Mawson Craton is comprised of the Gawler Craton (South Australia), Terre Adélie Coast, Miller Range and Bunger Hills (Antarctica). (b) Correlation of lithologies between the southern Gawler Craton and Terre Adélie coast (after Fitzsimons 2003, Ménot et al. 2007). In situ sample sites are marked in red, erratic samples are marked in blue, with sample numbers for each site labled. Red asterisk represents the virtual position of the Redbanks Charnockite in this reconstruction.

GEOLOGICAL SETTING

Due to extensive ice cover, Antarctica remains one of the largest regions on Earth where we lack basic understanding of the basement geology (Aitken et al. 2014). From the limited outcrop, it has been determined that east Antarctica is composed of several continental blocks, including the Terre Adélie Craton, each with affinities to cratons in Africa, India or Australia (Figure 1; Fitzsimons 2003, Boger 2011). From the coastal outcrops of Terre Adélie, two domains have been identified, correlating to Archean basement and overlying Paleoproterozoic sequences (Figure 1; eg. Peucat et al. 1999, Ménot et al. 2005, Di Vincenzo et al. 2007, Duclaux et al. 2008, Gapais et al. 2008). The basement is composed of orthogneiss, the protolith of which was intruded c. 2800–2700 Ma (Nd model ages, Ménot et al. 2007, Duclaux et al. 2008) and subordinate paragneiss (Figure 2; Stillwell 1918, Duclaux et al. 2008). The basement records a polyphase metamorphic evolution c. 2500–2400Ma, characterised by M1 metamorphic conditions which increase in grade from amphibolite (5 kbar, 700–800 ºC; Monnier 1995) in the west to granulite facies (7.5–10.5kbar, 750–850 ºC; Ménot et al. 2005) in the east between Port Martin and the Mertz Glacier (Ménot et al. 2005, Duclaux et al. 2008). A later M2 event c. 1700Ma generated amphibolite facies conditions across most of the Terre Adélie Craton (4–6.6 kbar, 700–800 ºC; Stüwe and Oliver 1989, Peucat et al. 1999, Ménot et al. 2005, Di Vincenzo et al. 2007), except to the west, at Cape Hunter, where greenschist facies metamorphism is recorded (Ménot et al. 2005, Di Vincenzo et al. 2007). The M2 event was transpressive (Ménot et al. 2005) but the pervasiveness of the event is controversial, recording either a local resetting event related to deformation along shear zones (SHRIMP U–Pb on zircon, $^{40}Ar/^{39}Ar$ laserprobe biotite dating; Oliver and Fanning 2002, Duclaux et al. 2008, Gapais et al.

2008) or a regionally pervasive event that affected the Terre Adélie Craton as a whole ($^{40}Ar/^{39}Ar$ laserprobe biotite dating; Di Vincenzo et al. 2007). Payne et al. (2009) suggest this event records the amalgamation of the Terre Adélie–Gawler Craton and the Miller Range. The Terre Adélie Craton was not reworked by the later c. 500 Ma Ross Orogeny, which is pervasive to the east of the Mertz Shear Zone (Gapais et al. 2008).

The Gawler Craton has a complex and prolonged tectonic history spanning c. 3200 – 1500Ma. Palaeoarchaean (c. 3400 – 3250 Ma) crust was reworked to form c. 3150Ma granites, exposed in a narrow belt in the eastern Gawler Craton (Belousova et al. 2009, Fraser et al. 2010). Following this, there is no known record of significant tectonic activity until the onset of bimodal magmatism c. 2560–2470 Ma (Hand et al. 2007). This magmatism was terminated by high temperature metamorphism and deformation during the c. 2465–2410 Ma Sleafordian Orogeny (Figure 2; Hand et al. 2007). This was followed by the poorly constrained Miltalie Event, which included widespread sedimentation with magmatism in the eastern and southern Gawler Craton (Hand et al. 2007), including the 2011 ± 7 Ma intrusion of the Redbanks Charnockite into the Cape Carnot Gneiss, the Australian correlative of the Cape Gray Orthogneiss (Oliver and Fanning 1997, Fitzsimons 2003, Payne et al. 2009, Jagodzinski et al. 2012). The c. 1730–1690 Ma Kimban Orogeny reworked the Palaeoproterozoic basins and Archean basement in a predominantly transpressional orogenic system. Magmatism in the Terre Adélie and Gawler Cratons in the interval c. 1620–1570 Ma is represented by volcanics at Rocher Janet, the St Peter and Hiltaba suites and the Gawler Range Volcanics (Peucat et al. 2002, Hand et al. 2007).

Geographically precise reconstructions of the Mawson Craton are possible using the Price Metasediments in the southern Gawler Craton and Cape Hunter Phyllite in Antarctica as the piercing point (Figure 1; Oliver and Fanning 1997). The Price Metasediments and Cape Hunter Phyllite are both narrow (~5km wide) belts of very distinctive Mn-rich garnet–chlorite–magnetite phyllitic schist enclosed by higher grade amphibolite and granulite facies lithologies. Both these phyllitic lithologies have detrital zircon populations indicating a unimodal provenance region of c. 1765 Ma (Lane et al. 2015). Such precise geographic and geological correlation within the Mawson Craton implies that the Redbanks Charnockite was unambiguously formerly in close proximity to the rocks of Terre Adélie. Herein, events in the Mawson Craton will be described using the Gawler Craton terminology, Sleafordian and Kimban, for simplicity.

Recent geophysical models were used to propose broad scale tectonic domains in east Antarctica based on magnetic, gravity and subglacial topography data (Aitken et al. 2014). Combined with the known geology that outcrops along the coast of the Terre Adélie Craton (e.g. Peucat et al. 1999, Oliver and Fanning 2002, Ménot et al. 2005, Ménot et al. 2007, Gapais et al. 2008), the geophysical models and interpretations provide some potential insight into the largely unconstrained geology of the interior of east Antarctica. Quantitative ice flow maps (Rignot et al. 2011b) allow constraints to be placed on the provenance of erratic material such as that found at Cape Denison (Figure 3), and show that the total (western) portion of the ice drainage basin for sourcing Cape Denison moraines occupies roughly 380,000 km^2.

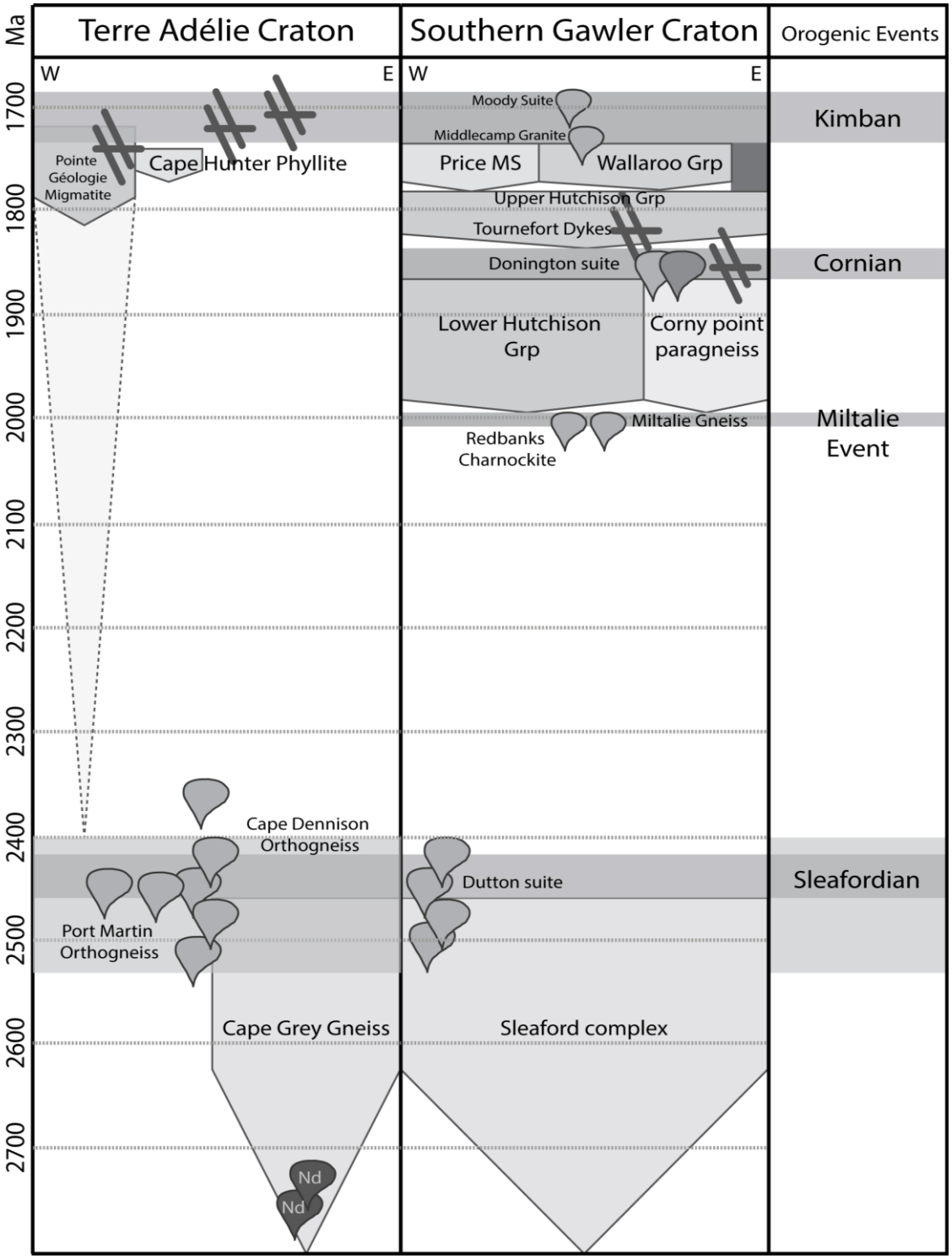

Figure 2: Time–space plot of the Mawson Craton, divided into the Antarctic (Terre Adélie Craton) portion and Australian (Gawler Craton) portion (after Fitzsimons 2003, Payne et al. 2009, Dutch et al. 2010). Additional data from Sheraton et al. (1989), Monnier et al. (1996), Oliver and Fanning (1997), Ménot et al. (2007), Duclaux et al. (2008), and Jagodzinski et al. (2012).

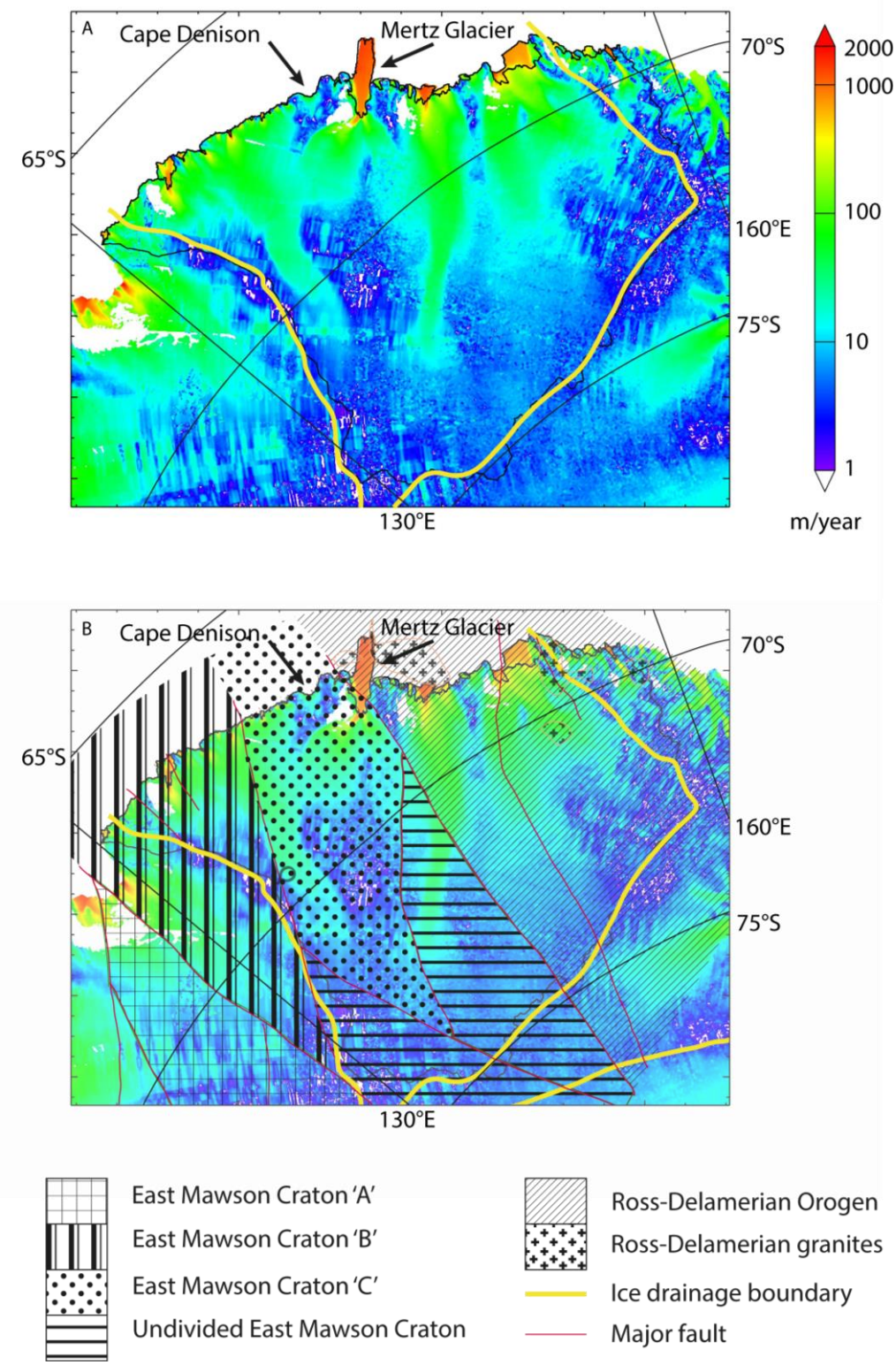

Figure 3: Ice flow and geophysical interpretation maps of the eastern part of the Mawson Craton, Antarctica, and the Phanerozoic Ross–Delamerian Orogen. (a) Ice flow map of the Terre Adélie coast (after Rignot et al. 2011a). Blue indicates the slowest moving ice and red indicates fastest moving ice. (b) ice flow sampling of interpreted geophysical domains (after Rignot et al. 2011a, Aitken et al. 2014). Geophysical domains (East Mawson Craton 'A', 'B' and 'C') are labelled after Aitken et al. (2014) and correspond to proposed terranes in the Terre Adélie Craton. Moraines at Cape Denison sample the East Mawson Craton.

ANALYTICAL METHODS

Geochronology

In situ monazite U–Pb Laser Ablation Inductively Coupled Mass Spectrometry (LA–ICP–MS) geochronology was collected for in situ and erratic samples from the Australian Antarctic Expedition archives, and the sample RB2012-02, from the Redbanks Charnockite.

Analytical techniques for U–Pb isotopic dating of monazite follow those of Payne et al. (2008). Prior to U–Pb analysis monazites were imaged in thin section using a Phillips XL-30 Field Emission Scanning Electron Microscope (FESEM). U–Pb isotopic analyses were obtained using a New Wave 213nm Nd–YAG laser in a He ablation atmosphere, coupled to an Agilent 7500cs/7500s ICP–MS at Adelaide Microscopy, University of Adelaide. Ablation of monazites was performed in situ with a frequency of 5 Hz and a spot size of 15 μm, with a total acquisition time of 80 s, including 30 s of background measurement, 10 s of the laser firing with the shutter closed to allow for beam stabilization, and 40 s of sample ablation. Isotopes measured were ^{204}Pb, ^{206}Pb, ^{207}Pb and ^{238}U for dwell times of 10, 15, 30 and 15 ms respectively.

Data analysis and correction techniques for elemental fractionation and mass bias follow those of Howard et al. (2011) using the program ‘Glitter’, where a 1% uncertainty is assigned to the age of the primary monazite standard MADel (TIMS normalisation data: ^{207}Pb/^{206}Pb age = 491.7 Ma; ^{206}Pb/^{238}U age = 514.8 Ma; ^{207}Pb/^{235}U age = 510.4 Ma; Payne et al. (2008)).

Instrument drift was also corrected for with the application of a linear correction and by standard bracketing every 10 analyses for monazite. Weighted average ages collected throughout the course of this study for in-house monazite standard 222 were $^{207}Pb/^{206}Pb$ = 458.8±4.5 Ma (n=154, MSWD=0.70), $^{206}Pb/^{238}U$ = 451.0±1.9 Ma (n=138, MSWD=3.6), and $^{207}Pb/^{235}U$ = 451.5±1.7 Ma (n=137, MSWD=3.2) and MADel are $^{207}Pb/^{206}Pb$ = 492.3±3.5 Ma (n=237, MSWD=0.45), $^{206}Pb/^{238}U$ = 518.8±1.1 Ma (n=221, MSWD=1.5), and $^{207}Pb/^{235}U$ = 514.4±1.3 Ma (n=227, MSWD=2.4). Individual standard analyses are provided in Appendix A.

Data were filtered for concordance, calculated using Equation 1, using a threshold of ± 5% concordance to remove discordant and reversely discordant data.

$$concordance = \frac{^{207}Pb/^{206}Pb\ Age\ (Ma)}{^{206}Pb/^{238}U\ Age\ (Ma)} \times 100 \quad (1)$$

Data were then filtered for common lead and analyses with $^{204}Pb/^{206}Pb$ and ratios greater than 0.001 were excluded. Weighted average age plots for each sample were made using the Microsoft Excel plug-in Isoplot (Ludwig 2012), with statistical outliers excluded. Remaining data were then plotted using Isoplot to produce Tera–Wasserburg concordia diagrams, and concordia and weighted average ages were calculated for each sample and a probability density plot was produced for the entire dataset.

Bulk-rock and mineral chemistry

BULK-ROCK CHEMISTRY

Whole-rock geochemical analyses for phase equilibria forward modelling was undertaken by Wavelength Dispersive X-ray Fluorescence (WD–XRF) spectrometry at the Department of Earth and Environment, Franklin and Marshall College, Lancaster

PA, USA. Major elements were analysed on fused disks prepared using a lithium tetraborate flux. Trace elements were analysed by XRF in briquettes prepared using copolywax.

MINERAL CHEMISTRY

Quantitative analysis of mineral chemistry and collection of elemental X-ray maps were conducted at Adelaide Microscopy, the University of Adelaide, using a Cameca SXFive electron microprobe. A beam current of 20 nA, accelerating voltage of 15 kv and beam size of 3 µm were used for all point analyses. Routine analyses were made for SiO_2, ZrO_2, TiO_2, ZnO, Al_2O_3, V_2O_3, Cr_2O_3, FeO, MnO, MgO, CaO, BaO, Na_2O, K_2O, P_2O_5, Cl and F on Wavelength Dispersive Spectrometers. Analysis for sample 1809041A from the Redbanks Charnockite was conducted by K. Lane. Representative analyses for each mineral and representative values for each element are supplied in Appendix B. Qualitative compositional mapping used a beam current of 150 nA, accelerating voltage of 15 kV, a dwell time of 50 ms and a step size of 13 µm. For each sample, elements Mg, Ca, Mn, Al and Fe were mapped with wavelength dispersive spectrometers (WDS) and Ce, K, Na, P, Si, Ti and Z were mapped with energy dispersive spectrometers (EDS). Additionally elements Cl, Cr, F, O, S, V, Y, Zn, Au, La, Nd, Pb, Sm, Th and U were mapped with WDS for sample AAE784. Maps for sample 784 were collected by R. Dutch.

Phase equilibria modelling

Phase equilibria forward models were calculated using the software program THERMOCALC v.3.40 with the latest internally consistent thermodynamic dataset, tc-ds62.txt (Powell and Holland 1988, Holland and Powell 2011). Forward models predict

the stability of phases (mathematical models of minerals) in pressure–temperature–composition (*P*–*T*–*X*) space. Forward models were calculated for the geologically realistic system of MnNCKFMASHTO ($MnO–Na_2O–CaO–K_2O–FeO–MgO–Al_2O_3–SiO_2–H_2O–TiO_2–Fe_2O_3$). The activity-composition (*a*–*x*) models of White et al. (2002) were used for spinel and magnetite; non-Mn-bearing phases—silicate melt, muscovite, plagioclase and K-feldspar—used the *a*–*x* models of White et al. (2014a); and Mn-bearing phases—garnet, orthopyroxene, cordierite, chlorite, biotite and ilmenite—used the *a*–*x* models from White et al. (2014b). Whole-rock XRF analyses recast to molar oxide percent were used as input for the forward modelling of each sample.

Calculations in THERMOCALC are non-automated and based on the user specifying the stable assemblage, either based on the appearance of an assemblage in a sample or the known stability of assemblages from the literature. The forward model output is calculated as stable assemblage field boundaries (lines) and phase assemblage field boundary intersections (points), where field boundaries represent the zero abundance of a phase and phase assemblage field boundary intersections represent the zero abundance of two phases (e.g. Powell et al. 1998). The initial stable assemblage is determined by performing a Gibbs energy minimisation calculation at a set pressure–temperature (*P*–*T*) condition. The forward model is built around that initial assemblage with each line manually calculated in logical order to determine which minerals appear or disappear as a function of pressure, temperature and/or composition (*X*). In addition, the so-called ‘starting guesses’ (values for compositional variables for phases with which THERMOCALC commences its iterative least-squares calculation for a reaction with a phase at zero mode or an intersection where two phases have zero mode) require regular

updating as the forward model is calculated in different parts of *P–T–X* space. Therefore a single forward model commonly comprises > 150–200 total manual mineral reaction and intersection calculations. As a result, a single forward model can typically take upwards of 50 hours to build, and in many cases >100 hours.

Calculations in Perple_X (Connolly and Petrini 2002, Connolly 2005) are based on Gibbs energy minimisation over a user-specified gridded *P–T* or *T–X* range. The calculation of forward models in Perple_X is automated such that the user only need specify the rock ('bulk') composition, the list of solid-solution phases to be used by the calculation process, the filename of the thermodynamic dataset and the *P–T–X* range. *T–M* (where *M* refers to amount of a specified compositional variable) forward models have been calculated in Perple_X for the sake of time constraints.

The most uncertain variables of a rock composition are Fe_2O_3 and H_2O, commonly requiring that these be constrained with *T–M* type forward models prior to the calculation of the *P–T* forward model. The choice of pressure at which to calculate the *T–M* diagrams is based on broadly estimating the pressure at which the petrographically-determined peak metamorphic assemblage is stable. The FeO:Fe_2O_3 ratio and H_2O content of each sample was explored using calculated $T–M_O$ and $T–M_{H2O}$ diagrams, respectively, using Perple_X with the thermodynamic dataset of Holland and Powell (1998; 2004 update, filename hp04ver.dat). $T–M_O$ and $T–M_{H2O}$ forward models were calculated in the same chemical system (MnNCKFMASHTO) as the pressure–temperature forward models. The *a–x* models used for the Perple_X calculations are as follows: garnet and silicate melt (White et al. 2007), K-feldspar and plagioclase

(Holland and Powell 2003), biotite and cordierite (Holland and Powell 1998), muscovite and paragonite (Coggon and Holland 2002), ilmenite and hematite (White et al. 2000) and orthopyroxene, magnetite and spinel (White et al. 2002). From these models, calculated at 6 kbar in this study, the $FeO:Fe_2O_3$ ratio and H_2O content for the sample was determined by choosing a bulk composition with an Fe_2O_3 and, in turn, H_2O amount that enabled the peak assemblage, as determined from petrography, to be stable, and having the chemistry of the phase measured by electron microprobe satisfied. The T–M_O and T–M_{H2O} forward models are provided in Appendix C. The (bulk) composition corresponding to an appropriate $FeO:Fe_2O_3$ ratio and H_2O content was then used for P–T forward modelling.

RESULTS

Metamorphic petrography and sample selection

Antarctic samples were selected from the Australian Antarctic Expedition archives (Mawson 1940) on the basis of mineral assemblages useful for forward modelling. South Australian samples were collected by M. Hand and R. Dutch from the Redbanks Charnockite in the southern Gawler Craton (Table 1). Peak and retrograde mineral assemblages have been interpreted on the basis of grain size and microstructural context. The mineralogy of all samples is summarised in Table 1, and hand specimen and outcrop photographs are shown in Figure 4. Samples for which phase equilibria forward models were calculated are described in full below.

Table 1: Summary of mineralogy and analyses for all samples

Sample	Location	Unit	Mineralogy	*gechron.(detailed)*	*gechron.(recon.)*	*geochem.*	*forward model*	*element maps*	*probe data*	*figure*
				Analysis						
AAE757	In situ, Aurora Peak	Cape Gray Gneiss	opx–g–ksp–pl–cd–mt–bi-q		x	x				4a
AAE784	In situ, Cape Gray	Cape Gray Gneiss	g–cd–pl–ksp–bi–opx–mt–ilm–sill–q	x		x	x	x^	x	4b 5a,b
AAE980	In situ, Stillwell Island	Stillwell Is. Metapelite	g–bi–cd–pl–sill–q	x		x	x		x	4c 5c,d
RB2012-02	In situ, Redbanks	Redbanks Charnockite	opx–g–bi–ksp–pl–q	x		x	x			4d 5e
RB2012-03	In situ, Redbanks	Redbanks Charnockite	g–opx–ksp–pl–q			x				4d 5f
1809041A	In situ, Redbanks	Redbanks Charnockite	g–opx–ksp–pl–q						x*	4d
AAE100	Erratic, Cape Denison	undefined	bi–sill–cd–chl–ksp–q		x	x				4e
AAE162A	Erratic, Cape Denison	undefined	g–sill–bi–mu–pl–cd–tor–q		x	x			x	4f
AAE526	Erratic, Cape Denison	undefined	g–sill–bi–q		x	x		x	x	4g
AAE526A	Erratic, Cape Denison	undefined	g–bi–cd–q		x	x				4h
AAE612	Erratic, Cape Denison	undefined	cd–bi–chl–sill–cor		x	x			x	4i
AAE801	Erratic, Cape Denison	undefined	g–cd–sill–mt–ksp–q		x	x				4j
AAE813	Erratic, Cape Denison	undefined	g–sill–bi–pl–q		x	x				4k
AAE907	Erratic, Cape Denison	undefined	g–cd–sill–mt–q	x		x	x	x	x	4l 5g,h
AAE1233	Erratic, Cape Denison	undefined	g–sill–bi–pl–q		x	x	x			4m 5i,j

^ data collected by R. Dutch; * data collected by K. Lane; mineral abbreviations after (Holland and Powell 1998)

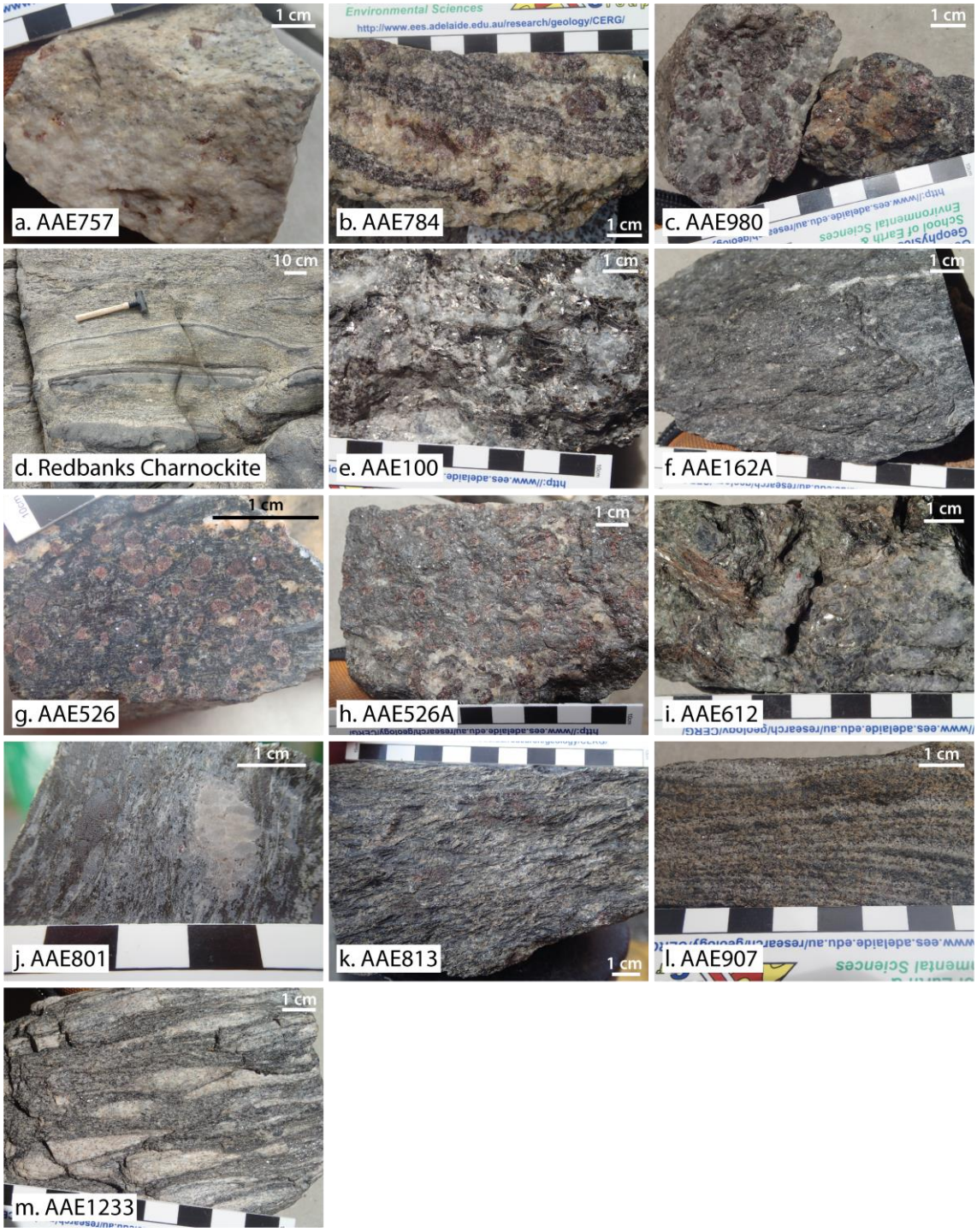

Figure 4: Hand sample and field photographs. (a) AAE757, hand sample, pyroxene–alkali-feldspar gneiss, in situ, Aurora Peak; (b) AAE784, hand sample, migmatitic garnet–cordierite gneiss, in situ, Cape Gray; (c) AAE980, hand sample, garnet–plagioclase–cordierite–biotite gneiss, in situ, Stillwell Island; (d) Redbanks Charnockite, outcrop, migmatised orthopyroxene–garnet–biotite charnockite gneiss; (e) AAE100, hand sample, biotite–sillimanite–garnet–cordierite paragneiss, erratic, Cape Denison(CD); (f) AAE162A, hand sample, biotite–muscovite–sillimanite gneiss, erratic, CD (g) AAE526, hand sample, garnet–sillimanite gneiss, erratic, CD; (h) AAE526A, hand sample, garnet–biotite gneiss, erratic, CD; (i) AAE612, hand sample, biotite–chlorite–cordierite–sillimanite gneiss, erratic, CD; (j) AAE801, hand sample, magnetite–sillimanite–quartz schist, erratic, CD; (k) AAE813, hand sample, sillimanite–garnet–biotite gneiss, erratic, CD; (l) AAE907, hand sample, garnet–cordierite–sillimanite gneiss, erratic, CD; (m) AAE1233, hand sample, sillimanite–biotite gneiss, erratic, CD.

IN SITU SAMPLES

AAE784

The coarse grained minerals in this sample are garnet, orthopyroxene, cordierite, biotite, magnetite, ilmenite, K-feldspar, plagioclase and quartz. At the scale of the hand specimen, the rock is migmatitic and coarse grained, with leucosomes defined by light-coloured layers comprised mostly of feldspars and containing elongate garnet porphyroblasts up to 1cm in diameter, and rare orthopyroxene (Figure 4b). Melanosomes are defined by dark coloured layers primarily composed of biotite, cordierite and garnet. In thin section, the sample consists of two domains, of which the first described is the majority (Figure 5a). Biotite is coarse grained, unoriented and tabular. Cordierite occurs as aggregates of fine grains, commonly containing abundant fine-grained blebs of biotite ± magnetite ± garnet. Garnet is coarse grained, up to 1 mm diameter, but has poor crystal habit. Feldspars and garnet are systematically separated by cordierite. Coarse-grained biotite and feldspars can be found in contact with each other, commonly also in the presence of magnetite and ilmenite. A weak fabric is defined by oriented zones of fine-grained cordierite. The second domain (Figure 5b) contains coarse-grained orthopyroxene and garnet which are systematically separated from coarse-grained K-feldspar and plagioclase (as perthite) by a multilayer corona. From the orthopyroxene to the feldspars the layers of the corona are organised thus: (1) acicular biotite, which grows approximately radially outward from the orthopyroxene and is intergrown with cordierite and quartz; (2) fine-grained garnet forming an aggregated layer with 5% quartz; (3) symplectic cordierite and quartz. Coarse-grained orthopyroxene and garnet in this domain are systematically separated by biotite, quartz and cordierite. The edges of the grains of perthite are systematically replaced by

plagioclase forming a layer with minor quartz, approximately 4 mm wide between the orthopyroxene and the cordierite-bearing domain. The orthopyroxene is highly fractured, with the cracks filled by biotite. The interpreted peak assemblage is garnet–plagioclase–liquid–K-feldspar–orthopyroxene–cordierite–ilmenite–quartz and the interpreted post-peak or overprinting assemblage is garnet–plagioclase–K-feldspar–biotite–cordierite–ilmenite–quartz.

AAE980

The coarse grained minerals consist of garnet, biotite, sillimanite, cordierite, pyrite, plagioclase, quartz, ilmenite and rutile. In hand specimen, the sample is composed of garnet porphyroblasts, up to 1 cm in diameter, with aggregates up to 3 cm, which are found in a matrix of feldspars, cordierite, biotite and quartz (Figure 4c). Garnet porphyroblasts are subhedral and the hand sample contains no apparent foliation. In thin section, the sample has two domains. The first is dominated by coarse-grained garnet the second is comprised of cordierite, plagioclase, sillimanite and biotite with rare porphyroblasts of garnet. The first domain is comprised of 85% garnet by area, with grains up to 20 mm across that are heavily fractured, with minor crack infill of cordierite, biotite and sillimanite. The garnet contains inclusions of pyrite, ilmenite, monazite and biotite. Ilmenite is systematically separated from garnet by biotite ± cordierite. Rare pyrite inclusions are up to 5 mm, and are in contact with the garnet, with some growth of biotite surrounding the pyrite grains. The biotite within the garnet-rich domain appears in two distinct styles. The first is strongly pleochroic from light yellow to deep red–brown and occurs as inclusions up to 2mm in diameter in garnet, occasionally separated from the garnet by coronae of cordierite; the second, moderately pleochroic, from straw yellow to orange brown. The second biotite style is more

abundant in this domain and occurs mainly as crack fill. Monazite inclusions (up to 200 μm) in garnet are moderately abundant. Sillimanite occurs as crack fill in garnet, in contact with cordierite, ilmenite, biotite and garnet. Sillimanite mostly has an anhedral grain shape with abundant inclusions of biotite, but can also be found rarely as acicular inclusions in cordierite.

In the second domain, the grainsize of all of the minerals is smaller. The domain is dominated by cordierite, plagioclase, quartz and biotite with inclusions of randomly oriented acicular sillimanite. Biotite has the same optical properties as biotite included in garnet in the first domain. Sillimanite also occurs as larger aggregated blebs, which are found in contact with coarse grained biotite, cordierite and plagioclase, and have a greater abundance in proximity to garnet porphyroblasts. Inclusions of finely intergrown ilmenite and rutile occur within garnet. The interpreted peak assemblage is garnet–plagioclase–liquid–biotite–rutile–sillimanite–quartz and the interpreted post-peak or overprinting assemblage is garnet–plagioclase–liquid–biotite–cordierite–ilmenite–quartz.

REDBANKS CHARNOCKITE

This is a highly migmatised charnockitic granulite where the c. 2000 Ma protolith intruded a c. 2450 Ma metasedimentary granulite. The charnockite is migmatised and heterogeneous at the outcrop scale, with cm–scale zones of homogeneous mineralogy (Figure 4d). Leucosomes are defined by light coloured layers made primarily of feldspar; melanosomes are defined by dark coloured layers containing biotite ± garnet ± orthopyroxene, with the foliation primarily defined by biotite. Two separate mineral assemblages from ~1m^2 of outcrop are described below.

RB2012-02

Orthopyroxene, garnet, K-feldspar, plagioclase, antiperthite, cordierite and quartz are the coarse grained minerals in this sample, all found in contact with each other. The sample has a weak foliation, defined by coarse grained orthopyroxene. Biotite is rare (<1% by area of the sample) and occurs as isolated grains. Medium grained (up to 1 mm) feldspars, cordierite and quartz form a matrix which comprises 70% by area of the sample. Garnet and orthopyroxene are both seen to occur around each other (Figure 5e). Minor magnetite and ilmenite are found in contact with coarse grained minerals. The interpreted peak assemblage is garnet–plagioclase–liquid–K-feldspar–orthopyroxene–magnetite–ilmenite–quartz.

RB2012-03

This sample is much coarser grained than others from this locality. The sample is dominated by a fabric defined by biotite grains up to 5 mm long and 1 mm wide, comprising 40% of the thin section, and elongate grains of orthopyroxene up to 1.5 cm long and 5 mm wide, which comprise 25% of the section (Figure 5f). Subhedral to euhedral poikiloblastic garnet up to 8 mm diameter contain inclusions of quartz, biotite and cordierite and comprise 25% by area of the sample. Garnet is commonly found in contact with fabric-forming biotite and less commonly with orthopyroxene. Coarse- to medium-grained quartz, feldspars and cordierite comprise 10% by area of the sample. Minor magnetite and ilmenite are found in contact with coarse grained minerals. All coarse-grained minerals are found in contact with each other. The interpreted peak assemblage is garnet–plagioclase–liquid–biotite–orthopyroxene–magnetite–ilmenite–quartz.

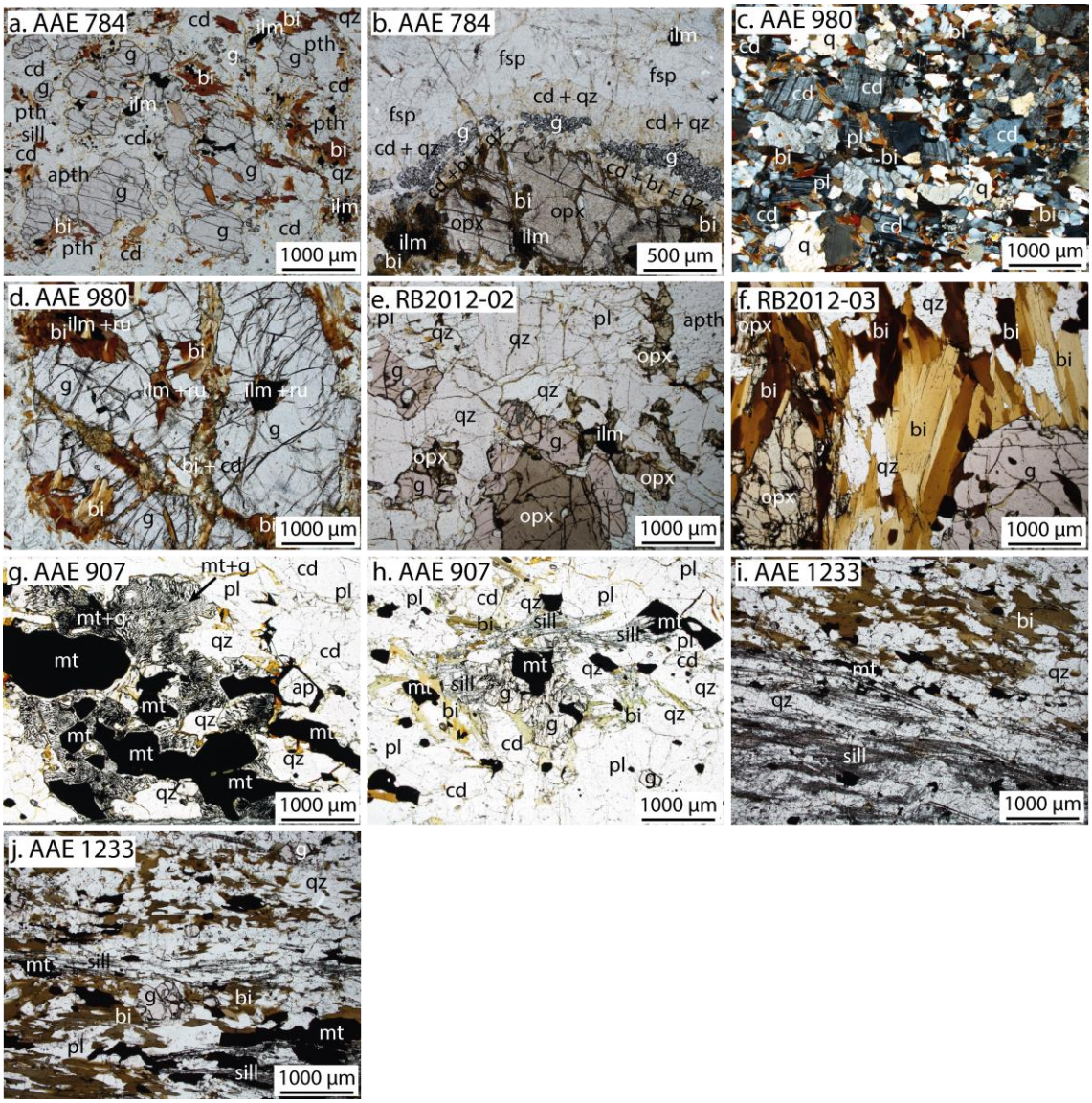

Figure 5: Photomicrographs of key petrological relationships. Photo micrographs are taken in plane polarised light unless specified. (a) AAE784, bulk assemblage. Garnet + biotite + feldspar break down to form cordierite; (b) AAE784, multilayer corona separating coarse grained orthopyroxene + garnet from K-feldspar and plagioclase. From the orthopyroxene to the feldspars the layers of the corona are organised thus: (1) biotite + cordierite + quartz; (2) garnet + quartz; (3) symplectic cordierite + quartz; (c) AAE980, cross polarised light. Matrix (bulk of sample) of biotite + plagioclase + quartz + sillimanite is overprinted by cordierite. (d) AAE980. Porphyroblast of garnet with inclusions of ilmenite ± rutile, cracks are filled by second generation biotite ± cordierite; (e) RB2012-02, corase grained garnet grows around coarse grained orthopyroxene in a matrix of plagioclase + K-feldspar + quartz; (f) RB2012-03, coarse grained biotite defines the foliation and is found in contact with coarse grained, elongate orthopyroxene and porphyroblastic garnet; (g) AAE907, coarse grained magnetite, quartz and plagioclase separated by fine grained garnet–magnetite symplectites; (h) AAE907, coarse grained magnetite + garnet + sillimanite + biotite + plagioclase + cordierite in contact. (i) AAE1233, contact between domains dominated by coarse grained biotite (top right) and sillimanite (bottom left); (j) AAE1233, garnet + magnetite + sillimanite within the biotite domain.

ERRATIC SAMPLES

AAE907

The coarse-grained minerals in this sample are garnet, sillimanite, cordierite, magnetite, quartz, biotite, plagioclase and K-feldspar . At the scale of the hand specimen, the sample has a strongly banded fabric, with fine alternating light and dark layers (Figure 4l). Dark layers are composed majorly of magnetite and garnet, with minor quartz. Light layers are composed primarily of feldspars and cordierite. In thin section, these layers remain apparent, with areas of greater and lesser abundance of magnetite, and a fabric defined by aggregated biotite, magnetite and sillimanite up to 10 mm long. Coarse-grained magnetite up to 3mm diameter is found in contact with coarse-grained cordierite and quartz, which dominate the rock and are approximately equal in abundance. Fine grained intergrowths of magnetite and garnet are found in contact with coarse grained magnetite (Figure 5g) and are spatially constrained to areas with low abundance of sillimanite and biotite. Magnetite is also found in contact with an assemblage of subhedral garnet, biotite and acicular to blocky sillimanite ± chlorite and as fine grained inclusions within large cordierite grains (Figure 5h). Where garnet is isolated from magnetite and biotite, it forms subhedral to euhedral grains up to 4mm. The sample contains monazite, found mostly as inclusions within cordierite, and occurring almost exclusively within the magnetite-rich areas of the rock. The interpreted peak assemblage is garnet–plagioclase–liquid–K-feldspar–biotite–cordierite–magnetite–ilmenite–sillimanite–quartz.

AAE1233

The coarse grained minerals in this sample are biotite, ilmenite, sillimanite, quartz and minor garnet, cordierite, plagioclase and tourmaline. All of these minerals are found in contact with each other. The hand specimen has lineations defined by fine grained sillimanite and biotite (Figure 4m). These two minerals form distinct zones, seen as elongate sillimanite rich, biotite poor sections up to 1cm wide, 0.5cm high and 10 cm long, found within a biotite rich matrix. In thin section, the sample is strongly layered, defined by sillimanite and biotite which each form alternating layers (Figure 5i). Sillimanite occurs as acicular grains up to 2 mm long which form aggregates up to 2 mm wide and 10 mm long. Coarse-grained biotite is anhedral to subhedral with grains up to 3 mm long, containing abundant inclusions of monazite, generally less than 20 μm in size. Garnet is subhedral up to 2 mm diameter, inclusion free and occurs more commonly in biotite-rich layers (Figure 5j). Ilmenite is abundant, together comprising 20% by area of the sample. They are evenly distributed throughout, but are coarser-grained (up to 4 mm) within the biotite-bearing layers. Quartz comprises 30% by area of the sample, in some places containing acicular sillimanite grains in various orientations. Cordierite and plagioclase are both minor in abundance, with cordierite appearing as fine-grained aggregates within the biotite layers. Accessory tourmaline grains up to 2 mm diameter can be found in contact with coarse-grained sillimanite, biotite, ilmenite and quartz. The interpreted peak assemblage is garnet–plagioclase–liquid–K-feldspar–biotite–cordierite–ilmenite–sillimanite–quartz.

Monazite LA–ICP–MS U–Pb geochronology

Detailed (>5 analyses) in situ U–Pb monazite geochronology was collected for samples AAE784 (Cape Gray orthogneiss), AAE980 (Stillwell Island metapelite), RB2012-02

from the Redbanks Charnockite and AAE612 and AAE907 from the Cape Denison moraines (Appendix D). Reconnaissance (≤5 analyses) in situ U–Pb monazite geochronology was collected for samples AAE757 from Aurora Peak and AAE100, AAE162A, AAE526, AAE526A, AAE801, AAE813 and AAE1233 from the Cape Denison moraines (Appendix D). Data are presented on Terra–Wasserberg Concordia diagrams, with in situ samples (Figure 6) and erratic samples (Figures 7 and 8) shown in separate diagrams for comparison, and a probability density plot of $^{207}Pb/^{206}Pb$ for all samples (Figure 9). U–Pb analyses reveal two age populations, each of which has a broad spread (c. 1660–1720 Ma, c. 2390–2430 Ma), with no apparent difference in ages from included versus matrix monazite. Results from monazite U–Pb geochronology are summarised in Table 2.

Table 2: Summary of results from monazite LA–ICP–MS U–Pb geochronology

sample	analyses	individual monazite grains	rejected	excluded (concordance)	excluded (statistical outlier)	$^{207}Pb/^{206}Pb$ age spread (Ma)	weighted average $^{207}Pb/^{206}Pb$ age (Ma)	*n*	MSWD	Figure
AAE784	32	26	–	8	2	2638.7–2256.0	2420 ± 10	22	1.4	5
AAE980	23	17	–	8	2	2459.8–1843.3	2425 ± 16	13	1.1	5
AAE757	5	1	–	2	–	2356.3–2271.0	2315 ± 110	3	4.5	5
RB2012-02	15	14	–	–	–	1717.0–1681.8	1700 ± 12	15	0.23	5
AAE100	5	5	–	–	–	1733.8–1705.4	1719 ± 21	5	0.27	6
AAE162A	4	4	–	1	–	1671.6–1643.1	1662 ± 25	3	0.12	6
AAE526	4	4	–	–	–	1819.7–1705.2	1695 ± 18	4	0.30	6
AAE562A	5	5	–	–	–	1707.8–1683.6	1695 ± 18	5	0.30	6
AAE612	27	9	–	4	–	2413.7–1692.7	2392 ± 17 1707 ± 10	7 16	0.36 0.23	6
AAE801	5	5	–	1	–	1748.2–1627.9	1711 ± 37	5	1.2	7
AAE813	4	4	–	–	–	1702.6–1670.4	1689 ± 20	4	0.5	7
AAE907	25	20	1	10	–	1563.2–1690.0	1673 ± 12	14	0.32	7
AAE1233	5	5	–	–	–	1900.6–1563.2	1691 ± 150	5	27	7

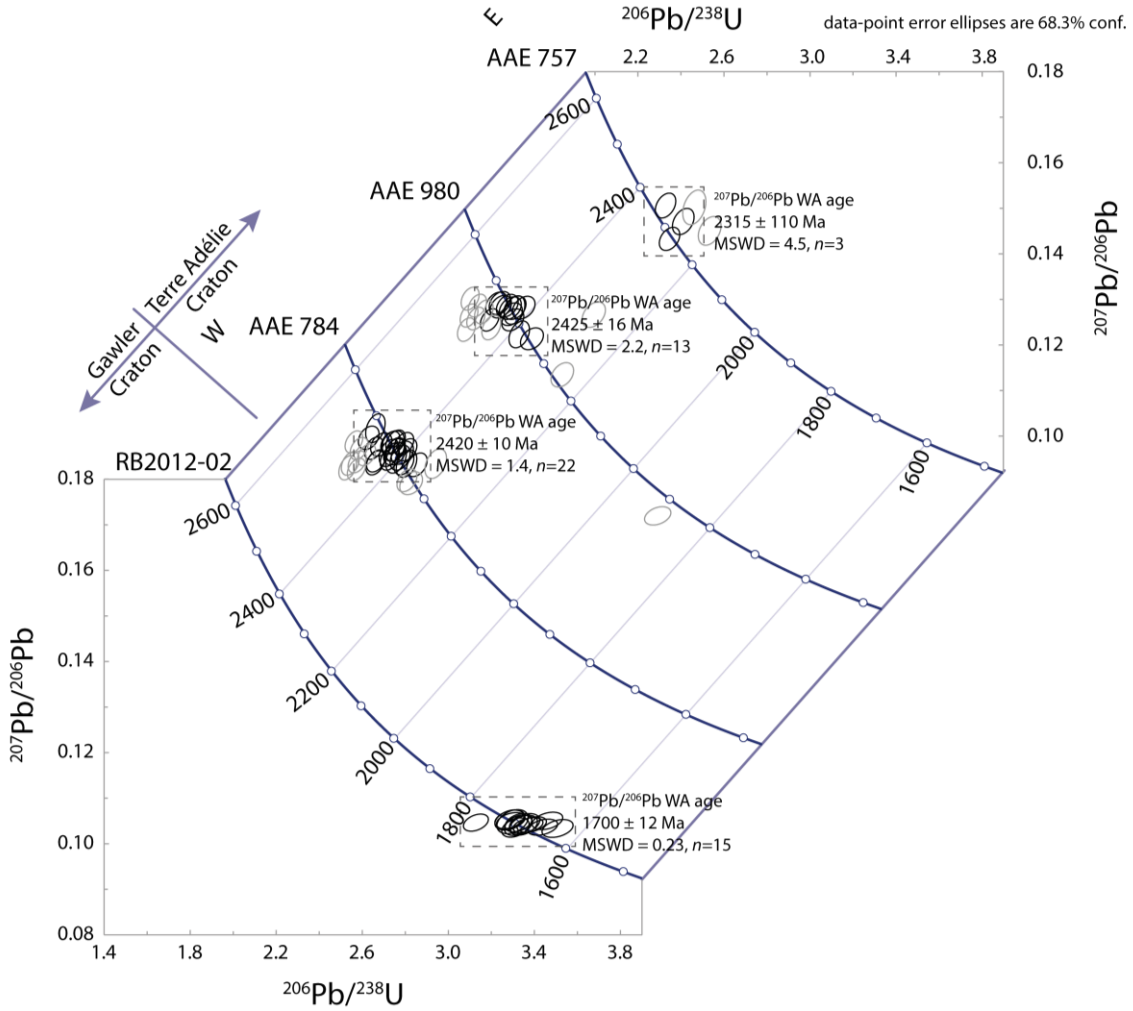

Figure 6: In situ monazite LA–ICP–MS U–Pb geochronology for in situ samples. Tera–Wasserburg Concordia diagrams for individual samples RB2012-02, AAE784, AAE980 and AAE757. The most concordant analyses (conc. 100 ± 5%) are shown with black outlines. Analyses that were excluded from weighted mean age calculations appear as grey ellipses. WA = weighted average.

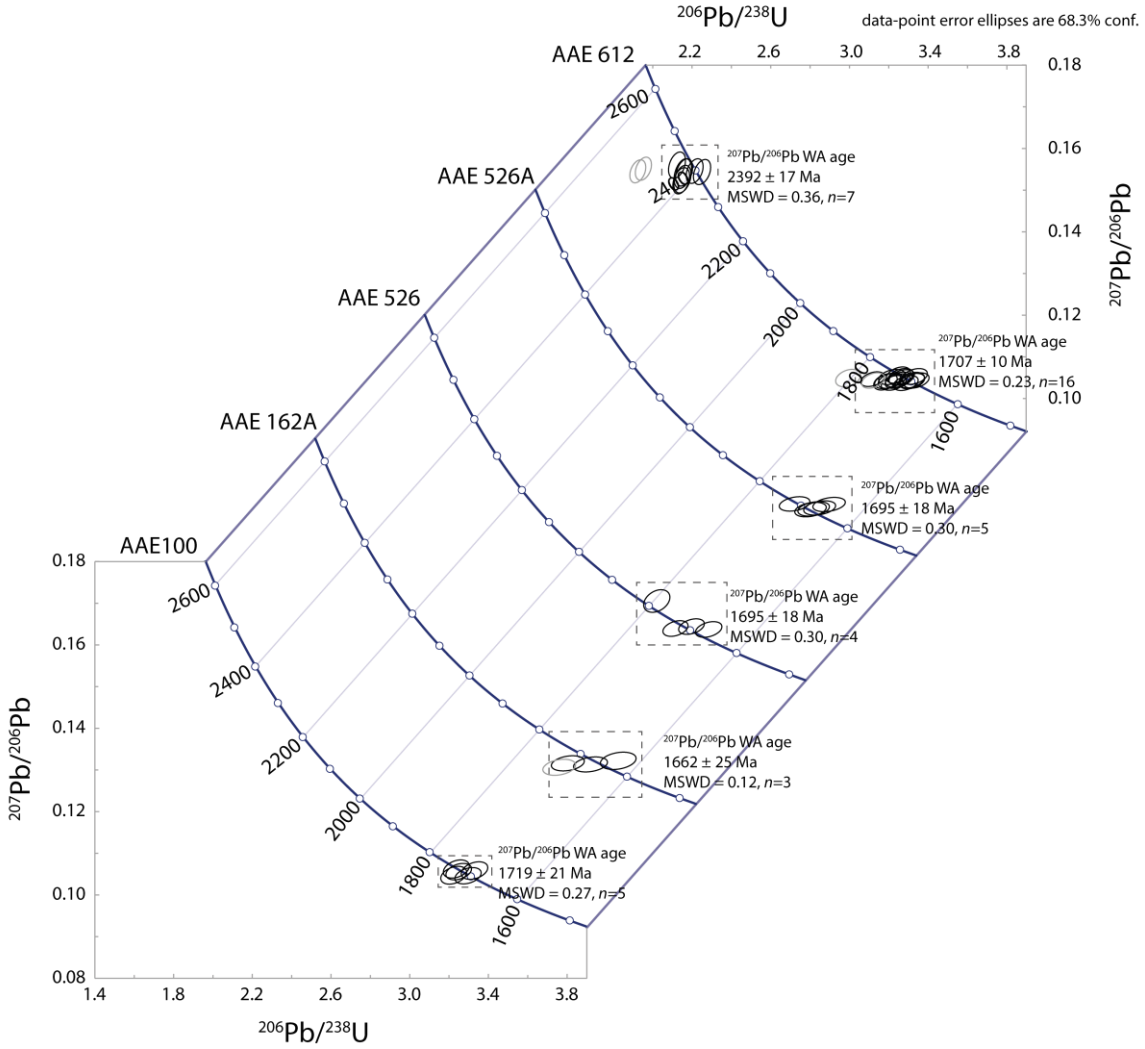

Figure 7: In situ monazite LA–ICP–MS U–Pb geochronology for erratic samples AAE100, AAE162A, AAE526, AAE526A and AAE612. Tera–Wasserburg Concordia diagrams for individual samples AAE100, AAE162A, AAE526, AAE526A and AAE612.The most concordant analyses (conc. 100 ± 5%) are shown with black outlines. Analyses that were excluded from weighted mean age calculations appear as grey ellipses. WA = weighted average.

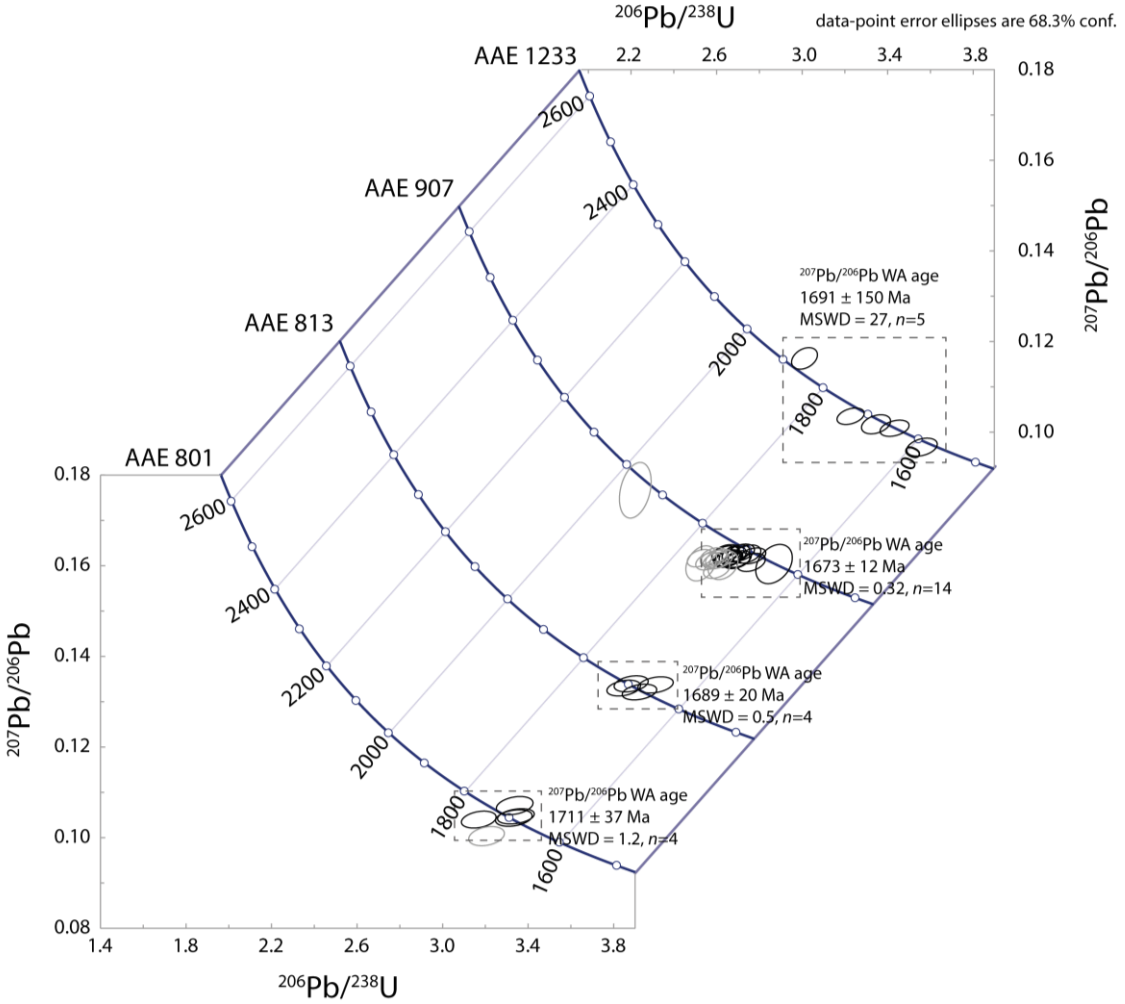

Figure 8: In situ monazite LA–ICP–MS U–Pb geochronology for erratic samples AAE801, AAE813, AAE907 and AAE1233. Tera–Wasserburg Concordia diagrams for individual samples AAE801, AAE813, AAE907 and AAE1233. The most concordant analyses (conc. 100 ± 5%) are shown with black outlines. Analyses that were excluded from weighted mean age calculations appear as grey ellipses. WA = weighted average.

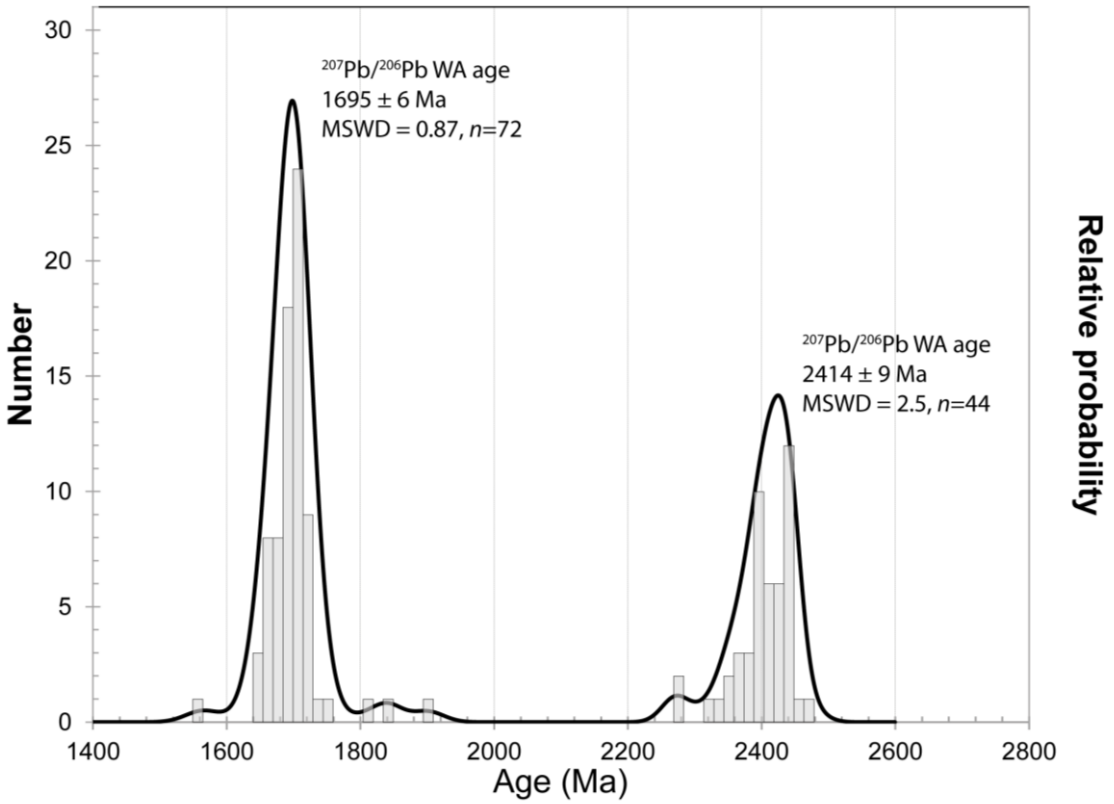

Figure 9: In situ monazite LA–ICP–MS U–Pb geochronology. Cumulative frequency histogram of $^{207}Pb/^{206}Pb$ ages and probability density plot for all concordant analyses (n = 124, conc. 100 ± 5%). WA = weighted average.

Bulk-rock chemistry

Bulk-rock geochemistry was collected for samples AAE784, AAE980, RB2012-02, RB2012-03, AAE 907 and AAE1233 to provide input for *T–M* and *P–T* forward model calculations. Table 3 shows the compositions used in the forward modelling, recast from weight percent oxides to normalised mole percent. There is a 1:1 ratio between Fe_2O_3 and excess O therefore 'O' for the mole percent bulk composition is equal to the moles of Fe_2O_3. Bulk-rock geochemical data are provided in Appendix E.

Table 3: Bulk-rock chemistry used for phase equilibria forward modelling

	AAE784		AAE980		AAE907		AAE1233		RB2012-02		RB2012-03	
	wt%	N mol%	wt%	N mol%	wt%	N mol%	wt%	N mol%	wt%	N mol%	wt%	N mol%
SiO_2	60.93	66.37	45.95	50.39	62.42	71.46	62.98	69.37	69.72	74.83	46.14	48.10
TiO_2	1.07	0.88	0.97	0.80	0.18	0.15	0.83	0.69	0.81	0.65	2.49	1.95
Al_2O_3	18.09	11.61	21.92	14.17	12.15	8.20	15.15	9.83	12.22	7.73	14.97	9.20
Fe_2O_3	1.88	–	0.17	–	12.78	–	1.15	–	2.74	–	3.77	–
FeO	5.55	–	15.16	–	4.93	–	9.34	–	4.19	–	13.72	–
O	–	0.77	–	0.07	–	5.50	–	0.48	–	1.11	–	1.48
FeO*	–	6.60	–	14.04	–	15.72	–	9.56	–	5.98	–	14.92
MnO	0.14	0.13	0.34	0.32	1.32	1.28	0.36	0.34	0.11	0.10	0.17	0.15
MgO	4.54	7.37	5.61	9.17	2.43	4.15	2.80	4.60	1.75	2.80	7.68	11.93
CaO	0.90	1.05	3.31	3.89	1.51	1.85	0.62	0.73	1.98	2.28	1.92	2.14
Na_2O	1.78	1.88	2.83	3.01	1.14	1.27	0.76	0.81	2.53	2.63	1.57	1.59
K_2O	3.89	2.70	1.83	1.28	0.65	0.47	4.44	3.12	2.97	2.03	4.70	3.12
H_2O	0.60	2.18	0.82	3.00	0.25	0.95	0.39	1.43	0.58	2.08	2.41	8.38
Total	**99.37**	**101.54**	**98.91**	**100.14**	**99.75**	**111.00**	**98.82**	**100.96**	**99.60**	**102.22**	**99.54**	**102.96**
2O		1.54		0.14		11.00		0.96		2.22		2.96
Total - 2O		100.00		100.00		100.00		100.00		100.00		100.00

N mol% = normalised mol %, the input composition for forward modelling; FeO* = FeO + 2 Fe2O3, O ∝ Fe_2O_3.

Element maps

Electron microprobe elemental X-ray maps of AAE784 (Figure 10) show coarse and fine grained garnet have similar compositions and no apparent zoning. Coarse grained K-feldspar is mantled by plagioclase ± quartz. Cordierite dominates the matrix in the top third of the map, representative of the bulk rock assemblage. X-ray maps of AAE907 (Figure 11) show garnet–magnetite symplectites surrounding coarse grained magnetite. Finer grained garnet in the symplectites is less calcic and manganese-rich than the coarser grained areas. Maps are used to confirm the mineralogy of the rock and the sequence of mineral growth, used in the interpretation of forward models.

Pressure–temperature forward models

P–T forward models were calculated for samples from the Terre Adélie coast (AAE784 and AAE980), Redbanks Charnockite (RB2012-02 and RB2012-03) and erratics from Cape Denison (AAE907 and AAE1233) in order to constrain the metamorphic conditions in the central Mawson Craton. The results from the forward models are summarised in Table 4. The *P–T* results in concert with geochronology results will be used as the basis for discussion on polymetamorphism.

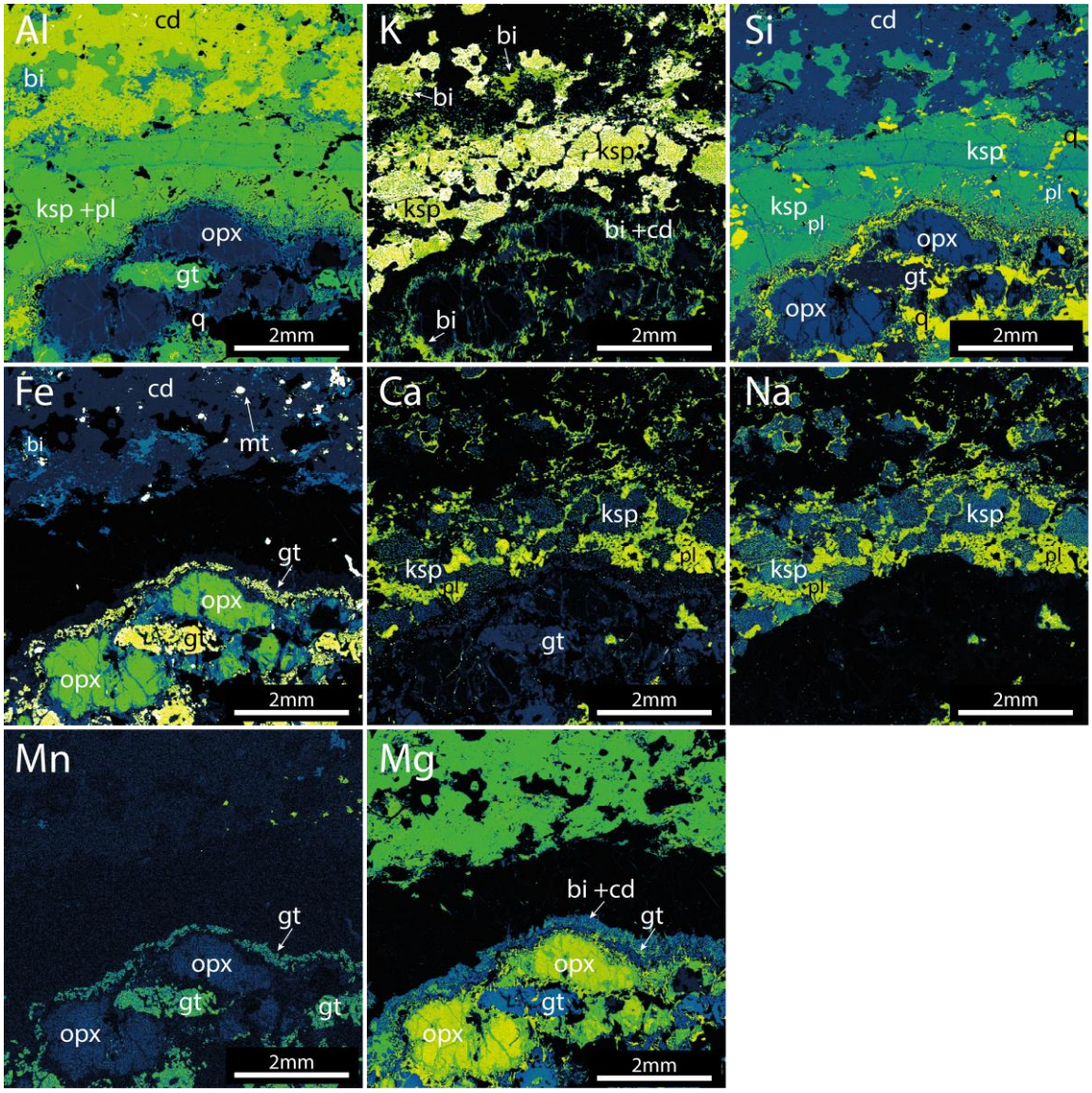

Figure 10: Electron microprobe elemental X-ray maps of AAE784. Qualitative elemental x-ray maps of Al, K, Si, Fe, Ca, Na, Mn and Mg are shown. Colour gradient from blue to white reflects an increasing concentration of that particular element. Mapped area corresponds to photomicrograph in Figure 5b. Coarse-grained orthopyroxene and garnet are systematically separated from coarse-grained K-feldspar and plagioclase by a multilayer corona. From the orthopyroxene to the feldspars the layers of the corona are organised thus: (1) biotite + cordierite + quartz; (2) garnet + quartz; (3) symplectic cordierite + quartz. Orthopyroxene and coronae, garnet and feldspars form a layer within the matrix of cd + bi + K-feldspar + plagioclase + garnet + ilmenite + magnetite.

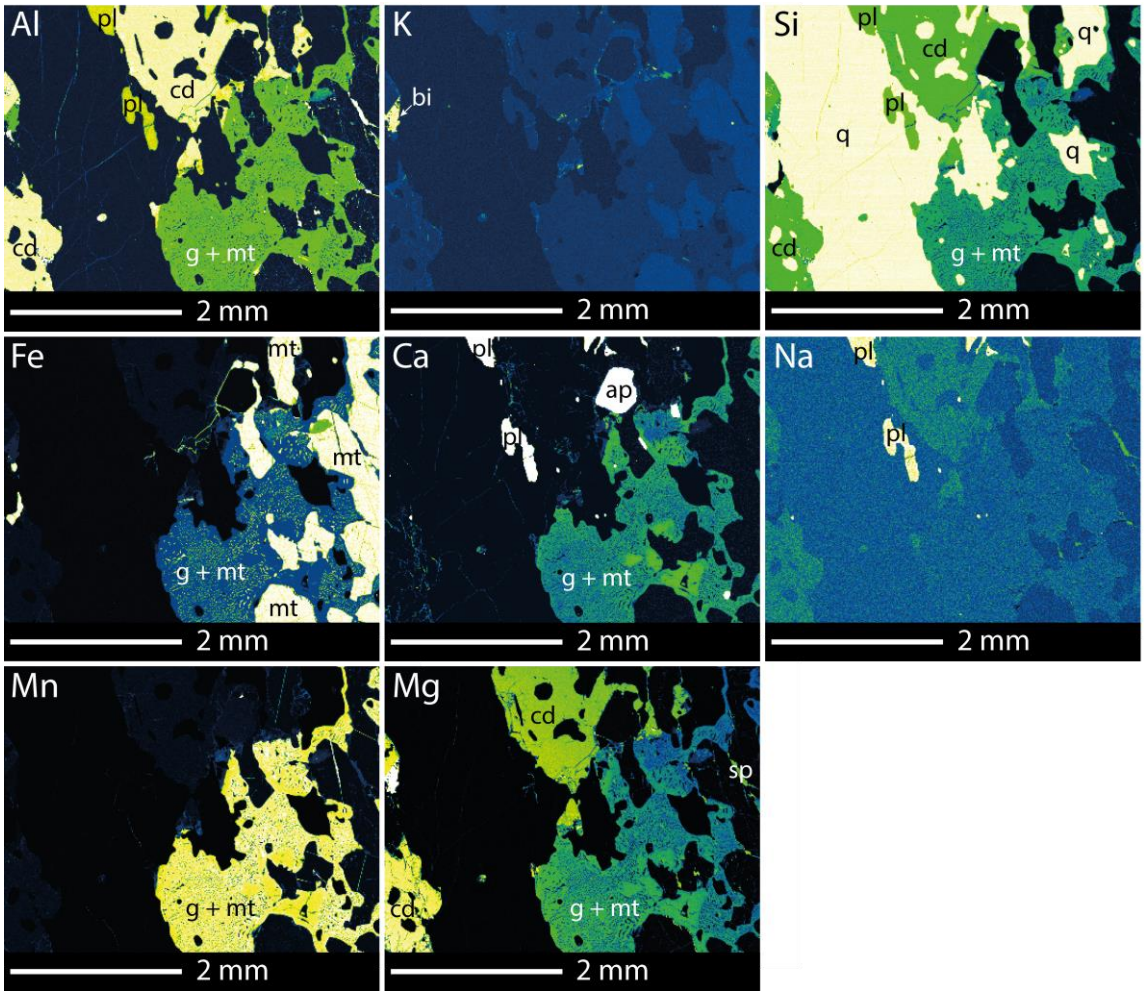

Figure 11: Electron microprobe elemental X-ray maps of AAE907. Qualitative elemental x-ray maps of Al, K, Si, Fe, Ca, Na, Mn and Mg are shown. Colour gradient from blue to white reflects an increasing concentration of that particular element. Mapped area corresponds to photomicrograph in Figure 5g. Coarse grained magnetite is in contact with symplectites of garnet + magnetite, and cordierite. Minor plagioclase, biotite and apatite are in contact with cordierite and quartz. Minor spinel is found as an inclusion in magnetite.

Table 4: Summary of results from *pressure–temperature* forward models.

sample	location	age (Ma)	first assemblage	*P–T* range	overprinting assemblage	*P–T* range	Figure
AAE784	in situ, Cape Gray	2420 ± 10	garnet–plagioclase–liquid –K-feldspar–orthopyroxene–cordierite–ilmenite–quartz	5.0–6.5 kbar 830–1000 °C	garnet–plagioclase–liqid–K-feldspar–biotite–cordierite–ilmenite–quartz	5.6–7.2 kbar 820–860 °C	11
AAE980	in situ, Stillwell Is.	2425 ± 16	garnet–plagioclase–liquid–biotite–rutile–sillimanite–quartz	6.4–8.7 kbar 690–740 °C	garnet–plagioclase–liquid–biotite–cordierite–ilmenite–quartz	5.0–6.5 kbar 700–750 °C	12
RB2012-02	in situ, Redbanks	1700 ± 12	garnet–plagioclase–liquid–K-feldspar–orthopyroxene–magnetite–ilmenite–quartz	4.3–10 kbar 830–1070 °C			13
RB2012-03	in situ, Redbanks		garnet–plagioclase–liquid–biotite–orthopyroxene–magnetite–ilmenite–quartz	4.4–7.6 kbar 710–840 °C			14
AAE907	erratic, Cape Denison	1673 ± 12	garnet–plagioclase–liquid–K-feldspar–biotite–cordierite–magnetite–ilmenite–sillimanite–quartz	5.7–7.2 kbar 760–830 °C			15
AAE1233	erratic, Cape Denison	1691 ± 150	garnet–plagioclase–liquid–K-feldspar–biotite–cordierite–ilmenite–sillimanite–quartz	5.1–6.0 kbar 780–820 °C			16

age = $^{207}Pb/^{206}Pb$ weighted average age, Figures 5, 6 and 7

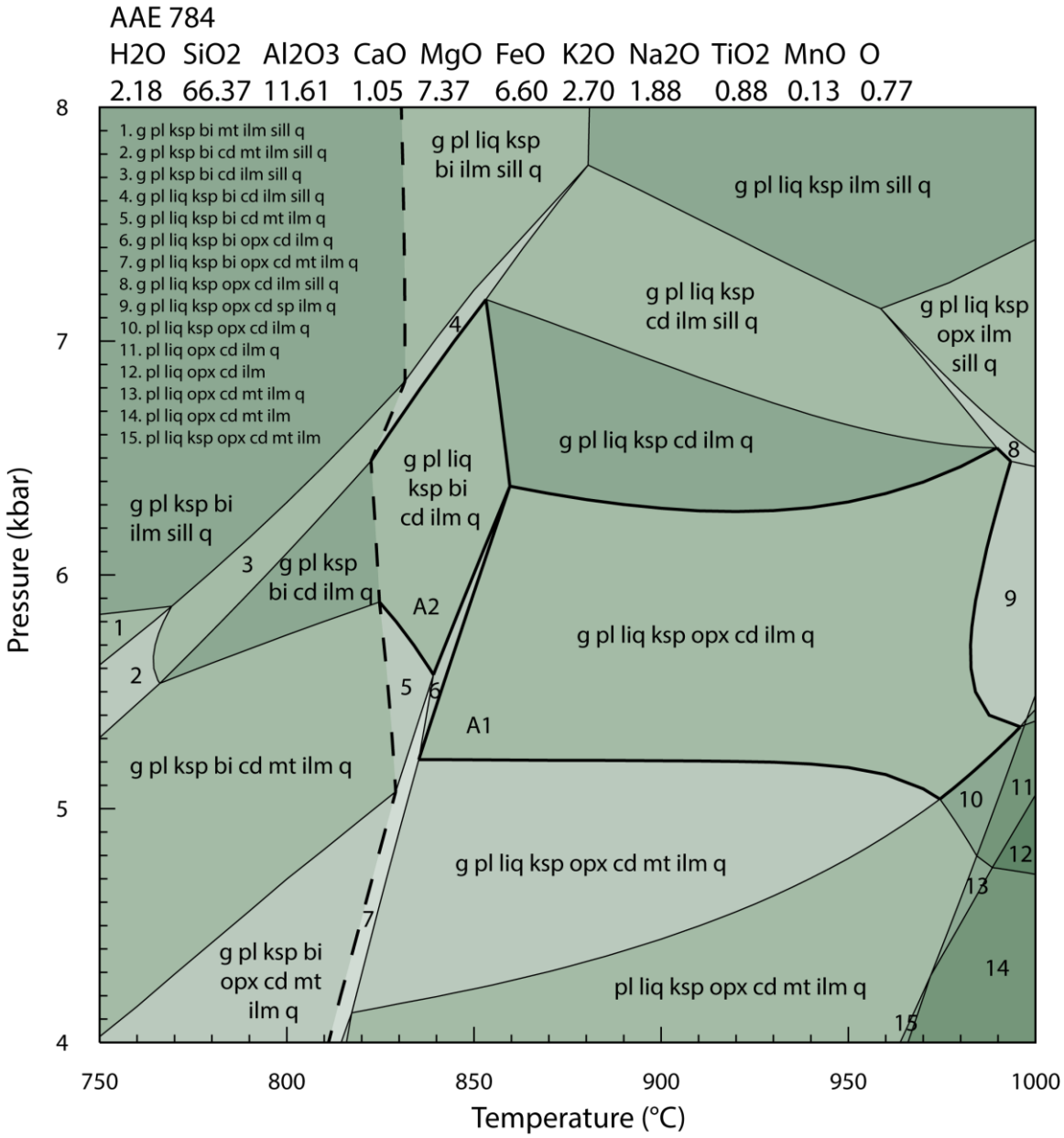

Figure 12: Calculated *P–T* forward model for sample AAE784 from the Cape Gray Gneiss. Bulk composition at the top of the diagram is expressed as mole percent. The field g–pl–liq–ksp–opx–cd–ilm–q, outlined in bold and labelled A1, indicates the first coarse-grained assemblage in the sample. The field labelled A2 and outlined in bold, indicates the *P–T* conditions of the overprinting assemblage g–pl–liq–ksp–bi–cd–ilm–q. The assemblages in the numbered fields are defined in the top left of the diagram. Mineral abbreviations from Holland and Powell (1998).

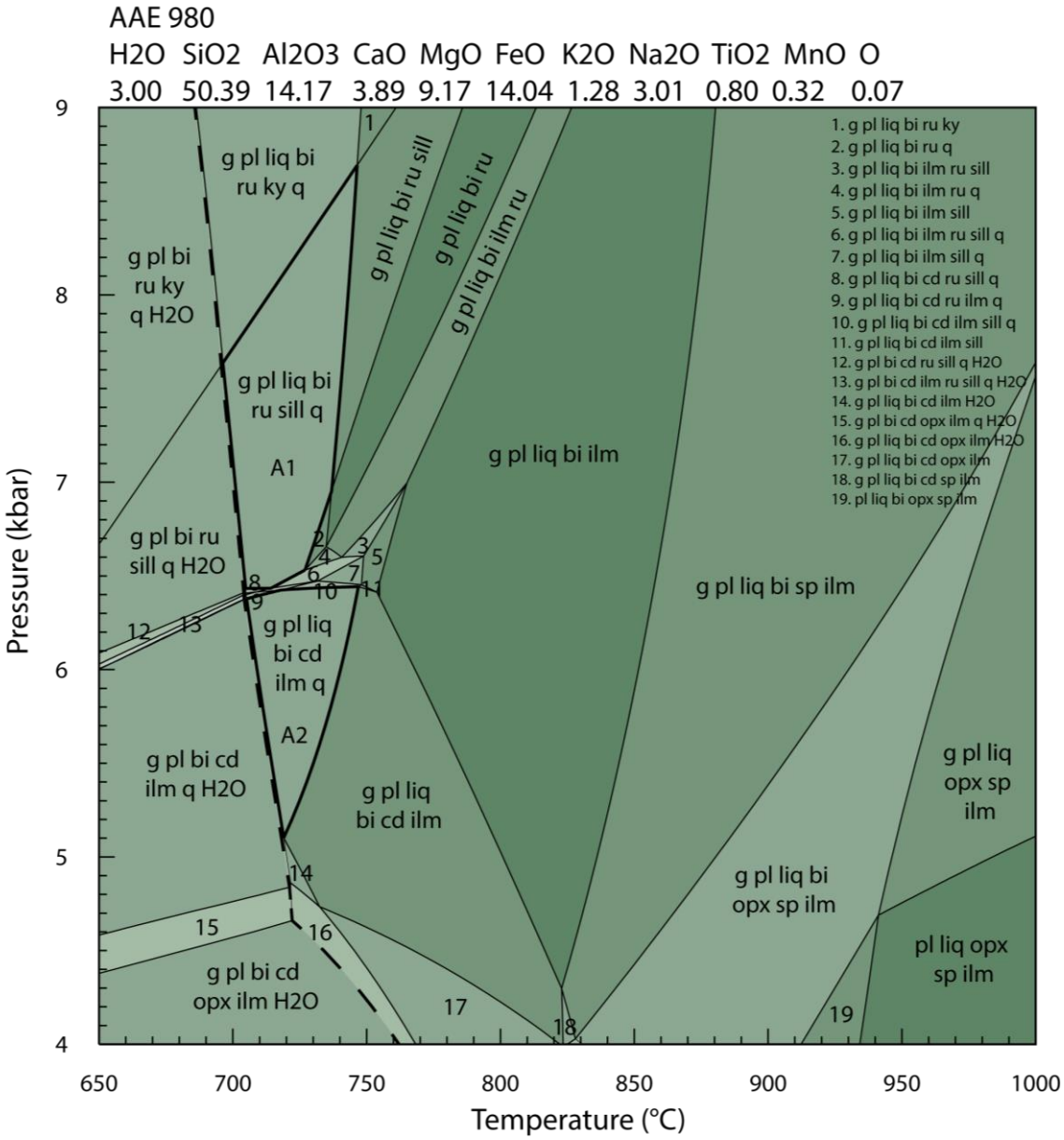

Figure 13: Calculated *P–T* forward model for sample AAE980 from the Stillwell Island Metapelite. Bulk composition at the top of the diagram is expressed as mole percent. The field g–pl–liq–bi–ru–sill–q, outlined in bold and labelled A1, indicates the first coarse-grained assemblage in the sample. The field g–pl–liq–bi–cd–ilm–q, outlined in bold and labelled A2, indicates the overprinting assemblage in the sample. The assemblages in the numbered fields are defined in the top right of the diagram. Mineral abbreviations from Holland and Powell (1998).

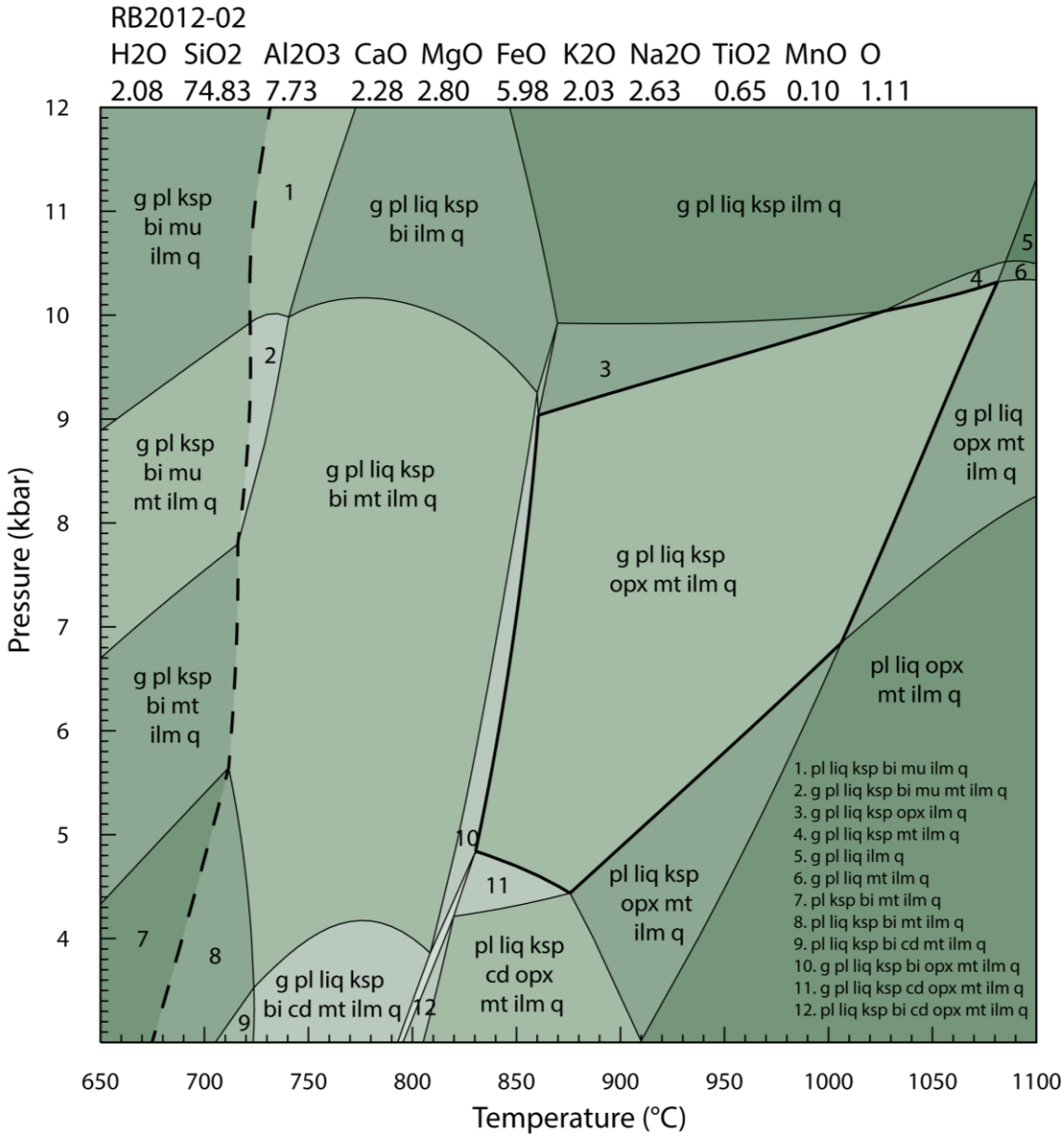

Figure 14: Calculated *P–T* forward model for sample RB2012-02 from the Redbanks Charnockite. Bulk composition at the top of the diagram is expressed as mole percent. The field g–pl–liq–ksp–opx–mt–ilm–q, outlined in bold, indicates the peak *P–T* conditions for this sample. The assemblages in the numbered fields are defined in the bottom right of the diagram. Mineral abbreviations from Holland and Powell (1998).

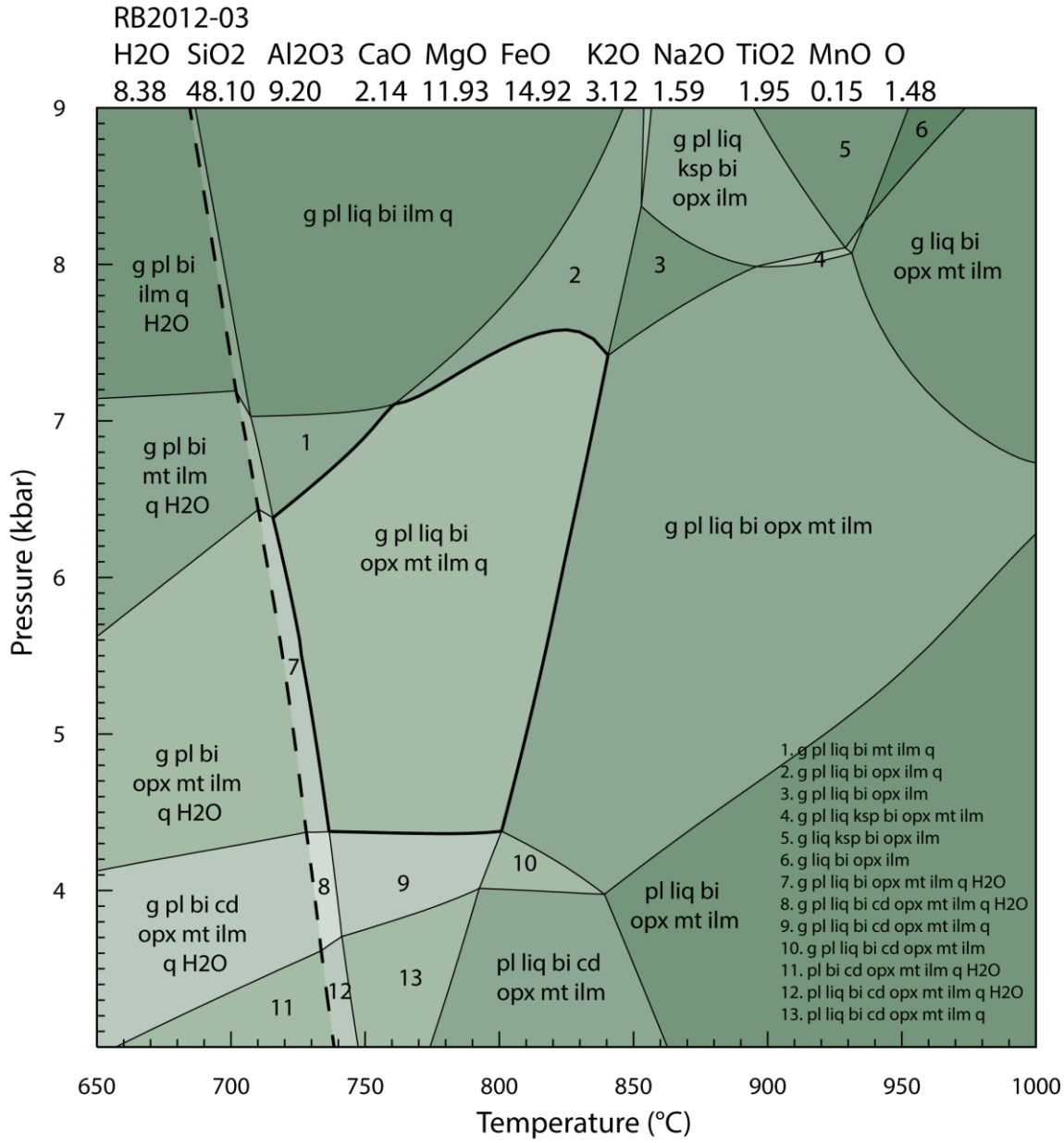

Figure 15: Calculated *P–T* forward model for sample RB2012-03 from the Redbanks Charnockite. Bulk composition at the top of the diagram is expressed as mole percent. The field g–pl–liq–bi–opx–mt–ilm–q, outlined in bold, indicates the peak *P–T* conditions for this sample. The assemblages in the numbered fields are defined in the bottom right of the diagram. Mineral abbreviations from Holland and Powell (1998).

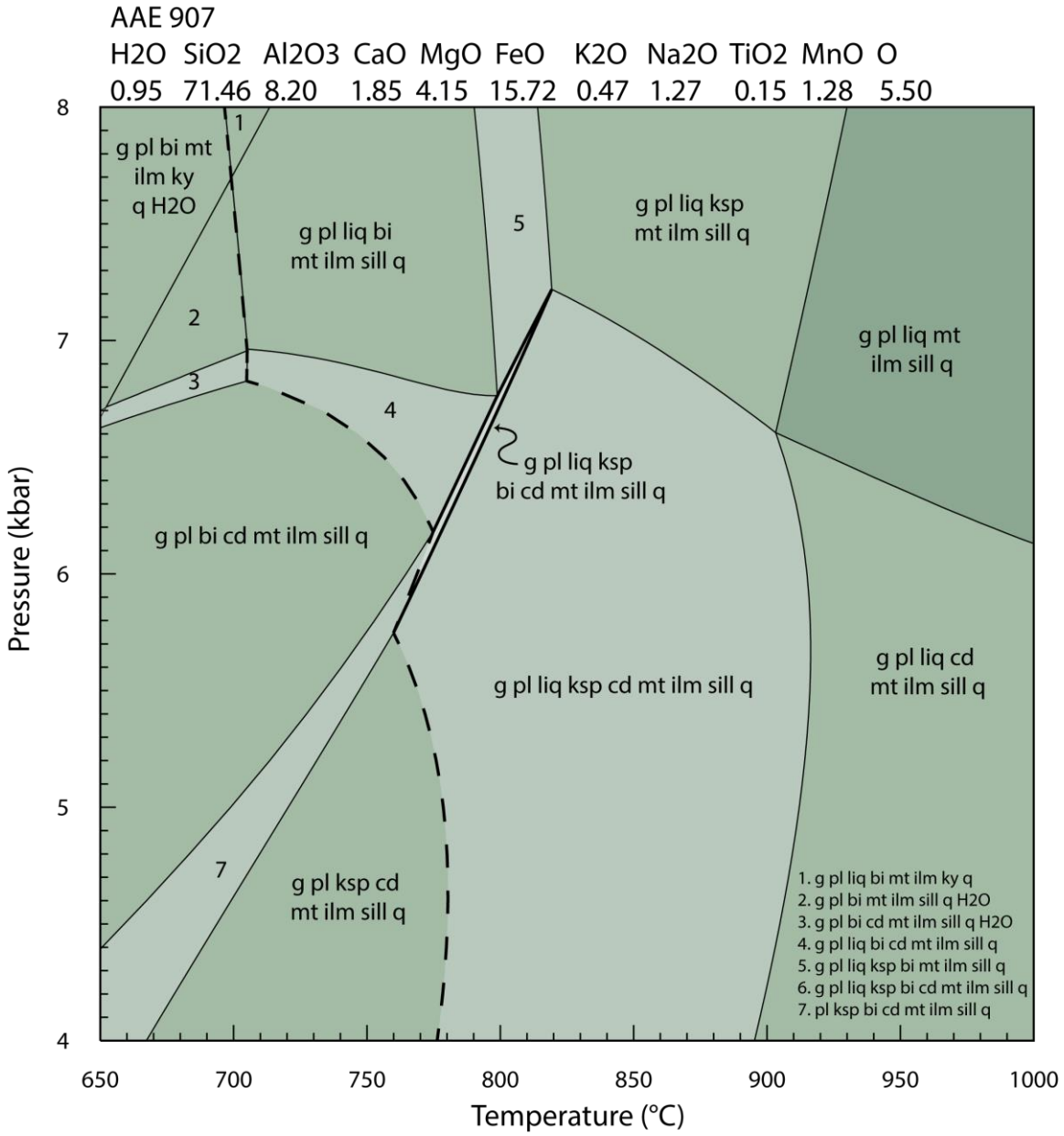

Figure 16: Calculated *P–T* forward model for sample AAE907, erratic from Cape Denison. Bulk composition at the top of the diagram is expressed as mole percent. The field g–pl–liq–ksp–bi–cd–mt–ilm–sill–q, outlined in bold, indicates the peak *P–T* conditions for this sample. The assemblages in the numbered fields are defined in the bottom right of the diagram. Mineral abbreviations from Holland and Powell (1998).

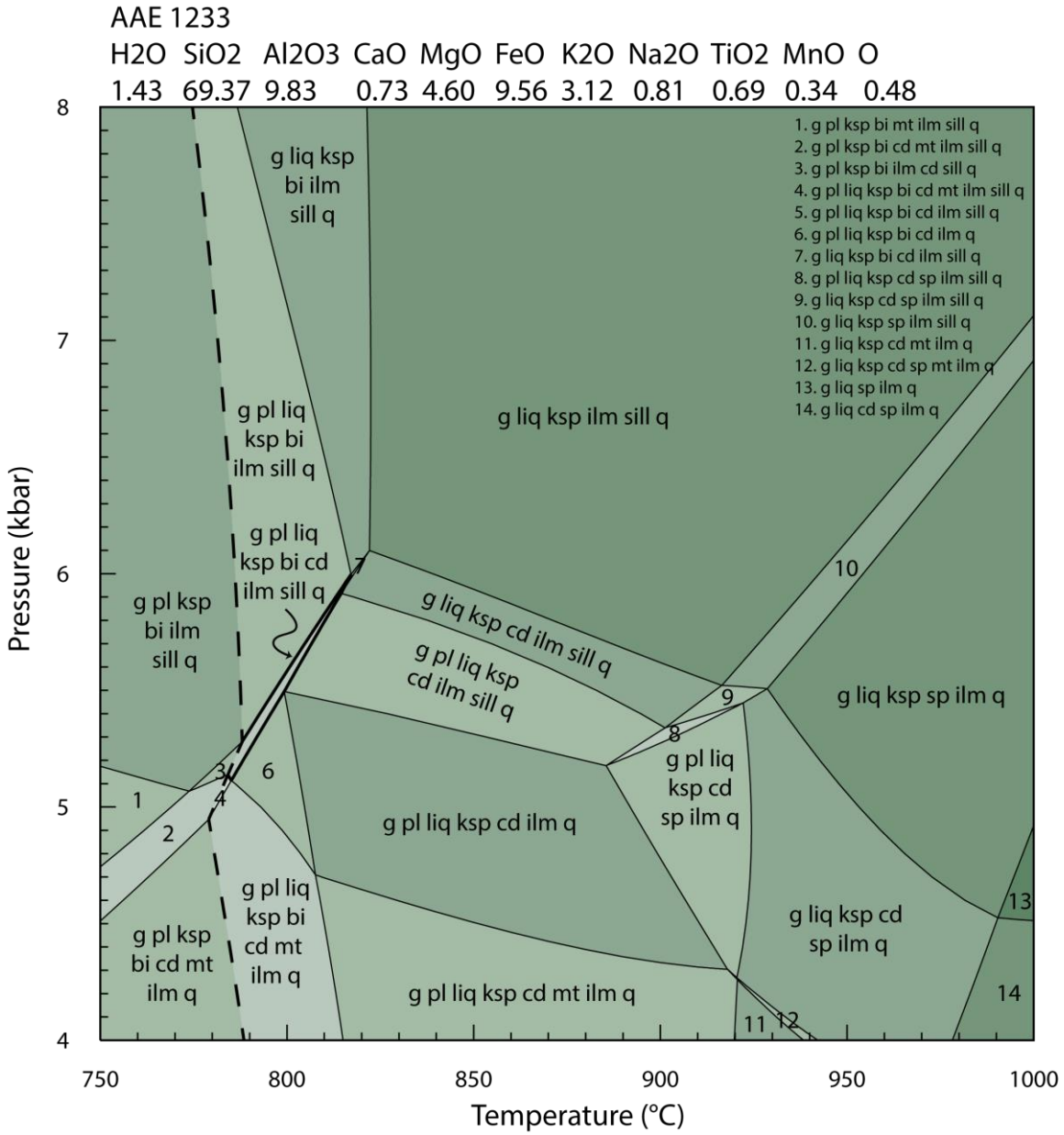

Figure 17: Calculated *P–T* forward model for sample AAE1233, erratic from Cape Denison. Bulk composition at the top of the diagram is expressed as mole percent. The field g–pl–liq–ksp–bi–cd–ilm–sill–q, outlined in bold, indicates the peak *P–T* conditions for this sample. The assemblages in the numbered fields are defined in the top right of the diagram. Mineral abbreviations from Holland and Powell (1998).

DISCUSSION

Geochronology

The samples dated in this study using monazite U–Pb geochronology all come from granulite facies metamorphic rocks. Given the propensity of monazite to grow during metamorphism (e.g. Parrish 1990, Rubatto et al. 2001, Fitzsimons et al. 2005, Kelsey et al. 2008, Gasser et al. 2012), and reactivity of monazite during metamorphism (Högdahl et al. 2012, Rubatto et al. 2013), it is interpreted here that the monazite ages record the timing of metamorphism. The monazite U–Pb geochronology collected from outcropping samples from the Cape Denison region reveals single populations that give ages of c. 2420 Ma. Sample AAE 757 gives a poorly constrained, potentially younger age around 2315 Ma; however, with more data, this age may converge with better constrained samples. The monazite U–Pb ages obtained from the coastal outcrops are similar to the electron microprobe-based Th–U–Pb ages reported for coastal areas further east (Duclaux et al. 2008).

In contrast to the ages obtained from the coastal samples, the ages obtained from erratics derived from northward flow ice (Figure 3) are, for the most part, significantly younger, c. 1700 Ma. The one exception is sample AAE 612, which contains two distinct age populations, the older of which (c. 2390 Ma) is similar to the ages obtained from the in situ samples, with the younger age population approximately the same as the age populations in the remainder of the dated erratics (Figure 8), and Palaeoproterozoic sequences west of Cape Denison (Ménot et al. 2007).

The age data from the erratics can be interpreted in two ways. One possibility is that in all but one sample, c. 2420 Ma monazite completely recrystallized at c. 1700 Ma. A second possibility is that samples that only contain the young monazite age population did not undergo metamorphism at c. 2420 Ma. As it is unknown how far inland the young samples were derived, aside from the absolute geographic limits imposed by the ice drainage basin, it is difficult to definitively interpret the significance of the younger-aged samples. However, two obvious alternatives exist. One, the samples that contain only young monazite were derived from a metamorphosed cover sequence deposited on a basement system that had been metamorphosed at c. 2420 Ma. This interpretation is consistent with previous work further west in the Terre Adélie Craton (Peucat et al. 1999, Ménot et al. 2007, Duclaux et al. 2008, Gapais et al. 2008).The other alternative is the young samples come from a terrane that has been juxtaposed against the c. 2420 Ma metamorphic terrane either around or after 1700 Ma. One test of this would be to determine the U–Pb ages and Hf isotopic composition of detrital zircons in the young samples and compare them with analogous data from the rock system that records c. 2420 Ma metamorphism. If the zircon populations of both share common ages and Hf compositions, it would suggest (although not prove) that the samples with the younger monazite were derived from a metamorphosed cover sequence, the protoliths of which were at least partly derived from the c. 2420 Ma metamorphic basement.

Of these alternatives the conservative interpretation is that samples containing only young monazite come from a cover sequence. In the Cape Denison region, the c. 1750 Ma Cape Hunter Phyllite (CHP; Oliver and Fanning 1997) forms a cover sequence on the c. 2420 Ma metamorphic basement, so this interpretation has some support in the

known geology. The CHP and its correlative Price Metasediments (PM) in the southern Gawler Craton (Oliver and Fanning 1997, Peucat et al. 1999) form a tightly constrained set of piercing points that allow the geology of the Terre Adélie coast to be precisely matched to the southern Gawler Craton (Oliver and Fanning 1997, Fitzsimons 2003). Aside from the CHP–PM, in the southern Gawler Craton the Hutchison Group (HG) forms an extensive cover sequence that overlies c. 2440 Ma basement (Hand et al. 2007, Szpunar et al. 2011). Both the PM and the HG are metamorphosed up to granulite grade (Hand et al. 2007, Lane et al. 2015), and conceivably cover sequences in Terre Adélie are similarly metamorphosed. Palaeoproterozoic sequences ~75 km to the west of Cape Denison show similar metamorphic ages to the CHP–PM (Peucat et al. 1999, Duclaux et al. 2008), although the metamorphic grade of the exposed rocks in these lithologies only reaches amphibolite facies (Monnier 1995).

The ages of the young monazite populations in the erratic samples correspond to the timing of the Kimban Orogeny which affected much of the Gawler Craton (Hand et al. 2007) , and to an unknown extent in the Terre Adélie Craton in Antarctica (Di Vincenzo et al. 2007, Duclaux et al. 2008). The young monazite U–Pb ages from the erratics span between c. 1720–1660 Ma (Figures 7 and 8). The extent of this age range may reflect the paucity of data in some of the samples. However, in the Fowler Belt in the western Gawler Craton, there is a continuum of monazite U–Pb ages in granulites ranging between c. 1710–1660 Ma (Howard 2012; unpublished PhD thesis, University of Adelaide). This is similar to the age range recorded in the Cape Denison erratics.

Polymetamorphism – age constraints

One of the erratic samples (AAE612) has both the young and old age populations. There is no obvious correlation between monazites of each age and the bulk silicate assemblage in the sample, and therefore it is not clear which age the silicate mineral assemblage in the rock relates to. If the samples that contain only c. 1700 Ma monazite do come from a cover sequence, then the sample with both c. 2420 Ma and c. 1700 Ma populations may come from the basement, and therefore record a polymetamorphic history. If this is the case, the single c. 2420 Ma age populations that come from the in situ samples AAE 784 and AAE 980 (Figure 6) are intriguing. Neither sample shows evidence for age resetting at c. 1700 Ma. This could mean that Kimban-aged metamorphism in the Cape Denison region was of sufficiently low temperature so as not to disturb monazite in the mostly anhydrous c. 2420 Ma granulites. Reconstruction of the rifted Mawson Craton shows the Cape Denison region is the continuation of the Sleaford Complex in the southern Gawler Craton (Figure 1). The southern Sleaford Complex underwent granulite facies reworking at c. 1700 Ma (Dutch et al. 2010, Jagodzinski et al. 2012) and the Kimban-aged structural trends continue into Terre Adélie (Di Vincenzo et al. 2007, Gibson et al. 2013, White et al. 2013). Although the reworked Sleaford Complex contains an extensive record of Kimban-aged metamorphism and deformation, Dutch et al. (2010; Figure 18) showed that rocks containing no geochronological record of Kimban-aged metamorphism are interleaved on a metre-scale with similar composition rocks that have highly modified or completely erased Sleafordian histories. This highlights the spatially complex way that polymetamorphism in basement terranes can be recorded.

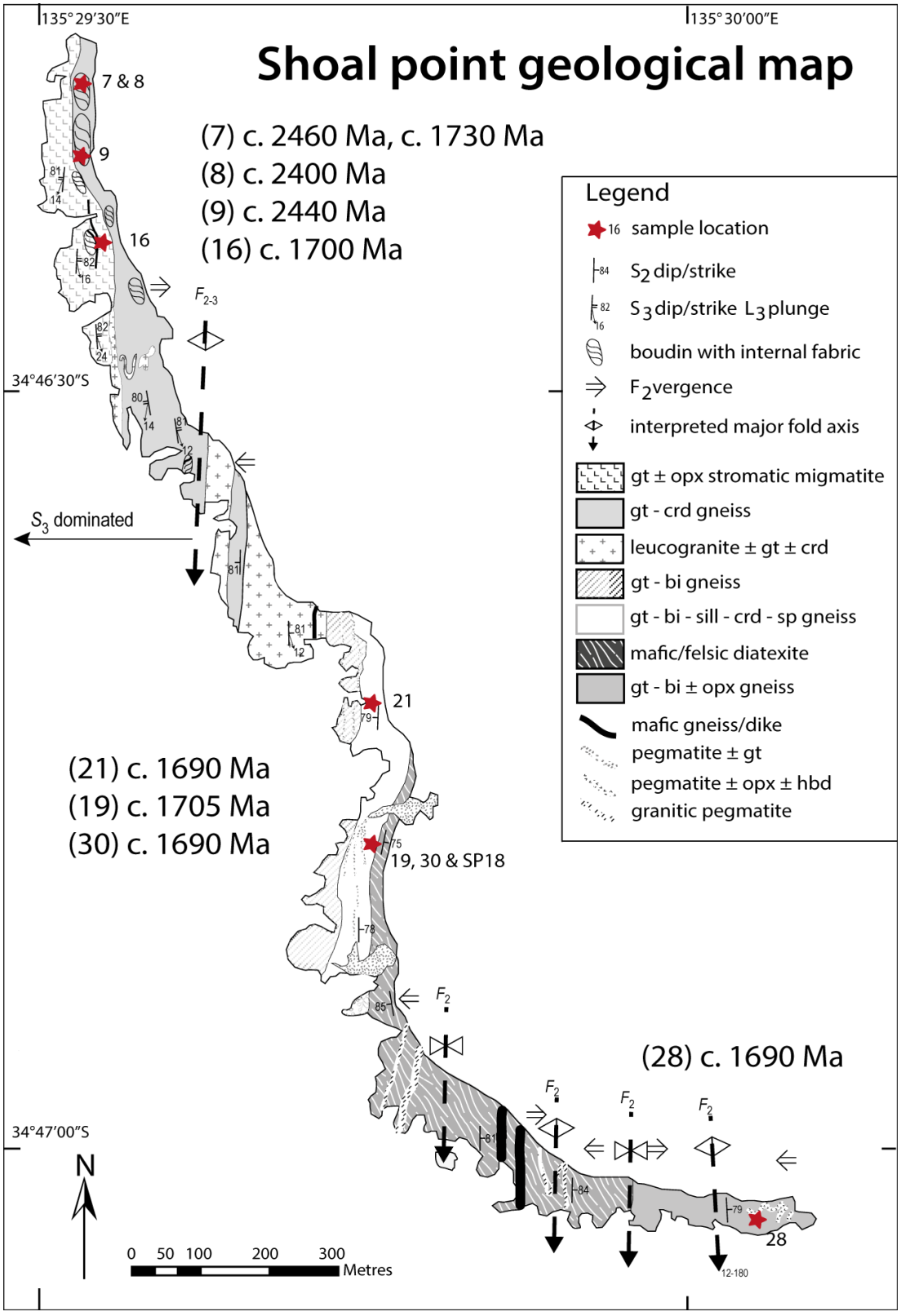

Figure 18: Shoal Point geological map. Structural and lithological map of shoal point with ages of samples from the section (after Dutch et al. 2010). Sample numbers for relevant ages are shown in brackets, red stars show sample locations. Samples indicated on this map do not form part of this study, but are presented here to highlight the spatial complexity of age distributions in rocks in high grade terranes that are visually similar.

Polymetamorphism – Metamorphic constraints

High grade terranes such as the Sleaford–Cape Denison Complex that have undergone high temperature reworking are problematic to interpret based on their metamorphic record because early generation metamorphic assemblages are variably overprinted by mineral assemblages that formed during subsequent events. This overprinting can create metamorphic reaction microstructures that suggest pressure–temperature evolutions that did not actually occur. For example, an assemblage that formed at 10 kbar and 850 °C at c. 2420 Ma could be partially overprinted by a c. 1700 Ma assemblage that formed at 5 kbar and 800 °C. The consequence would be the formation of mineral reaction microstructures that record the apparent high-temperature exhumation of the rock from 10 to 5 kbar. However, in reality the rock may have isobarically cooled at c. 2420 Ma back to a stable geotherm, been exhumed by 6 kbar between c. 2420 and c. 1700 Ma, and been reburied and reheated at c. 1700 Ma (Figure 19). The tectonic consequences of the apparent high-temperature decompression path as opposed to the comparatively pressure-insensitive cooling and heating paths are very different (Brown 1993, Vernon et al. 2008).

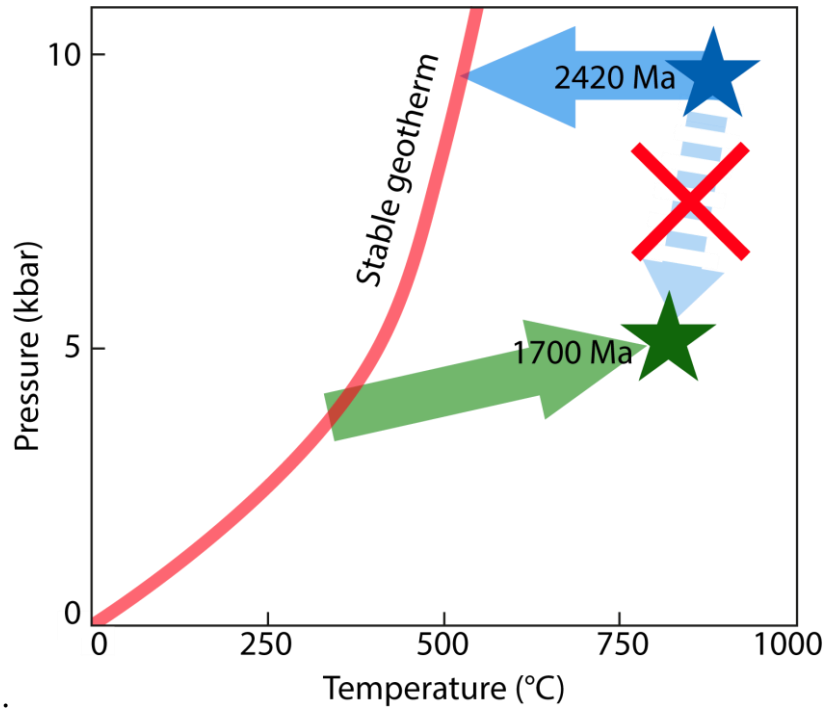

Figure 19: Schematic diagram showing potential problems with inferring P–T paths in reworked terranes. Solid arrows show the true *P–T* path taken by the sample, including two temporally distinct episodes of isobaric heating and cooling. Dashed arrow shows the apparent *P–T* path for the 2420 Ma event, inferred from the overprinting microstructural relationships that were produced during the c. 1700Ma event.

Fortunately in the Sleaford–Cape Denison Complex it is possibly to uniquely constrain the metamorphic evolution of the Kimban Orogeny using the metamorphic record in the Redbanks Charnockite (RBC), the protolith of which intruded metapelitic granulites of the Sleaford-Cape Denison Complex at c. 2007 Ma (Jagadinski et al 2012). Therefore the RBC does not contain a c. 2420 Ma metamorphic record. Metamorphic zircon in the RBC gives an age of 1722 ± 7 Ma (Jagodzinski et al. 2012), and metamorphic monazite gives 1700 ± 12 Ma (this study, Figure 6). *P–T* modelling of two garnet–orthopyroxene bearing migmatitic granulite samples from the RBC give conditions around 4.5–10.5 kbar and 720–1080 ºC (Figures 14 and 15) . Due to time constraints it has not been possible to undertake more extensive modelling that could be used to constrain the prograde Kimban history. However the results of *P–T* modelling from the RBC now

form a reference point with which to interpret the reaction microstructures developed in the older granulites in the Sleaford–Cape Denison Complex. They also form a useful reference point to compare to the modelled metamorphic conditions in the erratics that contain only young monazite ages.

Figure 20 shows the P–*T* results for the Antarctic samples that contain c. 2420 Ma monazite populations (AAE784 and AAE980). Also shown are the *P–T* constraints derived from the RBC and erratic samples (AAE907, AAE1233, RB2012-02 and RB2012-03) which contain only c. 1700 Ma monazite populations. The peak metamorphic grade for all modelled samples is granulite facies. Pressure–temperature constraints calculated for the peak assemblages in the in situ Antarctic samples (AAE784 and AAE980) are 5–11.5 kbar and 710–860 ºC (Table 4). For the erratic samples, calculated constraints are 5.1–7.2 kbar and 760–820 ºC. The peak fields for all modelled samples have similar thermal gradients (~90–180 ºC kbar), despite distinctly different monazite populations. This suggests one of two things: (1) the metamorphic grade of the c. 2420 event as recorded in samples AAE784 and AAE980 was very similar to the grade recorded for the c.1700 Ma event by samples AAE907, AAE1233, RB2012-02 and RB2012-03; or (2) The conditions recorded in the samples that contain c. 2420 Ma monazite record c.1700Ma conditions in overprinting assemblages, despite not recording this event in their monazite populations.

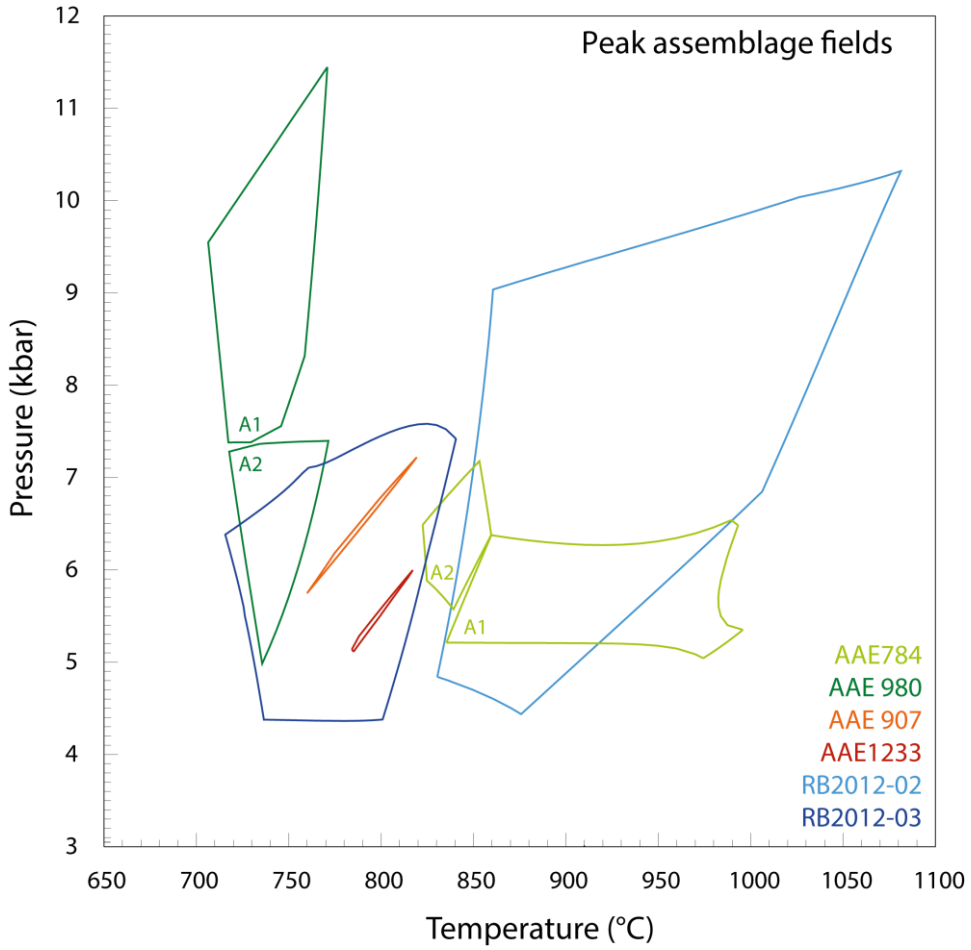

Figure 20: Summary of *P–T* constraints from forward models. Peak assemblage fields are shown for all modelled samples (Figures 12–17). Samples AAE784 and AAE980 show exclusively c. 2420 Ma monazite populations. Samples AAE907, AAE1233, RB2012-02 and RB2012-03 show exclusively c. 1700 Ma monazite populations.

Previous studies have suggested that the record of the c.1700 Ma event in the basement in Terre Adélie is limited to narrow, fluid-bearing anastomosed shear zones concentrated around the edges of the basement domain (Oliver and Fanning 2002, Ménot et al. 2007, Duclaux et al. 2008); however, the *P–T* constraints calculated in this study may indicate that the c.1700 Ma event was regionally pervasive. The peak conditions calculated here are higher grade than the amphibolite facies conditions previously recorded for the Kimban Orogeny in the Terre Adélie Craton (Peucat et al. 1999).

Both modelled samples with c. 2420 Ma geochronology (AAE784 and AAE980) record two separate peak assemblages. One of these assemblages (A2) corresponds to the Kimban conditions; therefore, these samples are interpreted to have been reworked during the Kimban Orogeny, despite having no Kimban record in their monazite populations. The apparent grade of the other recorded event in the samples AAE784 and AAE980 is inconsistent (Figure 20). Modelling for AAE784 suggests that the older event, interpreted from microstructural relationships containing orthopyroxene (A1), records higher temperatures, but similar pressures to the Kimban (Figure 12). In contrast, modelling for sample AAE980 suggests that the older event, as interpreted from reaction microstructures containing cordierite, sillimanite, ilmenite and rutile (A1), records similar temperature but higher pressure conditions than the Kimban event (Figure 13). This inconsistency may be explained by one or more of the following: (1) areas recording Sleafordian-aged assemblages have residual compositions and these form a relatively small part of the rock and are therefore not represented by the bulk composition of the rock, which is dominated by the Kimban-aged assemblage; (2) assumptions of the models do not accurately represent the reacting composition of the rock, with chosen O and H2O values having an effect on the stability fields of key minerals, such as orthopyroxene and rutile (Kelsey and Hand 2015).

Reworking of granulite facies rocks

Deciphering the record of multiple, temporally unrelated events in a terrane can be complex, especially where terrane has undergone extensive metamorphism and melt loss (Morrissey et al. in press). Differences in the record of polymetamorphism between samples may be due to the chemical heterogeneity of the protoliths (or melt-depleted residuum), not physical (pressure–temperature) heterogeneities experienced by a terrane

(Yakymchuk and Brown 2014, Morrissey et al. in press). However, this chemical heterogeneity generally cannot be quantified, as the pristine equivalents of reworked rock are commonly not available (Diener et al. 2008). Monazite and zircon are often interpreted as definitive records of terrane histories; however, the growth of these minerals is a complex function of both physical conditions (pressure and temperature) and multiple chemical components (Kelsey et al. 2008, Yakymchuk and Brown 2014). Monazite geochronology in this study reveals similar trends to those presented by Morrissey et al. (2015, in press; U–Pb LA–ICP–MS on monazite), from the polymetamorphic Rayner–Eastern Ghats terrane, which show distinctly different age populations that not only show spread but are organised in the terrane in a spatially "patchy" pattern. This type of "patchy" record of reworking is mirrored in a number of other reworked high grade terranes, including in the southern Gawler Craton (Dutch et al. 2010), the Anmatjira–Reynolds Range region in central Australia (Hand et al. 1992, Vernon 1996), the Strangways Metamorphic Complex in central Australia (Ballèvre et al. 2000), the Scottish Caledonides (Cutts et al. 2009) and Prydz Bay in east Antarctica (Dirks and Hand 1995, Kelsey et al. 2007) and the Bergen Arcs, Norway (e.g. Austrheim 1987, Boundy et al. 1992). The preservation of granulite facies mineral assemblages requires that loss of hydrous melt, produced by breakdown of hydrous minerals such as biotite, has occurred, otherwise the granulite facies mineral assemblage will be pervasively retrogressed with cooling (Brown 2002, White and Powell 2002). Thus, where melt has been retained or accumulated, rocks are less likely to preserve peak conditions, being locations of increased mineral growth on the retrograde path (Brown 2002). Such rocks are also more fertile (i.e. hydrous) and thus more likely to react when later subjected to granulite facies conditions (Morrissey et al. in press).

Additionally, older metamorphic fabrics may only be preserved in relatively low strain zones, such as in the hinges of folds (Hand et al. 1992). The record presented here is difficult to interpret in the absence of structural data, especially in the erratic samples where structural information is limited to the size of the hand specimen, and cannot be discussed in absolute terms. The preferred interpretation is that chemical heterogeneities caused by the depletion or accumulation of melt lead to inconsistent retrogression occurring either during the waning/exhumation stages of earlier events or between (high grade) events. The contrast between retrogressive and residual granulite parts of rocks being reheated is a mechanism for creating the inconsistencies in the record of ages and metamorphic reworking.

CONCLUSIONS

The in situ and erratic samples from the central Mawson Craton record two metamorphic monazite ages — c. 2420 Ma and c. 1700Ma — which correspond to the timings of the Sleafordian and Kimban Orogenies respectively in the southern Gawler Craton. In situ samples from Terre Adélie record exclusively c. 2420Ma and erratic samples exclusively c. 1700Ma, with the exception of erratic sample AAE612 which records both monazite populations. The calculated conditions of peak metamorphism are granulite facies across all samples, with the calculated constraints on Kimban conditions reaching 4.3–10kbar and 710–1010 ºC. Assemblages interpreted as c. 2420 in age constrain the peak of Sleafordian metamorphism to 5–11.5 kbar and 710–1000 ºC. Sleafordian-aged and Kimban-aged samples show similar metamorphic grades and thermal gradients in these samples, either due to the Sleafordian and Kimban reaching similar thermal grades at these sites or due to all of the samples recording predominantly Kimban-aged bulk silicate assemblages. This study reflects the findings

in other reworked high grade terranes of an inconsistent record of events between samples. This is interpreted to be due to heterogeneities in the depletion or accumulation of melt and subsequent retrogression, occurring either during the waning/exhumation stages of earlier events or between (high grade) events.

ACKNOWLEDGMENTS

Supervisors David Kelsey and Martin Hand are thanked for their ongoing support, creativity and guidance. Laura Morrissey and Naomi Tucker are thanked for valuable assistance with *P–T* modelling and processing of geochronological data. Ben Wade, Aoife McFadden and the rest of the staff of Adelaide Microscopy are thanked for assistance with SEM imaging, and electron microprobe and LA–ICP–MS analyses. Ros King and Katie Howard are thanked for their support and guidance throughout the year. Rian Dutch and Kathleen Lane are thanked for access to previously collected data.

REFERENCES

AITKEN A., YOUNG D., FERRACCIOLI F., BETTS P., GREENBAUM J., RICHTER T., ROBERTS J. L., BLANKENSHIP D. & SIEGERT M. 2014. The subglacial geology of Wilkes Land, East Antarctica. *Geophysical Research Letters* **41**, 2390-2400.

AUSTRHEIM H. 1987. Eclogitization of lower crustal granulites by fluid migration through shear zones. *Earth and Planetary Science Letters* **81**, 221-232.

BALLÈVRE M., MÖLLER A. & HENSEN B. 2000. Exhumation of the lower crust during crustal shortening: an Alice Springs (380 Ma) age for a prograde amphibolite facies shear zone in the Strangways Metamorphic Complex (central Australia). *Journal of Metamorphic Geology* **18**, 737-747.

BELOUSOVA E., REID A., GRIFFIN W. L. & O'REILLY S. Y. 2009. Rejuvenation vs. recycling of Archean crust in the Gawler Craton, South Australia: evidence from U–Pb and Hf isotopes in detrital zircon. *Lithos* **113**, 570-582.

BOGER S. D. 2011. Antarctica - Before and after Gondwana. *Gondwana Research* **19**, 335-371.

BOUNDY T., FOUNTAIN D. & AUSTRHEIM H. 1992. Structural development and petrofabrics of eclogite facies shear zones, Bergen Arcs, western Norway: implications for deep crustal deformational processes. *Journal of Metamorphic Geology* **10**, 127-146.

BROWN M. 1993. P–T–t evolution of orogenic belts and the causes of regional metamorphism. *Journal of the Geological Society* **150**, 227-241.

BROWN M. 2002. Retrograde processes in migmatites and granulites revisited. *Journal of Metamorphic Geology* **20**, 25-40.

COGGON R. & HOLLAND T. 2002. Mixing properties of phengitic micas and revised garnet-phengite thermobarometers. *Journal of Metamorphic Geology* **20**, 683-696.

CONNOLLY J. & PETRINI K. 2002. An automated strategy for calculation of phase diagram sections and retrieval of rock properties as a function of physical conditions. *Journal of Metamorphic Geology* **20**, 697-708.

CONNOLLY J. 2005. Computation of phase equilibria by linear programming: a tool for geodynamic modeling and its application to subduction zone decarbonation. *Earth and Planetary Science Letters* **236**, 524-541.

CUTTS K., HAND M., KELSEY D., WADE B., STRACHAN R., CLARK C. & NETTING A. 2009. Evidence for 930 Ma metamorphism in the Shetland Islands, Scottish Caledonides: implications for Neoproterozoic tectonics in the Laurentia–Baltica sector of Rodinia. *Journal of the Geological Society* **166**, 1033-1047.

DI VINCENZO G., TALARICO F. & KLEINSCHMIDT G. 2007. An 40 Ar–39 Ar investigation of the Mertz Glacier area (George V Land, Antarctica): implications for the Ross Orogen–East Antarctic Craton relationship and Gondwana reconstructions. *Precambrian Research* **152**, 93-118.

DIENER J., WHITE R. & POWELL R. 2008. Granulite facies metamorphism and subsolidus fluid-absent reworking, Strangways Range, Arunta Block, central Australia. *Journal of Metamorphic Geology* **26**, 603-622.

DIRKS P. & HAND M. 1995. Clarifying temperature-pressure paths via structures in granulite from the Bolingen Islands, Antarctica. *Australian Journal of Earth Sciences* **42**, 157-172.

DUCLAUX G., ROLLAND Y., RUFFET G., MÉNOT R.-P., GUILLOT S., PEUCAT J.-J., FANNING M., REY P. & PÊCHER A. 2008. Superimposed Neoarchaean and Paleoproterozoic tectonics in the Terre Adélie Craton (East Antarctica): Evidence from Th–U–Pb ages on monazite and 40Ar/39Ar ages. *Precambrian Research* **167**, 316-338.

DUTCH R., HAND M. & KELSEY D. 2010. Unravelling the tectonothermal evolution of reworked Archean granulite facies metapelites using in situ geochronology: an example from the Gawler Craton, Australia. *Journal of Metamorphic Geology* **28**, 293-316.

FANNING C., MOORE D., BENNETT V. & DALY S. 1996 The 'Mawson Continent': Archaean to Proterozoic crust in the East Antarctic Shield and Gawler Craton, Australia. A cornerstone in Rodinia and Gondwanaland. Geological Society of Australia Abstracts*.* pp. 135.

FITZSIMONS I., KINNY P., WETHERLEY S. & HOLLINGSWORTH D. 2005. Bulk chemical control on metamorphic monazite growth in pelitic schists and implications for U–Pb age data. *Journal of Metamorphic Geology* **23**, 261-277.

FITZSIMONS I. C. W. 2003. Proterozoic basement provinces of southern and southwestern Australia, and their correlation with Antarctica. *Geological Society, London, Special Publications* **206**, 93-130.

FRASER G., MCAVANEY S., NEUMANN N., SZPUNAR M. & REID A. 2010. Discovery of early Mesoarchean crust in the eastern Gawler Craton, South Australia. *Precambrian Research* **179**, 1-21.

GAPAIS D., PELLETIER A., MÉNOT R.-P. & PEUCAT J.-J. 2008. Paleoproterozoic tectonics in the Terre Adélie Craton (East Antarctica). *Precambrian Research* **162**, 531-539.

GASSER D., BRUAND E., RUBATTO D. & STÜWE K. 2012. The behaviour of monazite from greenschist facies phyllites to anatectic gneisses: an example from the Chugach Metamorphic Complex, southern Alaska. *Lithos* **134**, 108-122.

GIBSON G., TOTTERDELL J., WHITE L., MITCHELL C., STACEY A., MORSE M. & WHITAKER A. 2013. Pre-existing basement structure and its influence on continental rifting and fracture zone development along Australia's southern rifted margin. *Journal of the Geological Society* **170**, 365-377.

GONCALVES P., NICOLLET C. & MONTEL J.-M. 2004. Petrology and in situ U–Th–Pb Monazite Geochronology of Ultrahigh-Temperature Metamorphism from the Andriamena Mafic Unit, North–Central Madagascar. Significance of a Petrographical P–T Path in a Polymetamorphic Context. *Journal of Petrology* **45**, 1923-1957.

HAND M., DIRKS P., POWELL R. & BUICK I. 1992. How well established is isobaric cooling in Proterozoic orogenic belts? An example from the Arunta inlier, central Australia. *Geology* **20**, 649-652.

HAND M., REID A. & JAGODZINSKI L. 2007. Tectonic Framework and Evolution of the Gawler Craton, Southern Australia. *Economic Geology* **102**, 1377-1395.

HARLEY S. 1989. The origins of granulites: a metamorphic perspective. *Geological Magazine* **126**, 215-247.

HÖGDAHL K., MAJKA J., SJÖSTRÖM H., NILSSON K. P., CLAESSON S. & KONEČNÝ P. 2012. Reactive monazite and robust zircon growth in diatexites and leucogranites from a hot, slowly cooled orogen: implications for the Palaeoproterozoic tectonic evolution of the central Fennoscandian Shield, Sweden. *Contributions to Mineralogy and Petrology* **163**, 167-188.

HOLDAWAY M., GUIDOTTI C. V., NOVAK J. M. & HENRY W. E. 1982. Polymetamorphism in medium-to high-grade pelitic metamorphic rocks, west-central Maine. *Geological Society of America Bulletin* **93**, 572-584.

HOLLAND T. & POWELL R. 1998. An internally consistent thermodynamic data set for phases of petrological interest. *Journal of metamorphic Geology* **16**, 309-343.

HOLLAND T. & POWELL R. 2003. Activity–composition relations for phases in petrological calculations: an asymmetric multicomponent formulation. *Contributions to Mineralogy and Petrology* **145**, 492-501.

HOLLAND T. & POWELL R. 2011. An improved and extended internally consistent thermodynamic dataset for phases of petrological interest, involving a new equation of state for solids. *Journal of Metamorphic Geology* **29**, 333-383.

HOWARD K. E. 2012. Geotectonics in the Gawler craton: constraints from geochemistry, U–Pb geochronology and Sm–Nd and Lu–Hf isotopes.

JAGODZINSKI E. A., REID A. J. & HAND M. 2012. SHRIMP U–Pb geochronology of Archaean to Palaeoproterozoic rocks from the southern Eyre Peninsula. *DMITRE Resources and Energy Group. Geological Survey of South Australia*.

KELLY N. M. & HARLEY S. L. 2005. An integrated microtextural and chemical approach to zircon geochronology: refining the Archaean history of the Napier Complex, east Antarctica. *Contributions to Mineralogy and Petrology* **149**, 57-84.

KELSEY D., HAND M., CLARK C. & WILSON C. 2007. On the application of in situ monazite chemical geochronology to constraining P–T–t histories in high-

temperature (> 850° C) polymetamorphic granulites from Prydz Bay, East Antarctica. *Journal of the Geological Society* **164**, 667-683.

KELSEY D., CLARK C. & HAND M. 2008. Thermobarometric modelling of zircon and monazite growth in melt-bearing systems: Examples using model metapelitic and metapsammitic granulites. *Journal of Metamorphic Geology* **26**, 199-212.

KELSEY D. E. & HAND M. 2015. On ultrahigh temperature crustal metamorphism: Phase equilibria, trace element thermometry, bulk composition, heat sources, timescales and tectonic settings. *Geoscience Frontiers* **6**, 311-356.

LANE K., JAGODZINSKI E., DUTCH R., REID A. & HAND M. 2015. Age constraints on the timing of iron ore mineralisation in the southeastern Gawler Craton. *Australian Journal of Earth Sciences* **62**, 55-75.

LUDWIG K. 2012. User's manual for Isoplot version 3.75-4.15: a geochronological toolkit for Microsoft. *Excel Berkley Geochronological Center Special Publication*.

MAWSON D. 1940. Catalogue of Rocks and Minerals collected in Antarctic Regions. *University of Adelaide Australasian Antarctic Expedition (1911-14) Scientific Reports, Series A* **4**.

MÉNOT R., PELLETIER A., PEUCAT J., FANNING C. & OLIVER R. 1999 Petrological and structural constraints on the amalgamation of the Terre Adélie Craton (135-145 E), East Antarctica. 8th International Symposium on Antarctic Earth Sciences: Wellington, New Zealand. pp. 208.

MÉNOT R., PECHER A., ROLLAND Y., PEUCAT J., PELLETIER A., DUCLAUX G. & GUILLOT S. 2005. Structural Setting of the Neoarchean Terranes in the Commonwealth Bay Area (143-145° E), Terre Adélie Craton, East Antarctica. *Gondwana Research* **8**, 1-9.

MÉNOT R., DUCLAUX G., PEUCAT J., ROLLAND Y., GUILLOT S., FANNING M., BASCOU J., GAPAIS D. & PECHER A. 2007 Geology of the Terre Adélie craton (135–146 E). Antarctica: A Keystone in a Changing World–Online Proceedings of the 10th ISAES, edited by AK Cooper and CR Raymond et al., USGS Open-File Report.

MONNIER O. 1995 Le socle protérozoïque de Terre Adélie(Antarctique Est), son évolution tectono-métamorphique et sa place dans les reconstitutions du Proto-Gondwana.

MONNIER O., MÉNOT R.-P., PEUCAT J.-J., FANNING M. & GIRET A. 1996. Actualisation des données géologiques sur Terre Adélie (Antarctique Est): mise en évidence d'un collage tectonique au Protérozoïque. *CR Acad. Sci., Paris* **322**, 55-62.

MORRISSEY L. J., HAND M., KELSEY D. & WADE B. in press. Cambrian high-temperature reworking of the Rayner–Eastern Ghats terrane: constraints from the northern Prince Charles Mountains region, east Antarctica. *Journal of Petrology*.

OLIVER R. L. & FANNING C. M. 1997. Australia and Antarctica: precise correlation of Palaeoproterozoic terranes. *The Antarctic Region: geological evolution and processes. Sienna, Terra Antartica Publication*, pp. 163-172.

OLIVER R. L. & FANNING C. M. 2002. Proterozoic geology east and southeast of Commonwealth Bay, George V land, Antarctica, and its relationship to that of adjacent Gondwana terranes. *In* GAMBLE J. A., SKINNER D. N. B. & HENRYS S. eds. *Antarctica at the close of a millennium: proceedings of the 8th*

International Symposium on Antarctic Earth Sciences, Wellington 1999. The Royal Society of New Zealand Bulletin, 35 ed.

PARRISH R. R. 1990. U-Pb dating of monazite and its application to geological problems. *Canadian Journal of Earth Sciences* **27**, 1431-1450.

PAYNE J., HAND M., BAROVICH K. & WADE B. 2008. Temporal constraints on the timing of high-grade metamorphism in the northern Gawler Craton: implications for assembly of the Australian Proterozoic. *Australian Journal of Earth Sciences* **55**, 623-640.

PAYNE J. L., HAND M., BAROVICH K. M., REID A. & EVANS D. A. 2009. Correlations and reconstruction models for the 2500-1500 Ma evolution of the Mawson Continent. *Geological Society, London, Special Publications* **323**, 319-355.

PEARCE M. A., WHITE A. J. R. & GAZLEY M. F. 2015. TCInvestigator: automated calculation of mineral mode and composition contours for thermocalc pseudosections. *Journal of Metamorphic Geology*, n/a-n/a.

PEUCAT J., MÉNOT R., MONNIER O. & FANNING C. 1999. The Terre Adélie basement in the East-Antarctica Shield: geological and isotopic evidence for a major 1.7 Ga thermal event; comparison with the Gawler Craton in South Australia. *Precambrian Research* **94**, 205-224.

PEUCAT J., CAPDEVILA R., FANNING C., MÉNOT R., PÉCORA L. & TESTUT L. 2002. 1.60 Ga felsic volcanic blocks in the moraines of the Terre Adélie Craton, Antarctica: comparisons with the Gawler Range Volcanics, South Australia. *Australian Journal of Earth Sciences* **49**, 831-845.

POWELL R. & HOLLAND T. 1988. An internally consistent dataset with uncertainties and correlations: 3. Applications to geobarometry, worked examples and a computer program. *Journal of Metamorphic Geology* **6**, 173-204.

POWELL R., HOLLAND T. & WORLEY B. 1998. Calculating phase diagrams involving solid solutions via non-linear equations, with examples using THERMOCALC. *Journal of metamorphic Geology* **16**, 577-588.

REID A. J. & HAND M. 2012. Mesoarchean to Mesoproterozoic evolution of the southern Gawler Craton, South Australia. *Episodes-Newsmagazine of the InternationalUnion of Geological Sciences* **35**, p.216.

RIGNOT E., MOUGINOT J. & SCHEUCHL B. 2011a. MEaSUREs InSAR-based Antarctica Ice Velocity Map. DS14. Retrieved Date Accessed.

RIGNOT E., MOUGINOT J. & SCHEUCHL B. 2011b. Ice flow of the Antarctic ice sheet. *Science* **333**, 1427-1430.

RUBATTO D., WILLIAMS I. S. & BUICK I. S. 2001. Zircon and monazite response to prograde metamorphism in the Reynolds Range, central Australia. *Contributions to Mineralogy and Petrology* **140**, 458-468.

RUBATTO D., CHAKRABORTY S. & DASGUPTA S. 2013. Timescales of crustal melting in the Higher Himalayan Crystallines (Sikkim, Eastern Himalaya) inferred from trace element-constrained monazite and zircon chronology. *Contributions to Mineralogy and Petrology* **165**, 349-372.

SHERATON J., OLIVER R. & STÜWE K. 1989. Geochemistry of Proterozoic amphibolite dykes of Commonwealth Bay, Antarctica, and possible correlations with mafic dyke swarms elsewhere in Gondwanaland. *Precambrian research* **44**, 353-361.

STILLWELL F. L. 1918. Metamorphic rocks of Adelie Land. *University of Melbourne Australasian Antarctic Expedition (1911-14) Scientific Reports, Series A* **3**.

STÜWE K. & OLIVER R. 1989. Geological history of Adélie Land and King George V Land, Antarctica: evidence for a polycyclic metamorphic evolution. *Precambrian research* **43**, 317-334.

SZPUNAR M., HAND M., BAROVICH K., JAGODZINSKI E. & BELOUSOVA E. 2011. Isotopic and geochemical constraints on the Paleoproterozoic Hutchison Group, southern Australia: Implications for Paleoproterozoic continental reconstructions. *Precambrian Research* **187**, 99-126.

VERNON R. 1996. Problems with inferring P–T–t paths in low-P granulite facies rocks. *Journal of Metamorphic Geology* **14**, 143-153.

VERNON R., WHITE R. & CLARKE G. 2008. False metamorphic events inferred from misinterpretation of microstructural evidence and P–T data. *Journal of Metamorphic Geology* **26**, 437-449.

WHITE L. T., GIBSON G. M. & LISTER G. S. 2013. A reassessment of paleogeographic reconstructions of eastern Gondwana: Bringing geology back into the equation. *Gondwana Research* **24**, 984-998.

WHITE R., POWELL R., HOLLAND T. & WORLEY B. 2000. The effect of TiO2 and Fe2O3 on metapelitic assemblages at greenschist and amphibolite facies conditions: mineral equilibria calculations in the system K2O–FeO–MgO–Al2O3–SiO2–H2O–TiO2–Fe2O3. *Journal of Metamorphic Geology* **18**, 497-512.

WHITE R. & POWELL R. 2002. Melt loss and the preservation of granulite facies mineral assemblages. *Journal of Metamorphic Geology* **20**, 621-632.

WHITE R., POWELL R. & CLARKE G. 2002. The interpretation of reaction textures in Fe-rich metapelitic granulites of the Musgrave Block, central Australia: constraints from mineral equilibria calculations in the system K2O–FeO–MgO–Al2O3–SiO2–H2O–TiO2–Fe2O3. *Journal of metamorphic Geology* **20**, 41-55.

WHITE R., POWELL R. & HOLLAND T. 2007. Progress relating to calculation of partial melting equilibria for metapelites. *Journal of Metamorphic Geology* **25**, 511-527.

WHITE R., POWELL R., HOLLAND T., JOHNSON T. & GREEN E. 2014a. New mineral activity–composition relations for thermodynamic calculations in metapelitic systems. *Journal of Metamorphic Geology* **32**, 261-286.

WHITE R., POWELL R. & JOHNSON T. 2014b. The effect of Mn on mineral stability in metapelites revisited: new a–x relations for manganese-bearing minerals. *Journal of Metamorphic Geology* **32**, 809-828.

YAKYMCHUK C. & BROWN M. 2014. Behaviour of zircon and monazite during crustal melting. *Journal of the Geological Society* **171**, 465-479.

ZIRKLER A., JOHNSON T., WHITE R. & ZACK T. 2012. Polymetamorphism in the mainland Lewisian complex, NW Scotland–phase equilibria and geochronological constraints from the Cnoc an t'Sidhean suite. *Journal of Metamorphic Geology* **30**, 865-885.

ZWART H. 1962. On the determination of polymetamorphic mineral associations, and its application to the Bosost area (Central Pyrenees). *Geologische Rundschau* **52**, 38-65.

APPENDIX A: LA–ICP–MS MONAZITE U–PB GEOCHRONOLOGY STANDARD ANALYSES

Set	Analysis	207Pb/ 206Pb	1σ	206Pb/ 238U	1σ	207Pb/ 235U	1σ	% Conc.	207Pb/ 206Pb age (Ma)	1σ	206Pb/ 238U age (Ma)	1σ	207Pb/ 235U age (Ma)	1σ	204Pb/ 206Pb (%)	Rho (ρ)
757	STDMAD01	0.056	0.0007	0.083	0.0011	0.645	0.0094	111	463.40	27.95	514.80	6.42	505.50	5.80	0.017	0.5870
757	STDMAD02	0.057	0.0007	0.082	0.0011	0.641	0.0093	106	480.50	27.04	507.80	6.43	502.90	5.74	0.012	0.6163
757	STDMAD03	0.057	0.0007	0.086	0.0011	0.680	0.0099	106	500.80	26.98	532.80	6.75	526.80	5.98	0.000	0.6160
757	22201	0.055	0.0007	0.073	0.0010	0.560	0.0082	107	427.40	27.70	456.30	5.73	451.50	5.31	0.000	0.5837
757	22202	0.056	0.0007	0.071	0.0009	0.552	0.0081	98	454.50	27.46	444.80	5.59	446.30	5.29	0.000	0.5860
757	22203	0.055	0.0007	0.071	0.0009	0.538	0.0079	106	417.20	27.63	441.30	5.57	437.30	5.20	0.002	0.5952
757	22204	0.056	0.0008	0.075	0.0010	0.581	0.0093	102	457.80	30.58	466.40	6.07	464.80	6.00	0.000	0.5581
757	22205	0.055	0.0008	0.071	0.0010	0.546	0.0087	103	430.70	29.95	444.60	5.77	442.20	5.69	0.016	0.5744
757	22206	0.056	0.0008	0.071	0.0010	0.549	0.0090	97	456.40	31.18	442.20	5.79	444.30	5.89	0.006	0.5587
757	STDMAD04	0.055	0.0008	0.086	0.0012	0.659	0.0108	123	431.90	30.33	533.10	7.06	514.10	6.58	0.000	0.5756
757	STDMAD05	0.057	0.0008	0.082	0.0011	0.647	0.0106	102	497.40	30.90	509.00	6.78	506.70	6.56	0.000	0.5852
757	STDMAD06	0.057	0.0008	0.081	0.0011	0.638	0.0106	104	486.80	31.34	504.20	6.74	500.90	6.55	0.000	0.5749
757	STDMAD07	0.057	0.0009	0.088	0.0012	0.691	0.0125	111	491.50	35.76	543.20	7.25	533.30	7.52	0.000	0.5075
784-1	STDMAD-01	0.058	0.0007	0.087	0.0013	0.694	0.0114	106	511.60	26.97	540.70	7.88	534.90	6.85	0.006	0.6907
784-1	STDMAD-02	0.058	0.0007	0.086	0.0013	0.679	0.0109	103	512.80	25.68	529.20	7.68	526.00	6.59	0.013	0.7050
784-1	STDMAD-03	0.057	0.0007	0.084	0.0013	0.658	0.0106	110	474.90	26.26	522.10	7.58	513.30	6.46	0.000	0.7134
784-1	STDMAD-04	0.057	0.0006	0.082	0.0013	0.647	0.0101	105	488.10	23.85	510.50	7.54	506.40	6.22	0.010	0.7613
784-1	STDMAD-05	0.057	0.0006	0.085	0.0013	0.666	0.0104	107	490.10	23.88	524.60	7.75	518.10	6.35	0.011	0.7612
784-1	STDMAD-06	0.057	0.0006	0.084	0.0013	0.659	0.0103	106	492.20	23.91	519.30	7.69	514.20	6.32	0.006	0.7549
784-1	222-01	0.057	0.0007	0.076	0.0012	0.592	0.0094	98	478.20	25.64	470.80	6.91	472.00	6.02	0.005	0.7211
784-1	222-02	0.056	0.0007	0.075	0.0011	0.579	0.0093	102	457.70	25.24	465.40	6.82	464.00	5.95	0.020	0.7255
784-1	222-03	0.056	0.0007	0.074	0.0011	0.570	0.0091	102	451.20	25.36	459.80	6.75	458.30	5.91	0.000	0.7235
784-1	222-04	0.056	0.0007	0.072	0.0011	0.561	0.0090	98	458.30	25.09	450.90	6.64	452.00	5.83	0.000	0.7269
784-1	222-05	0.056	0.0007	0.072	0.0011	0.551	0.0089	101	441.10	25.81	446.70	6.61	445.70	5.85	0.000	0.7196
784-1	STDMAD-07	0.057	0.0006	0.084	0.0013	0.657	0.0105	105	494.40	24.27	517.10	7.74	512.80	6.41	0.007	0.7545

Set	Analysis	207Pb/ 206Pb	1σ	206Pb/ 238U	1σ	207Pb/ 235U	1σ	% Conc.	207Pb/ 206Pb age (Ma)	1σ	206Pb/ 238U age (Ma)	1σ	207Pb/ 235U age (Ma)	1σ	204Pb/ 206Pb (%)	Rho (ρ)
784-1	222-06	0.056	0.0007	0.073	0.0011	0.565	0.0092	97	466.20	25.91	452.90	6.79	455.10	5.98	0.002	0.7308
784-1	222-07	0.057	0.0007	0.072	0.0011	0.566	0.0093	94	480.60	26.19	450.70	6.76	455.60	6.02	0.000	0.7266
784-1	222-08	0.056	0.0007	0.074	0.0012	0.570	0.0095	100	457.30	26.44	458.10	6.89	457.80	6.13	0.002	0.7192
784-1	222-09	0.057	0.0007	0.074	0.0012	0.583	0.0100	92	498.30	28.23	460.20	6.97	466.50	6.41	0.019	0.7006
784-1	222-10	0.056	0.0007	0.074	0.0012	0.575	0.0099	101	457.40	28.57	461.90	6.99	461.00	6.41	0.000	0.6856
784-1	STDMAD-08	0.057	0.0006	0.085	0.0014	0.665	0.0108	110	478.90	24.26	526.80	8.04	517.80	6.58	0.011	0.7677
784-1	STDMAD-09	0.056	0.0006	0.087	0.0014	0.676	0.0110	114	469.70	24.25	537.30	8.21	524.50	6.65	0.008	0.7664
784-1	STDMAD-10	0.057	0.0006	0.083	0.0013	0.651	0.0106	106	484.30	24.45	514.50	7.89	508.90	6.53	0.000	0.7650
784-1	STDMAD-11	0.057	0.0007	0.082	0.0013	0.646	0.0110	104	491.00	27.38	509.10	7.75	505.70	6.76	0.024	0.7217
784-1	STDMAD-12	0.057	0.0006	0.085	0.0014	0.670	0.0110	108	488.90	24.61	528.30	8.12	520.90	6.69	0.000	0.7678
784-1	STDMAD-13	0.057	0.0006	0.083	0.0013	0.652	0.0107	104	493.90	24.64	513.30	7.91	509.60	6.59	0.012	0.7693
784-2	STDMAD-1	0.057	0.0007	0.094	0.0013	0.733	0.0107	120	481.80	25.43	577.00	7.65	558.00	6.26	0.008	0.6777
784-2	STDMAD-2	0.057	0.0006	0.083	0.0012	0.654	0.0092	107	484.80	24.04	516.70	6.83	510.70	5.65	0.012	0.6935
784-2	STDMAD-3	0.057	0.0007	0.083	0.0012	0.653	0.0095	103	497.00	25.35	513.70	6.83	510.50	5.83	0.000	0.6800
784-2	STDMAD-4	0.057	0.0007	0.086	0.0012	0.678	0.0099	108	494.70	25.38	532.80	7.08	525.60	5.97	0.014	0.6787
784-2	STDMAD-5	0.057	0.0006	0.084	0.0012	0.657	0.0094	106	489.60	24.77	518.10	6.89	512.70	5.78	0.000	0.6839
784-2	STDMAD-6	0.057	0.0006	0.083	0.0012	0.653	0.0094	104	494.70	24.67	514.20	6.84	510.50	5.75	0.015	0.6841
784-2	222-1	0.056	0.0007	0.072	0.0010	0.555	0.0083	102	439.90	25.91	450.00	6.03	448.10	5.41	0.019	0.6523
784-2	222-2	0.056	0.0006	0.071	0.0010	0.542	0.0078	99	444.10	24.50	439.40	5.89	440.00	5.16	0.000	0.6834
784-2	222-3	0.056	0.0006	0.071	0.0010	0.544	0.0079	99	445.50	24.93	440.20	5.90	440.90	5.22	0.014	0.6769
784-2	222-4	0.056	0.0006	0.070	0.0010	0.538	0.0078	96	450.80	24.73	434.50	5.81	437.00	5.15	0.006	0.6740
784-2	222-5	0.056	0.0007	0.068	0.0009	0.524	0.0078	97	439.30	25.93	425.50	5.69	427.60	5.18	0.004	0.6486
784-2	STDMAD-07	0.065	0.0007	0.091	0.0013	0.818	0.0117	72	782.90	23.25	560.90	7.44	606.70	6.54	0.071	0.6854
784-2	STDMAD-08	0.057	0.0007	0.083	0.0012	0.649	0.0094	107	479.50	25.40	514.40	6.82	508.00	5.79	0.025	0.6737
784-2	222-6	0.056	0.0007	0.072	0.0010	0.556	0.0083	101	445.20	26.32	449.90	6.01	449.00	5.42	0.000	0.6442

Set	Analysis	207Pb/ 206Pb	1σ	206Pb/ 238U	1σ	207Pb/ 235U	1σ	% Conc.	207Pb/ 206Pb age (Ma)	1σ	206Pb/ 238U age (Ma)	1σ	207Pb/ 235U age (Ma)	1σ	204Pb/ 206Pb (%)	Rho (ρ)
784-2	222-7	0.056	0.0008	0.071	0.0010	0.549	0.0088	100	444.40	29.25	444.50	6.01	444.30	5.76	0.000	0.6064
784-2	222-8	0.056	0.0008	0.070	0.0010	0.547	0.0087	94	465.20	29.60	438.80	5.94	443.00	5.73	0.013	0.6138
784-2	STDMAD-09	0.057	0.0007	0.084	0.0012	0.657	0.0095	105	492.60	25.09	517.50	6.85	512.80	5.79	0.000	0.6729
784-2	STDMAD-10	0.057	0.0007	0.084	0.0012	0.656	0.0095	108	482.30	25.59	518.70	6.85	511.90	5.83	0.003	0.6618
784-2	STDMAD-11	0.057	0.0006	0.083	0.0012	0.653	0.0092	103	500.00	24.32	512.50	6.82	510.00	5.67	0.012	0.6920
784-2	STDMAD-12	0.057	0.0007	0.083	0.0012	0.654	0.0097	105	489.90	26.18	515.70	6.88	510.80	5.95	0.000	0.6673
784-2	STDMAD-13	0.057	0.0007	0.085	0.0012	0.664	0.0097	110	478.80	26.22	525.70	6.94	516.90	5.95	0.003	0.6564
784-3	STDMAD-09	0.057	0.0006	0.083	0.0011	0.647	0.0092	105	485.00	25.07	511.60	6.66	506.60	5.65	0.000	0.6713
784-3	STDMAD-10	0.057	0.0007	0.083	0.0011	0.654	0.0094	105	492.70	25.50	515.40	6.77	511.00	5.78	0.005	0.6620
784-3	STDMAD-11	0.057	0.0006	0.082	0.0011	0.643	0.0089	104	488.50	23.59	507.80	6.71	504.10	5.48	0.011	0.6984
784-3	STDMAD-12	0.056	0.0006	0.083	0.0011	0.645	0.0090	110	466.10	23.99	514.00	6.75	505.10	5.56	0.002	0.6927
784-3	STDMAD-13	0.057	0.0006	0.085	0.0012	0.661	0.0094	110	477.80	24.77	524.10	6.87	515.40	5.73	0.002	0.6825
784-3	222-9	0.056	0.0006	0.074	0.0010	0.566	0.0079	103	443.50	24.73	458.00	5.90	455.50	5.13	0.006	0.6472
784-3	222-10	0.056	0.0006	0.074	0.0010	0.566	0.0079	104	439.10	24.11	458.80	6.00	455.40	5.14	0.017	0.6741
784-3	222-11	0.056	0.0007	0.073	0.0010	0.562	0.0086	100	451.80	27.24	453.30	6.10	452.90	5.60	0.003	0.6396
784-3	222-12	0.056	0.0006	0.070	0.0010	0.535	0.0075	99	438.10	23.92	434.90	5.70	435.30	4.95	0.012	0.6845
784-3	222-13	0.056	0.0007	0.071	0.0010	0.551	0.0081	98	453.60	25.43	444.20	5.91	445.50	5.27	0.007	0.6565
784-3	STDMAD-14	0.057	0.0007	0.087	0.0012	0.675	0.0097	114	471.20	25.39	535.90	7.02	523.60	5.87	0.000	0.6625
784-3	222-14	0.056	0.0008	0.073	0.0010	0.563	0.0091	97	463.20	30.38	451.60	6.09	453.40	5.90	0.035	0.5942
784-3	222-15	0.056	0.0007	0.070	0.0010	0.534	0.0078	99	439.00	25.38	433.70	5.78	434.40	5.17	0.013	0.6635
784-3	222-16	0.056	0.0007	0.068	0.0010	0.525	0.0080	97	439.90	26.89	426.80	5.75	428.70	5.31	0.018	0.6400
784-3	STDMAD-15	0.058	0.0007	0.090	0.0012	0.722	0.0106	102	544.50	25.46	554.30	7.33	552.10	6.23	0.014	0.6561
784-3	STDMAD-16	0.059	0.0007	0.084	0.0012	0.685	0.0102	93	562.80	25.99	522.40	6.97	529.80	6.15	0.037	0.6507
784-3	STDMAD-17	0.059	0.0007	0.084	0.0012	0.687	0.0103	92	569.50	25.55	522.50	6.98	531.10	6.18	0.025	0.6536
784-3	STDMAD-18	0.056	0.0007	0.091	0.0013	0.705	0.0104	122	459.50	26.36	561.80	7.43	541.90	6.19	0.000	0.6538

Set	Analysis	207Pb/ 206Pb	1σ	206Pb/ 238U	1σ	207Pb/ 235U	1σ	% Conc.	207Pb/ 206Pb age (Ma)	1σ	206Pb/ 238U age (Ma)	1σ	207Pb/ 235U age (Ma)	1σ	204Pb/ 206Pb (%)	Rho (ρ)
784-3	STDMAD-19	0.057	0.0007	0.083	0.0012	0.655	0.0096	103	501.20	25.80	513.80	6.84	511.40	5.90	0.000	0.6652
784-3	STDMAD-20	0.057	0.0007	0.082	0.0011	0.642	0.0095	104	486.20	26.26	507.40	6.77	503.50	5.87	0.000	0.6646
784-4	STDMAD-01	0.057	0.0006	0.085	0.0012	0.664	0.0095	110	479.50	24.88	525.80	6.96	517.20	5.78	0.000	0.6766
784-4	STDMAD-02	0.057	0.0006	0.084	0.0012	0.655	0.0093	109	478.10	23.99	519.30	6.92	511.70	5.69	0.000	0.7044
784-4	STDMAD-03	0.057	0.0007	0.084	0.0012	0.664	0.0098	106	492.70	26.57	522.90	6.93	517.20	5.97	0.000	0.6534
784-4	STDMAD-04	0.057	0.0008	0.083	0.0012	0.645	0.0105	107	476.20	30.89	511.80	6.86	505.30	6.48	0.000	0.5823
784-4	STDMAD-05	0.057	0.0006	0.083	0.0012	0.655	0.0094	105	493.00	24.47	515.70	6.88	511.40	5.76	0.000	0.6948
784-4	222-01	0.057	0.0007	0.074	0.0010	0.581	0.0084	96	481.30	25.55	461.50	6.11	464.80	5.37	0.000	0.6696
784-4	222-02	0.056	0.0006	0.073	0.0010	0.561	0.0081	99	457.60	24.79	451.60	5.97	452.50	5.24	0.010	0.6690
784-4	222-03	0.056	0.0006	0.074	0.0010	0.571	0.0080	104	442.40	23.35	461.70	6.09	458.30	5.15	0.000	0.6981
784-4	222-04	0.056	0.0007	0.071	0.0010	0.553	0.0084	97	460.40	27.57	444.80	5.92	447.30	5.47	0.000	0.6311
784-4	222-05	0.056	0.0006	0.073	0.0010	0.562	0.0079	99	456.10	23.58	452.40	6.01	452.90	5.15	0.000	0.6957
784-4	STDMAD-06	0.057	0.0007	0.084	0.0012	0.661	0.0096	105	495.90	25.23	519.70	6.92	515.20	5.88	0.031	0.6791
784-4	222-06	0.057	0.0007	0.078	0.0011	0.608	0.0086	100	482.10	25.34	482.70	6.27	482.50	5.46	0.016	0.6595
784-4	222-07	0.056	0.0006	0.074	0.0010	0.568	0.0079	103	446.30	23.55	458.70	6.00	456.50	5.11	0.000	0.6843
784-4	222-08	0.057	0.0007	0.072	0.0010	0.559	0.0082	93	478.40	26.23	445.90	5.91	451.20	5.36	0.008	0.6556
784-4	222-09	0.056	0.0009	0.077	0.0011	0.596	0.0105	104	458.90	35.30	478.20	6.43	474.70	6.69	0.000	0.5051
784-4	STDMAD-07	0.057	0.0006	0.086	0.0012	0.673	0.0096	107	492.40	24.99	529.30	6.90	522.40	5.80	0.019	0.6740
784-4	STDMAD-08	0.057	0.0007	0.084	0.0011	0.661	0.0095	106	491.70	25.57	520.80	6.80	515.30	5.81	0.000	0.6580
784-4	STDMAD-09	0.057	0.0007	0.088	0.0012	0.693	0.0100	111	491.20	26.34	545.20	7.03	534.70	6.01	0.040	0.6374
784-4	STDMAD-10	0.057	0.0007	0.084	0.0011	0.661	0.0096	106	491.30	26.90	521.00	6.72	515.40	5.89	0.000	0.6291
784-4	STDMAD-11	0.057	0.0008	0.082	0.0011	0.648	0.0099	102	497.70	28.80	509.40	6.61	507.20	6.10	0.000	0.5905
784-5	STDMAD-12	0.057	0.0007	0.103	0.0014	0.805	0.0115	129	487.70	25.89	629.30	8.05	599.40	6.46	0.096	0.6409
784-5	STDMAD-13	0.057	0.0006	0.091	0.0012	0.711	0.0097	118	475.60	23.81	562.20	7.27	545.30	5.77	0.000	0.6858
784-5	STDMAD-14	0.057	0.0006	0.086	0.0012	0.674	0.0093	108	489.70	23.91	530.90	6.92	523.10	5.66	0.000	0.6963

Set	Analysis	207Pb/ 206Pb	1σ	206Pb/ 238U	1σ	207Pb/ 235U	1σ	% Conc.	207Pb/ 206Pb age (Ma)	1σ	206Pb/ 238U age (Ma)	1σ	207Pb/ 235U age (Ma)	1σ	204Pb/ 206Pb (%)	Rho (ρ)
784-5	STDMAD-15	0.057	0.0006	0.084	0.0011	0.661	0.0092	104	500.70	23.91	518.60	6.79	515.20	5.62	0.000	0.6907
784-5	STDMAD-16	0.057	0.0006	0.083	0.0011	0.647	0.0090	107	480.60	24.20	512.40	6.70	506.50	5.57	0.000	0.6872
784-5	STDMAD-17	0.057	0.0006	0.082	0.0011	0.644	0.0090	103	491.80	23.99	507.70	6.66	504.80	5.53	0.014	0.6893
784-5	STDMAD-18	0.057	0.0006	0.091	0.0012	0.713	0.0099	117	479.40	23.89	562.60	7.35	546.30	5.88	0.000	0.6942
784-5	222-10	0.056	0.0007	0.072	0.0010	0.557	0.0085	99	452.60	27.79	448.80	5.91	449.30	5.51	0.000	0.6058
784-5	222-11	0.056	0.0009	0.071	0.0010	0.545	0.0094	98	449.00	33.31	440.00	5.94	441.40	6.16	0.000	0.5308
784-5	222-12	0.056	0.0007	0.072	0.0010	0.551	0.0082	100	447.40	26.73	445.30	5.90	445.50	5.40	0.000	0.6320
784-5	222-13	0.056	0.0007	0.074	0.0010	0.575	0.0085	99	466.80	27.12	459.90	6.05	461.00	5.51	0.000	0.6346
784-5	222-14	0.056	0.0006	0.071	0.0010	0.543	0.0074	100	441.40	22.96	440.20	5.76	440.30	4.89	0.000	0.6987
784-5	STDMAD-19	0.057	0.0006	0.084	0.0012	0.657	0.0094	106	489.80	24.47	518.30	6.86	512.90	5.73	0.028	0.6877
784-5	222-15	0.056	0.0006	0.078	0.0011	0.594	0.0085	111	435.30	24.01	481.50	6.38	473.40	5.38	0.000	0.6834
784-5	222-16	0.056	0.0006	0.076	0.0011	0.585	0.0083	106	446.30	23.74	471.90	6.29	467.50	5.33	0.000	0.6972
784-5	222-17	0.055	0.0006	0.074	0.0010	0.565	0.0082	108	426.40	24.42	460.60	6.21	454.70	5.30	0.000	0.6989
784-5	STDMAD-20	0.057	0.0007	0.087	0.0012	0.682	0.0099	107	498.10	25.30	535.10	7.13	528.00	5.99	0.033	0.6808
784-5	STDMAD-21	0.057	0.0006	0.085	0.0012	0.661	0.0096	110	477.30	24.93	523.60	7.04	515.00	5.90	0.000	0.6898
784-5	STDMAD-22	0.057	0.0007	0.084	0.0012	0.655	0.0097	106	487.40	25.61	517.30	6.99	511.70	5.97	0.040	0.6783
784-5	STDMAD-23	0.057	0.0007	0.083	0.0012	0.648	0.0100	106	483.20	27.85	513.10	6.90	507.50	6.13	0.000	0.6410
784-5	STDMAD-24	0.057	0.0007	0.082	0.0012	0.644	0.0100	106	480.10	27.32	510.20	6.98	504.70	6.17	0.006	0.6584
980	STDMAD-01	0.057	0.0007	0.091	0.0014	0.711	0.0116	119	473.20	26.45	563.20	8.37	545.60	6.91	0.000	0.7171
980	STDMAD-02	0.057	0.0006	0.088	0.0014	0.694	0.0110	109	499.60	23.53	544.00	8.17	535.30	6.58	0.000	0.7708
980	STDMAD-03	0.057	0.0006	0.084	0.0013	0.663	0.0105	104	501.20	23.56	519.90	7.83	516.30	6.41	0.004	0.7721
980	STDMAD-04	0.057	0.0006	0.084	0.0013	0.654	0.0103	109	475.70	23.53	519.00	7.81	510.90	6.35	0.000	0.7727
980	STDMAD-05	0.057	0.0006	0.082	0.0013	0.652	0.0103	101	507.20	23.16	510.60	7.69	509.80	6.34	0.000	0.7720
980	STDMAD-06	0.057	0.0006	0.088	0.0014	0.697	0.0110	109	500.60	23.48	546.10	8.20	537.20	6.60	0.000	0.7702
980	STDMAD-07	0.057	0.0006	0.086	0.0013	0.669	0.0106	111	477.00	23.59	530.10	7.97	520.10	6.45	0.004	0.7736
980	222-01	0.055	0.0006	0.074	0.0011	0.564	0.0089	107	429.10	23.87	459.00	6.86	453.90	5.75	0.003	0.7588

Set	Analysis	207Pb/ 206Pb	1σ	206Pb/ 238U	1σ	207Pb/ 235U	1σ	% Conc.	207Pb/ 206Pb age (Ma)	1σ	206Pb/ 238U age (Ma)	1σ	207Pb/ 235U age (Ma)	1σ	204Pb/ 206Pb (%)	Rho (ρ)
980	222-02	0.056	0.0006	0.072	0.0011	0.555	0.0087	100	447.20	23.28	448.90	6.70	448.50	5.67	0.000	0.7608
980	222-03	0.055	0.0006	0.071	0.0011	0.543	0.0084	103	431.10	23.21	442.60	6.62	440.60	5.54	0.004	0.7724
980	222-04	0.056	0.0006	0.071	0.0011	0.545	0.0085	101	440.00	23.35	442.40	6.60	441.80	5.61	0.000	0.7606
980	222-05	0.056	0.0006	0.072	0.0011	0.557	0.0087	100	450.80	22.33	449.40	6.79	449.50	5.68	0.000	0.7807
980	STDMAD-08	0.057	0.0006	0.082	0.0013	0.645	0.0103	104	488.90	23.87	509.40	7.68	505.60	6.34	0.017	0.7706
980	222-06	0.056	0.0006	0.071	0.0011	0.547	0.0087	101	439.90	24.19	444.00	6.63	443.20	5.70	0.000	0.7475
980	222-07	0.056	0.0006	0.070	0.0011	0.539	0.0086	97	449.40	24.20	435.60	6.51	437.80	5.65	0.000	0.7499
980	222-08	0.055	0.0006	0.070	0.0011	0.537	0.0086	102	428.00	24.77	438.00	6.55	436.30	5.65	0.000	0.7468
980	STDMAD-09	0.063	0.0008	0.085	0.0013	0.740	0.0121	72	723.90	24.91	523.50	7.81	562.40	7.04	0.057	0.7247
980	STDMAD-10	0.057	0.0006	0.086	0.0014	0.675	0.0109	105	502.40	24.19	529.00	7.99	524.00	6.59	0.005	0.7625
980	STDMAD-11	0.070	0.0008	0.085	0.0013	0.820	0.0131	58	917.50	22.15	528.40	7.98	607.90	7.32	0.080	0.7632
980	STDMAD-12	0.057	0.0006	0.086	0.0014	0.681	0.0110	105	506.50	23.95	532.60	8.04	527.60	6.61	0.003	0.7612
980	STDMAD-13	0.057	0.0006	0.083	0.0013	0.655	0.0106	104	497.10	24.45	514.70	7.78	511.40	6.47	0.000	0.7611
980	STDMAD-14	0.057	0.0006	0.083	0.0013	0.646	0.0104	106	481.10	24.49	511.80	7.75	506.20	6.44	0.000	0.7579
980	STDMAD-15	0.057	0.0006	0.084	0.0013	0.661	0.0107	107	486.10	24.59	521.70	7.90	515.00	6.54	0.000	0.7603
980-2	STDMAD-20	0.057	0.0007	0.086	0.0012	0.682	0.0100	106	505.30	25.60	533.30	7.09	528.00	6.05	0.037	0.6660
980-2	STDMAD-21	0.057	0.0006	0.084	0.0012	0.661	0.0094	109	480.80	24.02	522.70	7.00	514.90	5.76	0.000	0.7006
980-2	STDMAD-22	0.057	0.0006	0.083	0.0012	0.651	0.0093	105	490.20	24.07	513.40	6.89	509.10	5.72	0.030	0.7044
980-2	STDMAD-23	0.057	0.0006	0.082	0.0011	0.648	0.0094	103	493.70	24.95	510.60	6.80	507.50	5.77	0.000	0.6864
980-2	STDMAD-24	0.057	0.0006	0.082	0.0012	0.640	0.0093	105	481.00	24.50	507.30	6.82	502.50	5.74	0.000	0.6975
980-2	STDMAD-25	0.058	0.0007	0.092	0.0013	0.735	0.0108	109	521.50	25.82	569.00	7.55	559.40	6.32	0.000	0.6625
980-2	222-01	0.057	0.0007	0.074	0.0010	0.579	0.0084	98	472.10	25.29	462.10	6.17	463.70	5.41	0.000	0.6727
980-2	222-02	0.056	0.0007	0.075	0.0011	0.586	0.0088	100	466.60	26.88	468.40	6.31	468.00	5.63	0.022	0.6447
980-2	222-03	0.056	0.0007	0.072	0.0010	0.556	0.0083	98	455.60	26.03	448.00	6.02	449.10	5.42	0.012	0.6594
980-2	222-04	0.057	0.0007	0.073	0.0011	0.576	0.0093	92	495.20	28.49	455.20	6.39	461.80	5.97	0.024	0.6455

Set	Analysis	207Pb/ 206Pb	1σ	206Pb/ 238U	1σ	207Pb/ 235U	1σ	% Conc.	207Pb/ 206Pb age (Ma)	1σ	206Pb/ 238U age (Ma)	1σ	207Pb/ 235U age (Ma)	1σ	204Pb/ 206Pb (%)	Rho (ρ)
980-2	222-05	0.057	0.0007	0.075	0.0011	0.584	0.0094	95	485.40	28.91	463.40	6.48	467.10	6.05	0.000	0.6443
980-2	STDMAD-26	0.058	0.0007	0.091	0.0013	0.722	0.0109	109	514.90	25.24	561.10	7.61	551.90	6.41	0.036	0.6756
980-2	STDMAD-27	0.057	0.0006	0.093	0.0013	0.736	0.0107	112	509.60	24.12	572.70	7.69	560.10	6.26	0.007	0.6960
980-2	222-06	0.056	0.0008	0.077	0.0011	0.592	0.0096	106	449.20	29.81	476.80	6.48	472.00	6.15	0.006	0.5973
980-2	222-07	0.056	0.0006	0.078	0.0011	0.601	0.0087	109	443.70	24.31	485.10	6.50	477.70	5.52	0.000	0.6854
980-2	222-08	0.056	0.0009	0.075	0.0011	0.584	0.0108	100	467.00	36.38	466.70	6.45	466.70	6.89	0.000	0.5175
980-2	STDMAD-28	0.057	0.0007	0.085	0.0012	0.669	0.0106	108	488.10	28.13	527.40	7.28	520.00	6.45	0.015	0.6551
980-2	STDMAD-29	0.057	0.0007	0.084	0.0012	0.662	0.0098	105	493.80	25.50	520.90	7.06	515.80	6.01	0.008	0.6831
980-2	STDMAD-30	0.057	0.0007	0.084	0.0012	0.658	0.0098	104	497.30	25.58	517.20	7.01	513.40	6.00	0.004	0.6846
980-2	STDMAD-31	0.057	0.0007	0.083	0.0012	0.655	0.0100	105	492.50	27.26	515.80	6.92	511.40	6.13	0.000	0.6498
980-2	STDMAD-32	0.057	0.0008	0.083	0.0012	0.653	0.0104	105	491.50	29.07	514.50	6.97	510.10	6.39	0.000	0.6216
RB02-1	STDMAD-01	0.057	0.0008	0.082	0.0010	0.651	0.0095	102	500.30	29.72	510.90	5.98	508.80	5.87	0.000	0.4960
RB02-1	STDMAD-02	0.057	0.0008	0.083	0.0010	0.653	0.0096	104	496.00	29.83	513.90	6.02	510.40	5.88	0.000	0.5080
RB02-1	STDMAD-03	0.057	0.0008	0.084	0.0010	0.663	0.0097	105	497.30	29.52	521.30	6.10	516.60	5.90	0.017	0.5058
RB02-1	STDMAD-04	0.057	0.0007	0.084	0.0010	0.654	0.0091	108	479.30	27.41	518.10	6.12	510.80	5.59	0.014	0.5627
RB02-1	STDMAD-05	0.057	0.0010	0.082	0.0011	0.641	0.0114	105	484.60	37.29	506.90	6.29	502.70	7.03	0.003	0.4289
RB02-1	222-01	0.056	0.0007	0.073	0.0009	0.564	0.0079	100	453.30	27.03	454.90	5.41	454.40	5.12	0.000	0.5545
RB02-1	222-02	0.057	0.0009	0.073	0.0009	0.565	0.0090	96	471.50	33.29	451.70	5.41	454.80	5.85	0.006	0.4603
RB02-1	222-03	0.056	0.0013	0.070	0.0010	0.539	0.0129	99	440.20	52.48	437.60	5.80	437.80	8.50	0.016	0.2751
RB02-1	222-04	0.057	0.0009	0.074	0.0009	0.576	0.0094	96	476.60	33.91	459.00	5.54	461.80	6.04	0.021	0.4538
RB02-1	222-05	0.056	0.0008	0.071	0.0009	0.547	0.0082	98	451.40	29.91	441.90	5.26	443.20	5.36	0.000	0.5026
RB02-1	STDMAD-06	0.057	0.0007	0.087	0.0011	0.681	0.0097	113	476.20	27.95	539.50	6.45	527.40	5.86	0.014	0.5541
RB02-1	STDMAD-07	0.057	0.0007	0.087	0.0011	0.678	0.0096	113	476.40	27.84	537.10	6.43	525.50	5.83	0.000	0.5645
RB02-1	222-06	0.055	0.0007	0.077	0.0010	0.585	0.0086	112	426.10	29.11	476.00	5.71	467.40	5.48	0.000	0.5348
RB02-1	222-07	0.056	0.0007	0.075	0.0010	0.580	0.0085	102	458.60	28.84	465.90	5.68	464.50	5.49	0.025	0.5588

Set	Analysis	207Pb/ 206Pb	1σ	206Pb/ 238U	1σ	207Pb/ 235U	1σ	% Conc.	207Pb/ 206Pb age (Ma)	1σ	206Pb/ 238U age (Ma)	1σ	207Pb/ 235U age (Ma)	1σ	204Pb/ 206Pb (%)	Rho (ρ)
RB02-1	222-08	0.057	0.0008	0.074	0.0009	0.577	0.0087	97	474.00	30.38	460.60	5.57	462.70	5.61	0.022	0.5152
RB02-1	STDMAD-08	0.057	0.0010	0.084	0.0011	0.662	0.0118	107	489.50	37.60	522.20	6.47	516.00	7.23	0.009	0.4254
RB02-1	STDMAD-09	0.056	0.0008	0.084	0.0011	0.651	0.0098	111	468.70	29.58	518.50	6.35	509.30	6.03	0.000	0.5423
RB02-1	STDMAD-10	0.057	0.0008	0.084	0.0011	0.657	0.0100	107	486.80	29.89	518.80	6.38	512.80	6.11	0.000	0.5430
RB02-1	STDMAD-11	0.057	0.0008	0.082	0.0010	0.646	0.0101	102	498.90	31.16	507.90	6.18	506.10	6.20	0.012	0.5136
RB02-1	STDMAD-12	0.057	0.0008	0.082	0.0011	0.641	0.0098	104	485.60	30.01	507.00	6.26	503.10	6.06	0.003	0.5471
RB02-2	STDMAD-01	0.058	0.0007	0.092	0.0012	0.732	0.0105	110	514.80	25.22	568.30	7.31	557.60	6.16	0.000	0.6416
RB02-2	STDMAD-02	0.057	0.0006	0.085	0.0012	0.667	0.0094	109	485.50	24.92	526.90	6.82	519.00	5.75	0.041	0.6695
RB02-2	STDMAD-03	0.057	0.0007	0.084	0.0011	0.652	0.0096	109	476.10	26.91	517.30	6.69	509.70	5.90	0.000	0.6277
RB02-2	STDMAD-04	0.057	0.0007	0.083	0.0011	0.651	0.0095	103	498.00	26.38	512.00	6.62	509.30	5.82	0.007	0.6405
RB02-2	STDMAD-05	0.059	0.0007	0.083	0.0011	0.672	0.0097	91	560.80	25.16	513.10	6.71	521.70	5.91	0.000	0.6637
RB02-2	STDMAD-06	0.058	0.0006	0.092	0.0012	0.731	0.0102	110	516.80	23.88	567.00	7.26	556.90	5.96	0.000	0.6696
RB02-2	STDMAD-07	0.057	0.0006	0.086	0.0012	0.678	0.0094	109	487.90	24.10	534.20	6.94	525.40	5.71	0.038	0.6859
RB02-2	222-01	0.056	0.0006	0.080	0.0011	0.622	0.0086	106	468.20	24.66	496.40	6.37	491.40	5.37	0.000	0.6625
RB02-2	222-02	0.056	0.0006	0.074	0.0010	0.572	0.0078	98	465.10	23.38	458.00	5.98	459.00	5.07	0.000	0.6957
RB02-2	222-03	0.056	0.0006	0.072	0.0010	0.550	0.0077	101	441.70	23.72	446.20	5.87	445.30	5.06	0.034	0.6886
RB02-2	222-04	0.056	0.0007	0.070	0.0010	0.543	0.0079	98	448.00	25.17	439.10	5.80	440.40	5.20	0.000	0.6610
RB02-2	222-05	0.056	0.0006	0.071	0.0010	0.548	0.0079	99	447.50	24.17	442.80	5.93	443.40	5.17	0.010	0.6934
RB02-2	STDMAD-08	0.057	0.0006	0.082	0.0011	0.648	0.0091	101	505.40	24.16	508.10	6.62	507.40	5.61	0.057	0.6837
RB02-2	STDMAD-09	0.057	0.0006	0.082	0.0011	0.644	0.0091	103	492.90	24.53	507.90	6.62	505.10	5.60	0.032	0.6808
RB02-2	222-06	0.056	0.0006	0.070	0.0010	0.543	0.0075	97	452.70	23.49	438.30	5.72	440.50	4.94	0.022	0.6828
RB02-2	222-07	0.056	0.0006	0.071	0.0010	0.551	0.0077	99	448.60	24.21	444.90	5.75	445.40	5.02	0.000	0.6717
RB02-2	222-08	0.057	0.0006	0.071	0.0010	0.554	0.0078	93	477.00	24.57	441.70	5.79	447.30	5.10	0.041	0.6765
RB02-2	STDMAD-10	0.057	0.0007	0.091	0.0012	0.713	0.0106	114	490.00	27.98	560.10	7.18	546.40	6.27	0.000	0.6023
RB02-2	STDMAD-11	0.057	0.0007	0.083	0.0011	0.655	0.0094	105	491.70	25.55	516.10	6.75	511.50	5.78	0.000	0.6586

Set	Analysis	207Pb/ 206Pb	1σ	206Pb/ 238U	1σ	207Pb/ 235U	1σ	% Conc.	207Pb/ 206Pb age (Ma)	1σ	206Pb/ 238U age (Ma)	1σ	207Pb/ 235U age (Ma)	1σ	204Pb/ 206Pb (%)	Rho (ρ)
RB02-2	STDMAD-12	0.057	0.0007	0.085	0.0012	0.667	0.0096	109	484.40	25.52	527.00	6.85	519.00	5.82	0.000	0.6636
RB02-2	STDMAD-13	0.057	0.0008	0.084	0.0011	0.665	0.0103	104	501.10	29.35	521.30	6.77	517.40	6.30	0.000	0.5793
RB02-2	STDMAD-14	0.057	0.0007	0.083	0.0011	0.653	0.0095	103	497.70	26.71	512.90	6.63	510.00	5.85	0.025	0.6311
526	STDMAD1	0.057	0.0008	0.095	0.0012	0.751	0.0111	117	502.10	28.57	586.10	7.19	569.10	6.46	0.000	0.5597
526	STDMAD2	0.057	0.0007	0.085	0.0011	0.666	0.0097	105	496.00	28.19	523.20	6.45	518.10	5.93	0.000	0.5719
526	STDMAD3	0.057	0.0007	0.081	0.0010	0.635	0.0093	101	494.90	28.05	500.30	6.18	499.20	5.74	0.016	0.5840
526	STDMAD4	0.057	0.0007	0.086	0.0011	0.675	0.0096	107	496.90	26.59	529.80	6.57	523.60	5.80	0.000	0.6070
526	STDMAD5	0.057	0.0007	0.085	0.0011	0.668	0.0099	107	493.50	28.56	525.80	6.52	519.70	6.01	0.000	0.5695
526	222-1	0.057	0.0007	0.083	0.0011	0.650	0.0094	104	492.60	27.54	512.00	6.34	508.40	5.77	0.000	0.5913
526	222-2	0.064	0.0011	0.084	0.0011	0.741	0.0131	69	753.60	34.37	517.10	6.67	563.00	7.63	0.078	0.4650
526	222-3	0.057	0.0008	0.083	0.0011	0.653	0.0106	104	495.70	31.91	514.00	6.51	510.60	6.48	0.023	0.5235
526	222-4	0.072	0.0009	0.083	0.0011	0.819	0.0123	53	973.30	26.48	514.30	6.51	607.50	6.88	0.178	0.5727
526	222-5	0.057	0.0011	0.087	0.0012	0.688	0.0139	109	496.50	41.44	540.00	7.30	531.60	8.36	0.000	0.4263
526	222-6	0.064	0.0010	0.084	0.0012	0.743	0.0129	69	750.10	32.82	519.70	6.82	564.40	7.52	0.053	0.5090
526	STDMAD6	0.057	0.0008	0.085	0.0012	0.664	0.0104	111	476.00	29.57	526.70	6.82	517.20	6.34	0.006	0.5838
526	STDMAD7	0.057	0.0008	0.084	0.0011	0.656	0.0104	106	488.10	30.03	518.10	6.74	512.50	6.36	0.000	0.5841
526	STDMAD8	0.057	0.0008	0.083	0.0011	0.654	0.0104	106	488.20	30.04	516.40	6.73	511.10	6.36	0.000	0.5857
526	STDMAD9	0.056	0.0009	0.081	0.0011	0.632	0.0107	109	464.20	33.17	504.50	6.63	497.10	6.67	0.000	0.5312
526	STDMAD10	0.057	0.0009	0.083	0.0011	0.652	0.0112	102	503.50	32.86	511.10	6.79	509.50	6.87	0.035	0.5376
612-1	STDMAD1	0.057	0.0007	0.084	0.0012	0.666	0.0102	104	502.00	27.82	522.40	6.83	518.50	6.19	0.000	0.6148
612-1	STDMAD2	0.057	0.0007	0.085	0.0012	0.661	0.0100	109	479.70	27.63	523.60	6.85	515.40	6.09	0.004	0.6225
612-1	STDMAD3	0.057	0.0007	0.083	0.0011	0.651	0.0099	105	489.50	27.91	513.90	6.73	509.40	6.07	0.000	0.6190
612-1	STDMAD4	0.057	0.0007	0.083	0.0011	0.648	0.0099	105	487.70	28.35	511.40	6.72	507.00	6.12	0.000	0.6141
612-1	STDMAD5	0.057	0.0007	0.082	0.0011	0.642	0.0099	107	475.20	28.44	509.50	6.70	503.30	6.10	0.028	0.6104
612-1	STDMAD6	0.059	0.0008	0.086	0.0012	0.706	0.0108	92	581.10	27.35	533.50	7.00	542.40	6.41	0.030	0.6241

Set	Analysis	207Pb/ 206Pb	1σ	206Pb/ 238U	1σ	207Pb/ 235U	1σ	% Conc.	207Pb/ 206Pb age (Ma)	1σ	206Pb/ 238U age (Ma)	1σ	207Pb/ 235U age (Ma)	1σ	204Pb/ 206Pb (%)	Rho (ρ)
612-1	2221	0.056	0.0007	0.085	0.0012	0.659	0.0101	118	449.50	27.58	528.40	6.92	513.70	6.16	0.002	0.6210
612-1	2222	0.058	0.0007	0.083	0.0011	0.658	0.0099	100	513.30	26.67	513.30	6.74	513.20	6.07	0.002	0.6349
612-1	2223	0.057	0.0007	0.085	0.0012	0.667	0.0103	106	494.70	28.65	524.60	6.90	519.00	6.29	0.000	0.6112
612-1	2224	0.058	0.0008	0.088	0.0012	0.695	0.0111	106	512.10	29.05	541.50	7.14	535.70	6.62	0.000	0.5915
612-1	2225	0.057	0.0008	0.088	0.0012	0.692	0.0111	110	495.00	30.04	543.60	7.18	534.30	6.65	0.000	0.5880
612-1	2226	0.057	0.0008	0.084	0.0012	0.652	0.0105	109	475.80	30.56	517.60	6.86	509.90	6.47	0.008	0.5854
612-1	2227	0.066	0.0009	0.086	0.0012	0.786	0.0127	65	817.70	28.58	531.50	7.09	588.90	7.22	0.031	0.5824
612-1	2228	0.057	0.0008	0.087	0.0012	0.685	0.0115	110	488.20	32.47	539.40	7.21	529.60	6.96	0.000	0.5555
612-1	2229	0.057	0.0007	0.084	0.0012	0.662	0.0104	108	484.00	28.75	522.80	6.94	515.60	6.32	0.000	0.6160
612-1	22210	0.057	0.0007	0.086	0.0012	0.675	0.0106	109	487.90	28.82	531.90	7.08	523.60	6.42	0.021	0.6189
612-1	STDMAD7	0.057	0.0008	0.084	0.0012	0.658	0.0107	105	492.00	30.59	518.60	6.95	513.60	6.58	0.000	0.5909
612-1	STDMAD8	0.057	0.0008	0.084	0.0012	0.654	0.0107	109	476.20	30.56	519.10	6.96	511.20	6.56	0.003	0.5956
612-1	STDMAD9	0.058	0.0008	0.084	0.0012	0.677	0.0111	96	543.40	30.28	520.60	7.00	524.70	6.74	0.042	0.5851
612-1	STDMAD10	0.057	0.0008	0.083	0.0012	0.656	0.0108	105	492.20	31.05	516.90	6.95	512.30	6.65	0.000	0.5886
612-1	STDMAD11	0.057	0.0008	0.084	0.0012	0.663	0.0111	103	504.30	31.05	519.00	7.00	516.10	6.77	0.028	0.5805
612-2	STDMAD-01	0.057	0.0007	0.086	0.0011	0.669	0.0094	110	480.50	28.19	529.50	6.24	520.20	5.75	0.000	0.5443
612-2	STDMAD-02	0.057	0.0007	0.084	0.0010	0.657	0.0093	107	486.70	28.06	519.00	6.15	513.00	5.69	0.000	0.5479
612-2	STDMAD-03	0.058	0.0007	0.082	0.0010	0.654	0.0092	98	518.60	27.62	509.60	6.04	511.10	5.64	0.000	0.5452
612-2	STDMAD-04	0.058	0.0007	0.083	0.0010	0.661	0.0094	100	514.90	27.80	515.80	6.14	515.50	5.72	0.000	0.5504
612-2	STDMAD-05	0.057	0.0007	0.083	0.0010	0.649	0.0091	109	474.20	27.48	515.40	6.13	507.80	5.60	0.000	0.5660
612-2	222-01	0.057	0.0008	0.073	0.0009	0.567	0.0091	96	471.70	32.98	453.20	5.50	456.10	5.87	0.017	0.4812
612-2	222-02	0.056	0.0008	0.072	0.0009	0.560	0.0082	96	466.30	29.31	449.00	5.39	451.80	5.34	0.006	0.5288
612-2	222-03	0.056	0.0008	0.071	0.0009	0.555	0.0087	95	469.80	32.06	444.20	5.38	448.20	5.67	0.023	0.4861
612-2	STDMAD-06	0.057	0.0007	0.084	0.0011	0.657	0.0095	110	472.80	28.43	521.80	6.25	512.70	5.80	0.011	0.5459
612-2	STDMAD-07	0.057	0.0009	0.089	0.0012	0.703	0.0123	111	498.40	35.97	550.80	6.80	540.70	7.30	0.029	0.4442

Set	Analysis	207Pb/ 206Pb	1σ	206Pb/ 238U	1σ	207Pb/ 235U	1σ	% Conc.	207Pb/ 206Pb age (Ma)	1σ	206Pb/ 238U age (Ma)	1σ	207Pb/ 235U age (Ma)	1σ	204Pb/ 206Pb (%)	Rho (ρ)
612-2	STDMAD-08	0.058	0.0008	0.086	0.0011	0.681	0.0101	104	512.60	28.63	531.20	6.40	527.60	6.10	0.014	0.5336
612-2	STDMAD-09	0.057	0.0008	0.084	0.0011	0.659	0.0099	106	489.20	29.70	520.00	6.29	514.30	6.02	0.000	0.5420
612-2	STDMAD-10	0.057	0.0008	0.083	0.0011	0.652	0.0100	106	484.70	30.60	515.60	6.26	509.90	6.13	0.015	0.5174
612-2	STDMAD-11	0.057	0.0008	0.084	0.0011	0.664	0.0102	103	506.10	30.17	519.50	6.32	516.90	6.22	0.000	0.5180
612-3	STDMAD-01	0.057	0.0008	0.086	0.0011	0.676	0.0106	105	504.40	30.62	529.30	6.55	524.50	6.40	0.023	0.5221
612-3	STDMAD-02	0.057	0.0009	0.082	0.0011	0.647	0.0108	104	489.80	33.71	510.80	6.40	506.90	6.62	0.000	0.4920
612-3	STDMAD-03	0.058	0.0008	0.083	0.0011	0.662	0.0102	98	524.20	30.03	514.10	6.37	515.80	6.21	0.000	0.5441
612-3	STDMAD-04	0.057	0.0007	0.084	0.0011	0.662	0.0097	105	496.30	28.29	520.20	6.43	515.70	5.93	0.006	0.5760
612-3	STDMAD-05	0.057	0.0007	0.083	0.0011	0.653	0.0095	103	496.70	28.02	513.30	6.37	510.20	5.84	0.000	0.5735
612-3	222-01	0.056	0.0009	0.072	0.0010	0.556	0.0098	99	452.30	35.75	448.20	5.72	448.70	6.39	0.000	0.4617
612-3	222-02	0.057	0.0008	0.072	0.0009	0.564	0.0090	93	483.90	32.03	448.00	5.64	453.90	5.86	0.000	0.5233
612-3	222-03	0.057	0.0009	0.071	0.0009	0.552	0.0093	93	474.80	33.99	440.60	5.59	446.10	6.05	0.000	0.4938
612-3	222-04	0.056	0.0008	0.073	0.0010	0.561	0.0092	103	441.50	32.54	454.20	5.74	452.00	5.99	0.033	0.5085
612-3	222-05	0.057	0.0008	0.071	0.0009	0.558	0.0087	93	476.10	30.74	445.10	5.60	450.10	5.66	0.007	0.5360
612-3	STDMAD-06	0.057	0.0008	0.084	0.0011	0.657	0.0105	106	490.00	31.98	518.20	6.48	512.90	6.42	0.000	0.5219
612-3	STDMAD-07	0.057	0.0008	0.084	0.0011	0.653	0.0102	108	479.80	30.77	517.50	6.46	510.50	6.24	0.006	0.5370
612-3	222-06	0.056	0.0010	0.072	0.0010	0.550	0.0101	101	442.40	37.30	445.60	5.84	445.00	6.63	0.000	0.4537
612-3	222-07	0.056	0.0009	0.073	0.0010	0.558	0.0094	102	442.60	33.03	452.00	5.83	450.30	6.11	0.034	0.5081
612-3	222-08	0.056	0.0008	0.072	0.0010	0.563	0.0089	96	467.80	30.72	451.00	5.79	453.70	5.78	0.038	0.5588
612-3	STDMAD-08	0.056	0.0008	0.084	0.0011	0.647	0.0101	112	460.40	29.70	517.30	6.63	506.90	6.20	0.006	0.5691
612-3	STDMAD-09	0.057	0.0008	0.083	0.0011	0.651	0.0105	106	486.20	31.42	514.30	6.59	509.00	6.43	0.000	0.5443
612-3	STDMAD-10	0.057	0.0008	0.084	0.0011	0.663	0.0105	105	495.70	30.29	521.20	6.71	516.40	6.39	0.043	0.5620
612-3	STDMAD-11	0.057	0.0010	0.082	0.0011	0.648	0.0117	102	500.20	36.13	509.20	6.66	507.40	7.21	0.000	0.4804
612-3	STDMAD-12	0.058	0.0008	0.085	0.0011	0.679	0.0110	102	518.90	31.48	527.80	6.79	525.90	6.66	0.020	0.5420
612-3	STDMAD-13	0.057	0.0008	0.085	0.0011	0.662	0.0109	109	480.90	32.61	524.10	6.75	516.00	6.68	0.015	0.5282

Set	Analysis	207Pb/ 206Pb	1σ	206Pb/ 238U	1σ	207Pb/ 235U	1σ	% Conc.	207Pb/ 206Pb age (Ma)	1σ	206Pb/ 238U age (Ma)	1σ	207Pb/ 235U age (Ma)	1σ	204Pb/ 206Pb (%)	Rho (ρ)
612-4	STDMAD-14	0.057	0.0008	0.088	0.0012	0.694	0.0112	111	492.30	31.81	545.50	6.95	535.20	6.72	0.028	0.5368
612-4	STDMAD-15	0.057	0.0008	0.085	0.0011	0.671	0.0103	104	503.20	29.34	525.50	6.62	521.20	6.23	0.000	0.5610
612-4	STDMAD-16	0.057	0.0008	0.084	0.0011	0.662	0.0107	106	490.00	31.52	521.60	6.75	515.60	6.55	0.000	0.5552
612-4	STDMAD-17	0.078	0.0026	0.084	0.0015	0.900	0.0291	46	1138.00	64.71	520.60	8.73	651.70	15.55	0.101	0.2186
612-4	STDMAD-18	0.057	0.0009	0.083	0.0011	0.650	0.0114	108	478.90	35.94	515.20	6.65	508.60	7.04	0.000	0.4802
612-4	STDMAD-19	0.057	0.0008	0.084	0.0011	0.658	0.0104	104	498.00	31.07	517.30	6.53	513.60	6.38	0.000	0.5361
612-4	222-08	0.057	0.0010	0.073	0.0010	0.570	0.0109	96	474.50	40.11	454.70	5.98	458.00	7.07	0.000	0.4260
612-4	222-09	0.057	0.0009	0.073	0.0010	0.568	0.0100	94	479.00	36.26	452.30	5.83	456.70	6.49	0.033	0.4676
612-4	222-10	0.056	0.0008	0.071	0.0009	0.553	0.0085	98	455.50	29.75	445.10	5.61	446.70	5.58	0.000	0.5454
612-4	222-11	0.056	0.0008	0.071	0.0009	0.549	0.0083	96	459.40	29.41	441.40	5.57	444.30	5.47	0.000	0.5641
612-4	222-12	0.056	0.0010	0.072	0.0010	0.551	0.0105	100	446.70	38.54	446.00	5.94	446.00	6.85	0.019	0.4525
612-4	222-13	0.056	0.0009	0.071	0.0009	0.547	0.0092	100	443.40	33.94	443.20	5.62	443.10	6.05	0.006	0.4793
612-4	STDMAD-20	0.057	0.0007	0.084	0.0011	0.661	0.0098	105	494.10	28.67	519.70	6.46	514.90	5.98	0.025	0.5715
612-4	STDMAD-21	0.057	0.0008	0.083	0.0011	0.647	0.0101	107	480.60	31.15	512.40	6.36	506.50	6.22	0.029	0.5242
612-4	222-14	0.056	0.0008	0.071	0.0009	0.551	0.0087	99	449.70	31.79	445.10	5.48	445.80	5.71	0.015	0.4911
612-4	222-15	0.056	0.0008	0.071	0.0009	0.549	0.0089	97	454.30	32.62	442.90	5.47	444.60	5.82	0.008	0.4845
612-4	222-16	0.058	0.0009	0.068	0.0009	0.542	0.0091	83	510.70	34.91	426.00	5.31	439.40	6.02	0.029	0.4610
612-4	STDMAD-22	0.057	0.0009	0.083	0.0011	0.648	0.0106	108	477.30	33.10	513.60	6.41	507.00	6.51	0.000	0.4954
612-4	STDMAD-23	0.057	0.0009	0.077	0.0010	0.605	0.0103	98	489.20	35.84	478.60	5.92	480.30	6.54	0.000	0.4332
612-4	STDMAD-24	0.057	0.0009	0.076	0.0010	0.591	0.0096	98	477.80	33.80	470.30	5.74	471.50	6.12	0.013	0.4578
612-4	STDMAD-25	0.057	0.0009	0.073	0.0009	0.573	0.0096	90	499.70	34.82	452.20	5.57	460.00	6.22	0.003	0.4496
612-4	STDMAD-26	0.056	0.0008	0.079	0.0010	0.608	0.0094	111	442.00	31.01	491.00	5.95	482.30	5.92	0.017	0.4918
612-4	STDMAD-27	0.071	0.0010	0.086	0.0011	0.844	0.0131	55	968.90	29.36	530.50	6.42	621.40	7.22	0.138	0.4792
612-4	STDMAD-28	0.057	0.0008	0.083	0.0011	0.653	0.0101	106	485.50	31.91	515.90	6.24	510.30	6.23	0.000	0.4905
612-4	STDMAD-29	0.058	0.0010	0.081	0.0010	0.643	0.0110	98	512.30	36.36	502.30	6.15	504.00	6.82	0.000	0.4217

Set	Analysis	207Pb/ 206Pb	1σ	206Pb/ 238U	1σ	207Pb/ 235U	1σ	% Conc.	207Pb/ 206Pb age (Ma)	1σ	206Pb/ 238U age (Ma)	1σ	207Pb/ 235U age (Ma)	1σ	204Pb/ 206Pb (%)	Rho (ρ)
612-4	STDMAD-30	0.057	0.0008	0.079	0.0010	0.619	0.0097	100	490.10	32.29	489.00	5.92	489.20	6.07	0.010	0.4834
612-4	STDMAD-31	0.057	0.0008	0.085	0.0011	0.666	0.0101	106	494.30	30.74	524.20	6.32	518.50	6.15	0.013	0.5000
801	STDMAD-01	0.058	0.0007	0.085	0.0014	0.672	0.0120	103	511.10	27.44	524.30	8.35	521.70	7.27	0.012	0.7293
801	STDMAD-02	0.057	0.0007	0.083	0.0014	0.650	0.0116	110	471.60	27.89	516.60	8.24	508.30	7.11	0.000	0.7342
801	STDMAD-03	0.057	0.0007	0.084	0.0014	0.655	0.0117	108	480.30	28.24	518.90	8.29	511.80	7.19	0.012	0.7315
801	STDMAD-04	0.058	0.0008	0.080	0.0014	0.637	0.0119	98	510.20	29.89	498.10	8.03	500.20	7.36	0.000	0.6962
801	STDMAD-05	0.057	0.0007	0.083	0.0014	0.653	0.0117	106	487.40	28.00	515.20	8.26	510.10	7.16	0.000	0.7342
801	222-01	0.057	0.0007	0.073	0.0012	0.566	0.0103	95	474.70	28.97	451.30	7.30	455.10	6.67	0.000	0.7217
801	222-02	0.056	0.0007	0.073	0.0012	0.559	0.0099	101	445.90	26.57	452.20	7.29	451.10	6.43	0.004	0.7494
801	222-03	0.056	0.0007	0.072	0.0012	0.558	0.0099	99	453.50	26.64	449.90	7.27	450.40	6.43	0.002	0.7453
801	222-04	0.059	0.0008	0.082	0.0014	0.665	0.0120	92	552.10	27.58	510.10	8.24	517.70	7.30	0.000	0.7313
801	222-05	0.058	0.0007	0.085	0.0014	0.688	0.0122	97	546.50	26.77	528.60	8.53	531.80	7.36	0.000	0.7482
801	STDMAD-06	0.057	0.0008	0.083	0.0014	0.656	0.0120	102	503.00	28.69	514.40	8.35	512.30	7.37	0.016	0.7261
801	222-06	0.056	0.0008	0.071	0.0012	0.549	0.0104	94	468.90	30.29	439.40	7.33	444.10	6.81	0.030	0.7197
801	222-07	0.056	0.0007	0.073	0.0012	0.562	0.0104	98	459.80	28.96	451.40	7.46	452.80	6.76	0.000	0.7293
801	222-08	0.060	0.0009	0.076	0.0013	0.627	0.0127	80	593.30	33.60	473.40	7.94	494.20	7.95	0.015	0.6622
801	222-09	0.056	0.0008	0.072	0.0013	0.561	0.0105	95	470.40	29.53	448.80	7.49	452.20	6.85	0.028	0.7322
801	STDMAD-07	0.057	0.0007	0.084	0.0015	0.660	0.0119	105	495.60	26.15	518.70	8.71	514.40	7.31	0.008	0.7826
801	STDMAD-08	0.057	0.0007	0.084	0.0015	0.662	0.0119	107	486.70	25.61	522.20	8.75	515.60	7.26	0.000	0.7851
801	STDMAD-09	0.057	0.0007	0.083	0.0015	0.653	0.0118	106	487.20	26.35	515.40	8.61	510.20	7.24	0.011	0.7737
801	STDMAD-10	0.057	0.0007	0.083	0.0015	0.655	0.0118	103	498.20	25.61	514.50	8.66	511.40	7.24	0.000	0.7902
801	STDMAD-11	0.057	0.0007	0.083	0.0015	0.648	0.0118	108	477.70	26.22	514.30	8.68	507.50	7.27	0.000	0.7823
813-2	STDMAD-01	0.056	0.0009	0.087	0.0014	0.668	0.0127	122	440.50	33.98	538.00	8.17	519.60	7.71	0.000	0.6105
813-2	STDMAD-02	0.057	0.0007	0.086	0.0013	0.677	0.0115	106	498.90	28.00	531.10	7.96	524.90	6.96	0.000	0.6961
813-2	STDMAD-03	0.057	0.0007	0.085	0.0013	0.664	0.0112	109	482.60	27.28	524.70	7.89	516.80	6.80	0.010	0.7141

Set	Analysis	207Pb/ 206Pb	1σ	206Pb/ 238U	1σ	207Pb/ 235U	1σ	% Conc.	207Pb/ 206Pb age (Ma)	1σ	206Pb/ 238U age (Ma)	1σ	207Pb/ 235U age (Ma)	1σ	204Pb/ 206Pb (%)	Rho (ρ)
813-2	STDMAD-04	0.057	0.0008	0.083	0.0013	0.655	0.0114	103	497.40	29.57	514.80	7.77	511.50	7.02	0.009	0.6758
813-2	STDMAD-05	0.057	0.0007	0.084	0.0013	0.656	0.0109	105	492.30	26.67	517.00	7.81	512.30	6.71	0.009	0.7221
813-2	STDMAD-06	0.130	0.0015	0.097	0.0015	1.740	0.0281	28	2103.80	19.78	595.50	8.91	1023.30	10.40	0.512	0.7463
813-2	222-01	0.056	0.0007	0.072	0.0011	0.557	0.0094	100	448.10	27.21	449.70	6.83	449.30	6.16	0.000	0.7096
813-2	222-02	0.055	0.0007	0.060	0.0009	0.455	0.0079	89	419.20	28.98	374.70	5.73	380.80	5.52	0.022	0.6847
813-2	222-03	0.056	0.0007	0.074	0.0012	0.570	0.0094	101	454.10	25.73	458.60	6.96	457.70	6.10	0.022	0.7352
813-2	222-04	0.056	0.0007	0.072	0.0011	0.559	0.0093	96	465.20	26.15	448.40	6.83	451.10	6.05	0.000	0.7322
813-2	222-05	0.057	0.0008	0.071	0.0011	0.558	0.0101	93	479.10	31.17	444.70	6.85	450.20	6.59	0.022	0.6643
813-2	222-06	0.057	0.0007	0.069	0.0011	0.539	0.0093	88	485.30	27.79	429.00	6.63	437.90	6.12	0.005	0.7194
813-2	222-07	0.056	0.0008	0.071	0.0011	0.546	0.0098	96	458.80	29.90	439.30	6.83	442.50	6.43	0.003	0.6877
813-2	222-08	0.056	0.0007	0.071	0.0012	0.548	0.0094	97	453.70	26.17	442.10	6.94	443.90	6.18	0.000	0.7376
813-2	222-09	0.056	0.0007	0.072	0.0012	0.557	0.0097	100	450.60	27.79	449.50	6.98	449.60	6.35	0.020	0.7089
813-2	STDMAD-07	0.057	0.0007	0.082	0.0013	0.640	0.0109	105	481.30	26.18	507.10	7.93	502.40	6.77	0.000	0.7501
813-2	STDMAD-08	0.057	0.0007	0.085	0.0014	0.670	0.0115	108	487.40	26.26	528.80	8.26	521.00	6.97	0.000	0.7522
813-2	STDMAD-09	0.058	0.0007	0.083	0.0014	0.661	0.0114	99	518.80	26.23	514.50	8.05	515.10	6.94	0.000	0.7455
813-2	STDMAD-10	0.056	0.0008	0.083	0.0014	0.642	0.0119	112	458.40	31.33	513.60	8.02	503.60	7.34	0.018	0.6714
813-2	STDMAD-11	0.057	0.0008	0.084	0.0014	0.657	0.0124	107	483.60	30.88	519.80	8.38	513.10	7.58	0.000	0.7004
813-2	STDMAD-12	0.058	0.0010	0.085	0.0014	0.674	0.0144	100	523.60	38.84	523.50	8.48	523.30	8.71	0.020	0.5864
813-2	STDMAD-13	0.057	0.0007	0.083	0.0014	0.645	0.0112	108	475.20	26.49	512.50	8.06	505.70	6.89	0.000	0.7458
813-2	STDMAD-14	0.057	0.0008	0.085	0.0014	0.670	0.0123	105	500.20	30.49	525.60	8.22	520.80	7.48	0.022	0.6799
907	STDMAD1	0.074	0.0009	0.090	0.0012	0.923	0.0134	53	1053.30	25.04	555.30	6.92	663.70	7.05	0.049	0.6000
907	STDMAD2	0.087	0.0011	0.089	0.0012	1.065	0.0153	40	1361.40	23.26	548.70	6.86	736.50	7.51	0.198	0.6081
907	STDMAD3	0.057	0.0007	0.083	0.0011	0.654	0.0098	103	499.60	28.22	513.90	6.45	511.10	5.99	0.000	0.5780
907	STDMAD4	0.057	0.0008	0.082	0.0011	0.648	0.0098	103	497.40	29.06	510.00	6.41	507.50	6.06	0.000	0.5784
907	STDMAD5	0.057	0.0008	0.086	0.0011	0.675	0.0103	111	480.20	29.33	534.30	6.71	524.00	6.23	0.000	0.5725

Set	Analysis	207Pb/ 206Pb	1σ	206Pb/ 238U	1σ	207Pb/ 235U	1σ	% Conc.	207Pb/ 206Pb age (Ma)	1σ	206Pb/ 238U age (Ma)	1σ	207Pb/ 235U age (Ma)	1σ	204Pb/ 206Pb (%)	Rho (ρ)
907	222-1	0.056	0.0008	0.076	0.0010	0.586	0.0095	108	439.00	30.58	474.70	6.23	468.50	6.09	0.027	0.5707
907	222-2	0.056	0.0008	0.075	0.0010	0.583	0.0098	99	469.40	32.65	466.10	6.15	466.60	6.26	0.000	0.5465
907	222-3	0.056	0.0008	0.074	0.0010	0.575	0.0095	101	458.30	31.49	461.80	6.07	461.10	6.10	0.000	0.5536
907	222-4	0.056	0.0008	0.075	0.0010	0.581	0.0092	100	465.30	30.37	464.90	5.98	464.90	5.88	0.000	0.5704
907	222-5	0.057	0.0007	0.075	0.0010	0.589	0.0087	98	480.20	27.72	468.50	5.93	470.40	5.55	0.000	0.6017
907	222-6	0.056	0.0008	0.076	0.0010	0.585	0.0098	109	434.40	32.76	475.00	6.11	467.90	6.27	0.002	0.5126
907	222-7	0.055	0.0010	0.075	0.0010	0.574	0.0107	108	430.70	37.78	466.90	6.15	460.70	6.90	0.000	0.4611
907	STDMAD6	0.060	0.0008	0.088	0.0012	0.727	0.0113	90	602.30	28.77	543.40	7.00	554.70	6.64	0.039	0.5841
907	STDMAD7	0.057	0.0008	0.084	0.0011	0.667	0.0104	104	501.50	29.47	522.70	6.75	518.60	6.34	0.000	0.5788
907	STDMAD8	0.057	0.0008	0.082	0.0011	0.647	0.0103	105	488.00	30.84	510.80	6.62	506.60	6.36	0.000	0.5660
907	STDMAD9	0.057	0.0008	0.084	0.0011	0.658	0.0104	108	482.60	30.42	520.10	6.74	513.10	6.37	0.000	0.5703
907	STDMAD10	0.056	0.0008	0.082	0.0011	0.636	0.0102	112	456.90	30.37	509.50	6.62	499.90	6.31	0.000	0.5668
907-2	STDMAD-01	0.058	0.0008	0.085	0.0011	0.676	0.0105	99	526.90	30.06	524.00	6.58	524.40	6.35	0.000	0.5564
907-2	STDMAD-02	0.057	0.0008	0.083	0.0011	0.653	0.0106	103	500.20	31.79	512.90	6.48	510.50	6.50	0.000	0.5285
907-2	STDMAD-03	0.057	0.0008	0.083	0.0011	0.652	0.0100	107	481.10	29.67	515.90	6.47	509.50	6.13	0.000	0.5643
907-2	STDMAD-04	0.058	0.0008	0.083	0.0011	0.671	0.0102	94	547.90	28.83	515.80	6.47	521.50	6.21	0.000	0.5649
907-2	STDMAD-05	0.057	0.0009	0.083	0.0011	0.654	0.0110	106	486.60	33.95	516.40	6.55	510.90	6.75	0.000	0.5027
907-2	STDMAD-06	0.057	0.0007	0.085	0.0011	0.665	0.0099	106	493.50	28.86	523.00	6.56	517.50	6.06	0.000	0.5777
907-2	222-01	0.057	0.0008	0.071	0.0009	0.559	0.0086	92	483.40	29.92	444.70	5.63	450.90	5.59	0.003	0.5570
907-2	222-02	0.056	0.0009	0.073	0.0010	0.561	0.0098	99	455.00	35.04	452.10	5.81	452.40	6.37	0.000	0.4828
907-2	222-03	0.056	0.0009	0.072	0.0010	0.561	0.0097	97	466.00	35.15	449.80	5.79	452.40	6.32	0.000	0.4811
907-2	222-04	0.056	0.0009	0.072	0.0010	0.553	0.0098	100	445.50	35.63	447.30	5.78	446.90	6.40	0.000	0.4777
907-2	222-05	0.056	0.0009	0.073	0.0010	0.564	0.0099	99	457.30	35.40	453.90	5.86	454.40	6.44	0.000	0.4778
907-2	STDMAD-07	0.057	0.0009	0.083	0.0011	0.650	0.0109	107	479.80	33.84	515.00	6.57	508.50	6.72	0.010	0.4992
907-2	STDMAD-08	0.057	0.0008	0.085	0.0011	0.661	0.0108	109	479.50	32.61	523.50	6.63	515.30	6.60	0.025	0.5150

Set	Analysis	207Pb/ 206Pb	1σ	206Pb/ 238U	1σ	207Pb/ 235U	1σ	% Conc.	207Pb/ 206Pb age (Ma)	1σ	206Pb/ 238U age (Ma)	1σ	207Pb/ 235U age (Ma)	1σ	204Pb/ 206Pb (%)	Rho (ρ)
907-2	222-06	0.056	0.0009	0.073	0.0010	0.566	0.0101	101	450.70	35.90	456.20	5.91	455.10	6.52	0.000	0.4720
907-2	222-07	0.056	0.0009	0.072	0.0010	0.558	0.0100	101	444.60	36.36	451.10	5.86	449.90	6.53	0.004	0.4685
907-2	222-08	0.056	0.0010	0.073	0.0010	0.557	0.0102	103	438.10	37.41	451.70	5.89	449.30	6.67	0.056	0.4475
907-2	STDMAD-09	0.057	0.0009	0.084	0.0011	0.656	0.0115	109	475.50	35.72	520.40	6.69	512.00	7.03	0.000	0.4731
907-2	STDMAD-10	0.057	0.0009	0.085	0.0011	0.666	0.0119	107	491.30	36.31	524.20	6.77	518.00	7.23	0.003	0.4728
907-2	STDMAD-11	0.057	0.0009	0.084	0.0011	0.654	0.0112	109	474.70	34.88	519.00	6.66	510.80	6.89	0.000	0.4921
907-2	STDMAD-12	0.057	0.0008	0.083	0.0011	0.651	0.0107	107	483.10	32.87	515.40	6.59	509.40	6.59	0.000	0.5239
907-2	STDMAD-13	0.057	0.0008	0.083	0.0011	0.655	0.0106	104	494.30	32.12	515.30	6.58	511.30	6.53	0.007	0.5315
907-3	STDMAD-14	0.057	0.0008	0.085	0.0011	0.671	0.0105	107	492.40	30.52	528.10	6.65	521.40	6.37	0.010	0.5470
907-3	STDMAD-15	0.057	0.0008	0.084	0.0011	0.659	0.0104	110	476.90	31.12	522.50	6.58	514.10	6.37	0.017	0.5365
907-3	STDMAD-16	0.057	0.0008	0.083	0.0011	0.650	0.0102	104	492.90	30.97	511.70	6.44	508.20	6.29	0.012	0.5398
907-3	STDMAD-17	0.058	0.0009	0.082	0.0011	0.662	0.0108	93	546.20	31.79	508.90	6.42	515.60	6.57	0.000	0.5157
907-3	STDMAD-18	0.057	0.0007	0.083	0.0011	0.644	0.0095	108	473.00	28.07	512.00	6.45	504.90	5.88	0.013	0.5877
907-3	STDMAD-19	0.057	0.0008	0.085	0.0011	0.669	0.0103	108	489.90	30.33	526.80	6.58	519.80	6.28	0.000	0.5486
907-3	222-09	0.056	0.0008	0.073	0.0010	0.568	0.0092	100	458.60	31.90	456.60	5.78	456.80	5.96	0.000	0.5199
907-3	222-10	0.056	0.0009	0.073	0.0010	0.568	0.0098	98	463.80	35.08	455.30	5.81	456.60	6.33	0.000	0.4741
907-3	222-11	0.056	0.0009	0.072	0.0010	0.554	0.0096	98	457.20	35.19	446.30	5.70	447.90	6.30	0.030	0.4667
907-3	222-12	0.056	0.0009	0.072	0.0009	0.552	0.0092	100	445.20	33.36	447.10	5.67	446.60	6.04	0.000	0.4874
907-3	222-13	0.056	0.0009	0.070	0.0009	0.543	0.0093	97	451.00	34.63	439.00	5.59	440.70	6.14	0.061	0.4767
907-3	STDMAD-20	0.060	0.0008	0.084	0.0011	0.692	0.0102	86	604.50	27.45	517.80	6.46	533.90	6.12	0.023	0.5789
907-3	STDMAD-21	0.057	0.0008	0.083	0.0011	0.655	0.0102	102	504.20	29.94	513.50	6.51	511.70	6.27	0.000	0.5512
907-3	222-14	0.056	0.0011	0.073	0.0010	0.560	0.0109	101	447.80	40.93	452.40	5.87	451.30	7.08	0.000	0.3943
907-3	222-15	0.056	0.0009	0.071	0.0009	0.548	0.0094	98	452.40	35.19	442.10	5.59	443.50	6.19	0.000	0.4523
907-3	222-16	0.055	0.0009	0.071	0.0009	0.534	0.0096	112	395.00	37.72	442.40	5.64	434.60	6.38	0.011	0.4275
907-3	STDMAD-22	0.059	0.0010	0.084	0.0011	0.678	0.0120	92	563.30	36.21	517.60	6.56	525.70	7.26	0.000	0.4373

Set	Analysis	207Pb/ 206Pb	1σ	206Pb/ 238U	1σ	207Pb/ 235U	1σ	% Conc.	207Pb/ 206Pb age (Ma)	1σ	206Pb/ 238U age (Ma)	1σ	207Pb/ 235U age (Ma)	1σ	204Pb/ 206Pb (%)	Rho (ρ)
907-3	STDMAD-23	0.131	0.0026	0.100	0.0014	1.813	0.0362	29	2116.00	34.39	616.00	8.35	1050.30	13.05	0.562	0.3602
907-3	STDMAD-24	0.057	0.0009	0.086	0.0011	0.673	0.0116	111	478.70	36.20	532.60	6.69	522.30	7.07	0.008	0.4459
907-3	STDMAD-25	0.056	0.0008	0.085	0.0011	0.662	0.0103	113	466.90	31.35	526.80	6.51	515.60	6.30	0.017	0.5177
907-3	STDMAD-26	0.057	0.0009	0.083	0.0011	0.650	0.0112	104	492.90	35.79	512.40	6.44	508.60	6.90	0.000	0.4493
907-3	STDMAD-27	0.057	0.0009	0.081	0.0011	0.641	0.0105	101	500.80	33.06	504.00	6.26	503.10	6.46	0.006	0.4784

APPENDIX B: MINERAL CHEMISTRY

Range of chemistry for selected minerals

		AAE784	AAE980	AAE907	1809041A
gt core	*x*(gt)	0.663–0.707	0.601–0.679	0.472–0.552	0.749–0.777
	X_{alm}	0.638–0.679	0.573–0.645	0.291–0.345	0.698–0.73
	X_{py}	0.243–0.311	0.261–0.333	0.06–0.278	0.209–0.234
	X_{grs}	0.02–0.022	0.028–0.047	0.035–0.046	0.044–0.055
	X_{sps}	0.015–0.021	0.013–0.02	0.306–0.387	0.013–0.016
gt rim	*x*(gt)	0.675–0.78	0.65–0.792	0.495–0.504	—
	X_{alm}	0.648–0.748	0.614–0.744	0.29–0.301	—
	X_{py}	0.21–0.275	0.168–0.305	0.17–0.189	—
	X_{grs}	0.019–0.022	0.027–0.054	0.042–0.043	—
	X_{sps}	0.017–0.023	0.015–0.028	0.362–0.371	—
gt symplectites	*x*(gt)	—	—	0.493–0.535	—
	X_{alm}	—	—	0.271–0.325	—
	X_{py}	—	—	0.094–0.224	—
	X_{grs}	—	—	0.032–0.041	—
	X_{sps}	—	—	0.335–0.442	—
opx	*y*(opx)	—	—	—	0.016–0.058
bi (matrix)	F(wt%)	—	0.33–0.44	0.67–0.82	—
	TiO(wt%)	—	3.04–4.18	0.75–1.77	4.46–4.75
	X_{Fe}	—	0.36–0.41	0.14–0.24	0.45–0.46
bi (crack)	F(wt%)	—	0.46–0.76	—	—
	TiO(wt%)	—	0.67–4.04	—	—
	X_{Fe}	—	0.21–0.35	—	—
cd	X_{Fe}	0.203–0.206	0.24–0.245	0.114–0.601	—
ksp	X_{Or}	0.87–0.89	0.56–0.91	—	0.79–0.88
pl	X_{ab}	—	0.68–0.76	0.6–0.6	0.7–0.72
	Ca(pl)	—	0.23–0.31	0.39–0.39	0.26–0.28
sp	Zn(wt%)	—	—	2.07–2.53	—
	Cr_2O_3(wt%)	—	—	0.024–0.041	—
ilm	MnO(wt%)	—	1.266–1.669	—	0.081–0.117
	TiO_2(wt%)	—	52.44–52.83	—	42.84–50.91

$X_{alm} = Fe^{2+}/(Fe^{2+}+Mg+Ca+Mn)$
$X_{py} = Mg/(Fe^{2+}+Mg+Ca+Mn)$
$X_{grs} = Ca/(Fe^{2+}+Mg+Ca+Mn)$
$X_{sps} = Mn/(Fe^{2+}+Mg+Ca+Mn)$
$x(gt) = Fe^{2+}/(Fe^{2+} + Mg)$

y(opx) = octahedrally-coordinated (M-site) Al in opx, calculated as Al + Si – 2 cations
$X_{Fe} = Fe/(Fe^{2+}+Mg)$
$X_{Or} = K/(K+Na+Ca)$
$X_{ab} = Na/(Na+Ca)$

Representative electron microprobe analyses

Mineral	AAE784				AAE907								AAE980	
	gt core	gt rim	cd	ksp	gt core	gt rim	gt (s)	bi	cd	mt (cg)	mt (s)	sp	gt core	gt rim
SiO_2	37.44	37.91	48.85	63.95	37.59	37.79	36.94	36.45	36.15	0.00	0.00	0.00	38.28	37.91
TiO_2	1.30	0.00	0.00	0.01	0.00	0.00	0.00	1.99	0.00	0.00	0.00	0.07	0.01	0.01
Al_2O_3	21.47	21.67	33.39	18.62	21.72	21.61	21.28	18.27	21.41	0.07	0.07	61.64	21.71	21.66
Cr_2O_3	0.09	0.15	0.00	0.00	0.01	0.00	0.02	0.00	0.00	0.05	0.01	0.04	0.10	0.05
FeO	29.86	30.83	4.85	0.02	17.00	16.38	16.97	5.97	17.17	93.92	92.37	15.58	29.60	31.60
MnO	0.74	0.83	0.02	0.00	14.17	16.09	15.42	0.21	15.23	0.28	0.72	2.70	0.86	0.75
MgO	8.07	7.66	10.66	0.00	8.34	7.53	7.44	20.90	7.56	0.02	0.01	14.03	8.34	6.70
ZnO	0.02	0.00	0.00	0.00	0.00	0.00	0.02	0.00	0.00	0.00	0.00	2.42	0.00	0.00
CaO	0.73	0.73	0.00	0.00	1.27	1.44	1.11	0.00	1.09	0.00	0.00	0.00	1.14	1.11
Na_2O	0.02	0.00	0.08	1.42	0.00	0.00	0.01	0.10	0.00	0.00	0.00	0.07	0.00	0.00
K_2O	0.00	0.00	0.02	14.60	0.00	0.00	0.00	9.06	0.00	0.00	0.00	0.00	0.00	0.00
Cl	0.00	0.00	0.00	0.01	0.00	0.01	0.00	0.00	0.00	0.00	0.00	0.00	0.00	0.01
F	0.00	0.04	0.00	0.00	0.00	0.00	0.00	0.74	0.00	0.27	0.24	0.00	0.00	0.05
Total	**99.73**	**99.80**	**97.87**	**98.62**	**100.08**	**100.84**	**99.21**	**93.36**	**98.62**	**94.50**	**93.33**	**96.55**	**100.04**	**99.82**
No. Oxygens	12	12	18	8	12	12	12	11	18	4	4	4	12	12
Si	2.93	2.97	4.97	2.98	2.91	2.93	2.91	2.65	4.34	0.00	0.00	0.00	2.97	2.98
Ti	0.08	0.00	0.00	0.00	0.00	0.00	0.00	0.11	0.00	0.00	0.00	0.00	0.00	0.00
Al	1.98	2.00	4.01	1.02	1.98	1.97	1.97	1.56	3.03	0.00	0.00	1.97	1.99	2.01
Cr	0.01	0.01	0.00	0.00	0.00	0.00	0.00	0.00	0.00	0.00	0.00	0.00	0.01	0.00
Fe^{3+}	0.01	0.05	--	--	0.19	0.18	0.21	--	--	1.96	1.97	0.03	0.07	0.01
Fe^{2+}	1.95	1.97	0.41	0.00	0.91	0.88	0.91	0.36	1.72	1.02	1.00	0.32	1.85	2.07
Mn^{2+}	0.05	0.05	0.00	0.00	0.93	1.05	1.03	0.01	1.55	0.01	0.02	0.06	0.06	0.05
Mg	0.94	0.89	1.62	0.00	0.96	0.87	0.87	2.26	1.35	0.00	0.00	0.57	0.97	0.79
Zn	0.00	0.00	0.00	0.00	0.00	0.00	0.00	0.00	0.00	0.00	0.00	0.05	0.00	0.00
Ca	0.06	0.06	0.00	0.00	0.11	0.12	0.09	0.00	0.14	0.00	0.00	0.00	0.09	0.09
Na	0.00	0.00	0.02	0.13	0.00	0.00	0.00	0.01	0.00	0.00	0.00	0.00	0.00	0.00
K	0.00	0.00	0.00	0.87	0.00	0.00	0.00	0.84	0.00	0.00	0.00	0.00	0.00	0.00
Cl	0.00	0.00	0.00	0.00	0.00	0.00	0.00	0.00	0.00	0.00	0.00	0.00	0.00	0.00
F	0.00	0.01	0.00	0.00	0.00	0.00	0.00	0.17	0.00	0.03	0.03	0.00	0.00	0.01
Total cations	**8.00**	**8.00**	**11.03**	**5.00**	**8.00**	**8.00**	**8.00**	**7.81**	**12.14**	**3.00**	**3.00**	**3.00**	**8.00**	**8.00**

Mineral	AAE980						1809041A	Redbanks Charnockite				
	bi in crack	bi in matrix	cd	pl	ksp	ilm	gt	bi	opx	pl	ksp	ilm
SiO_2	36.11	35.16	48.34	60.02	62.95	0.00	37.80	35.98	49.72	61.55	64.45	0.26
TiO_2	3.59	3.96	0.00	0.00	0.01	52.44	0.03	4.46	0.00	0.02	0.04	50.77
Al_2O_3	17.22	17.40	33.14	25.05	18.66	0.01	20.93	14.08	1.78	24.00	18.23	0.00
Cr_2O_3	0.05	0.15	0.00	0.00	0.00	0.06	0.03	0.00	0.01	0.00	0.00	0.02
FeO	13.35	15.78	5.76	0.07	0.00	44.86	32.58	18.30	30.88	0.10	0.06	47.46
MnO	0.00	0.02	0.04	0.00	0.00	1.67	0.64	0.05	0.18	0.03	0.02	0.09
MgO	14.70	12.82	10.24	0.00	0.00	0.18	5.88	11.94	16.01	0.01	0.00	0.26
ZnO	0.00	0.02	0.00	0.02	0.00	0.04	0.03	0.00	0.16	0.00	0.03	0.05
CaO	0.02	0.01	0.00	6.62	0.10	0.00	1.73	0.00	0.10	5.85	0.07	0.02
Na_2O	0.08	0.06	0.06	8.29	1.10	0.02	0.01	0.05	0.00	8.20	2.29	0.00
K_2O	9.26	9.13	0.00	0.13	14.64	0.00	0.00	9.69	0.00	0.35	13.61	0.00
Cl	0.06	0.05	0.00	0.00	0.00	0.00	0.00	0.00	0.00	0.00	0.00	0.00
F	0.46	0.33	0.00	0.00	0.00	0.09	0.00	0.00	0.00	0.00	0.00	0.00
Total	94.69	94.73	97.59	100.20	97.47	99.33	99.65	94.57	98.84	100.09	98.80	98.93
No. Oxygens	11	11	18	8	8	3	12	11	6	8	8	3
Si	2.68	2.65	4.96	2.67	2.97	0.00	3.00	2.77	1.95	2.73	2.99	0.01
Ti	0.20	0.22	0.00	0.00	0.00	1.00	0.00	0.26	0.00	0.00	0.00	0.97
Al	1.51	1.54	4.01	1.31	1.04	0.00	1.95	1.28	0.08	1.26	1.00	0.00
Cr	0.00	0.01	0.00	0.00	0.00	0.00	0.00	0.00	0.00	0.00	0.00	0.00
Fe^{3+}	--	--	--	--	--	0.00	0.05	--	0.01	--	--	0.04
Fe^{2+}	0.83	0.99	0.49	0.00	0.00	0.95	2.11	1.18	1.00	0.00	0.00	0.96
Mn^{2+}	0.00	0.00	0.00	0.00	0.00	0.04	0.04	0.00	0.01	0.00	0.00	0.00
Mg	1.63	1.44	1.57	0.00	0.00	0.01	0.69	1.37	0.94	0.00	0.00	0.01
Zn	0.00	0.00	0.00	0.00	0.00	0.00	0.00	0.00	0.00	0.00	0.00	0.00
Ca	0.00	0.00	0.00	0.32	0.10	0.00	0.15	0.00	0.00	0.28	0.00	0.00
Na	0.01	0.01	0.01	0.72	0.36	0.00	0.00	0.01	0.00	0.71	0.21	0.00
K	0.88	0.88	0.00	0.01	0.58	0.00	0.00	0.95	0.00	0.02	0.81	0.00
Cl	0.01	0.01	0.00	0.00	0.00	0.00	0.00	0.00	0.00	0.00	0.00	0.00
F	0.11	0.08	0.00	0.00	0.00	0.01	0.00	0.00	0.00	0.00	0.00	0.00
Total cations	**7.75**	**7.75**	**11.04**	**5.03**	**5.04**	**2.00**	**8.00**	**7.81**	**4.00**	**5.00**	**5.01**	**2.00**

APPENDIX C: T–X FORWARD MODELS

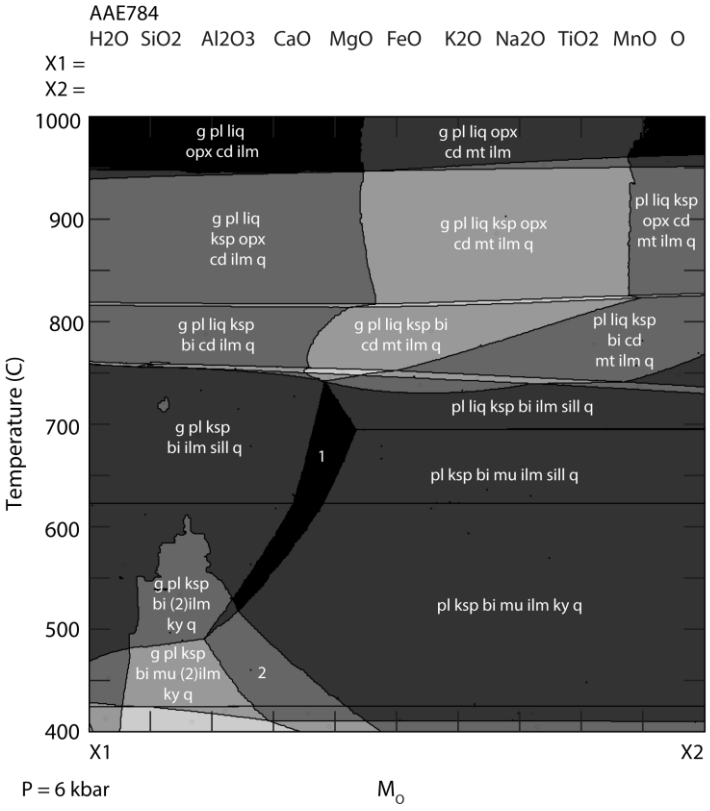

1. pl ksp bi ilm sill q
2. pl ksp bi mu (2)ilm ky q

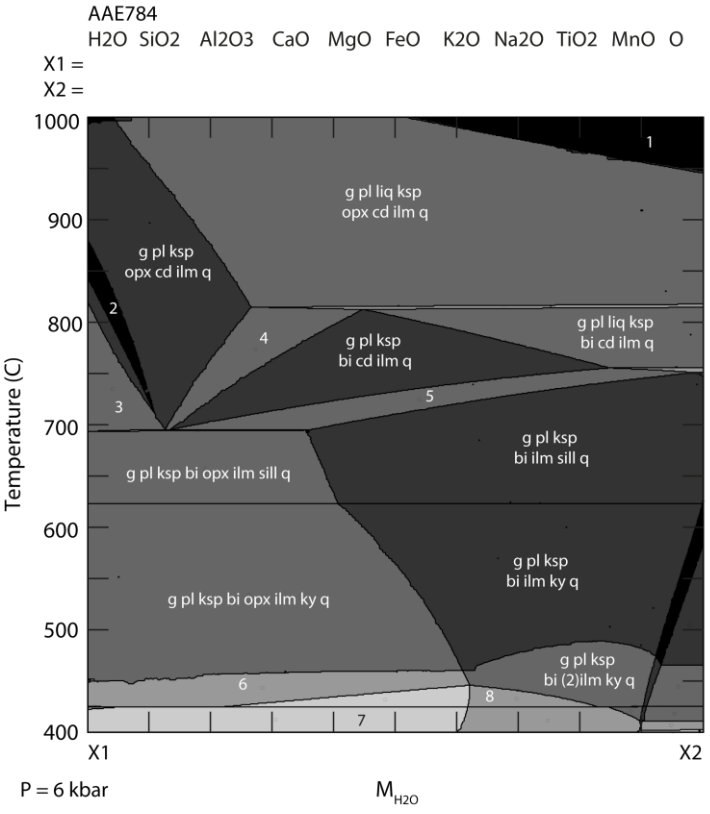

1. g pl liq opx cd ilm
2. g pl ksp cd ilm q
3. g pl ksp opx cd ilm sill q
4. g pl ksp bi opx cd ilm q
5. g pl ksp bi cd ilm sill q
6. g pl ksp bi opx (2)ilm ky q
7. g pl bi opx (2) ilm ky ab mic q
8. g pl ksp bi (2)ilm ky ab q

AAE980

	H2O	SiO2	Al2O3	CaO	MgO	FeO	K2O	Na2O	TiO2	MnO	O
X1 =	4.87	49.38	13.88	3.81	8.99	13.76	1.25	2.95	0.78	0.31	0.00
X2 =	5.12	51.88	14.58	4.00	9.44	14.46	1.32	3.10	0.82	0.33	5.06

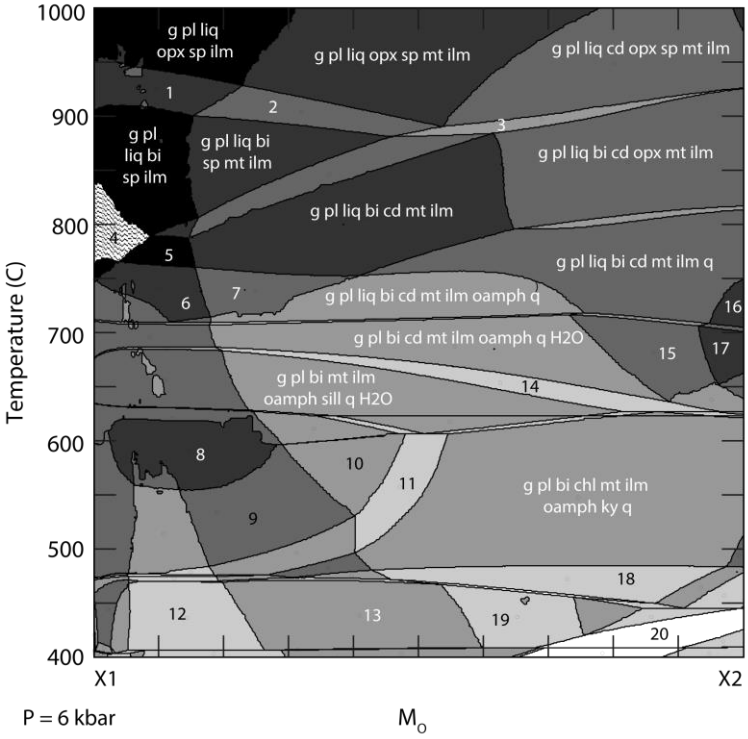

1. g pl liq bi opx mt ilm
2. g pl liq bi opx sp mt ilm
3. g pl liq bi cd opx sp mt ilm
4. g pl liq bi ilm
5. g pl liq bi cd ilm
6. g pl liq bi cd ilm oamph
7. g pl liq bi cd mt ilm oamph
8. g pl bi st ilm oamph q
9. g pl bi chl st oamph q
10. g pl bi chl st mt oamph q
11. g pl bi chl st mt oamph ky q
12. g pl ep bi (2)ilm oamph ky pa q
13. g pl ep bi ilm oamph ky pa q
14. g pl bi cd mt ilm oamph sill q H2O
15. g pl bi cd mt ilm q H2O
16. pl liq bi cd mt ilm q
17. pl bi cd mt ilm q H2O
18. g pl ep bi chl mt ilm oamph ky q
19. g pl ep bi mt ilm oamph ky pa q
20. g pl ep bi mt ilm oamph ky parg pa q

AAE980

	H2O	SiO2	Al2O3	CaO	MgO	FeO	K2O	Na2O	TiO2	MnO	O
X1 =	0.01	52.02	14.62	4.01	9.47	14.50	1.32	3.11	0.83	0.33	0.22
X2 =	4.88	49.49	13.91	3.82	9.01	13.79	1.26	2.95	0.79	0.31	0.21

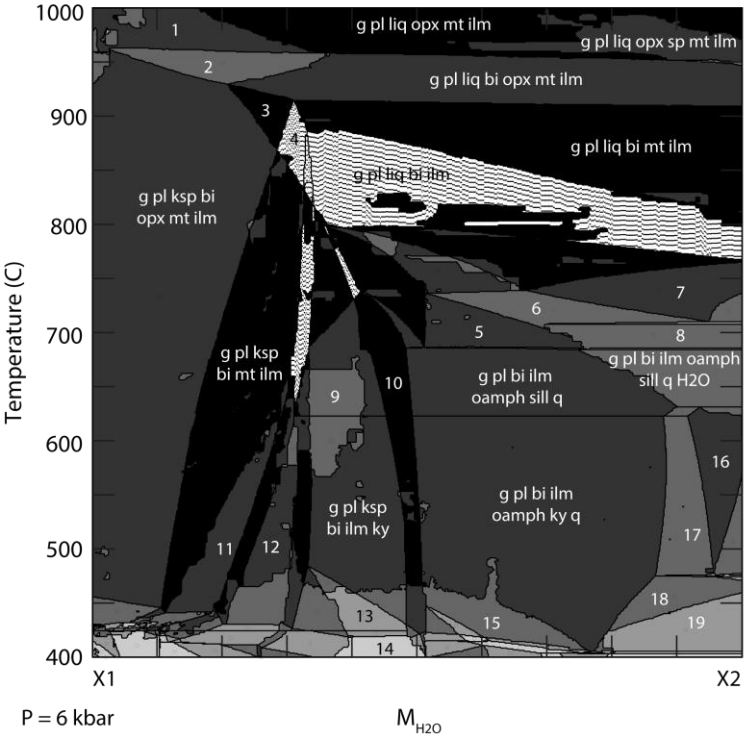

1. g pl liq ksp opx mt ilm
2. g pl liq ksp bi opx mt ilm
3. g pl bi opx mt ilm
4. g pl bi sp ilm
5. g pl bi cd ilm oamph q
6. g pl liq bi cd ilm oamph q
7. g pl liq bi cd ilm oamph
8. g pl bi cd ilm oamph H2O
9. g pl ksp bi (2) ilm sill q
10. g pl bi ilm sill q
11. g pl ksp bi mt ilm cor
12. g pl ksp bi ilm ky cor
13. g pl ksp bi opx (2)ilm ky q
14. g pl bi opx (2)ilm ky ab mic q
15. g pl bi (2)ilm oamph ky q
16. g pl bi st ilm oamph q
17. g pl bi st ilm oamph ky q
18. g pl bi ilm oamph ky pa q
19. g pl ep bi ilm oamph ky pa q

RB2012-02

	H2O	SiO2	Al2O3	CaO	MgO	FeO	K2O	Na2O	TiO2	MnO	O
X1 =	2.05	74.01	7.64	2.25	2.77	5.91	2.01	2.60	0.65	0.10	0.00
X2 =	2.10	75.57	7.81	2.30	2.83	6.04	2.05	2.66	0.66	0.10	2.11

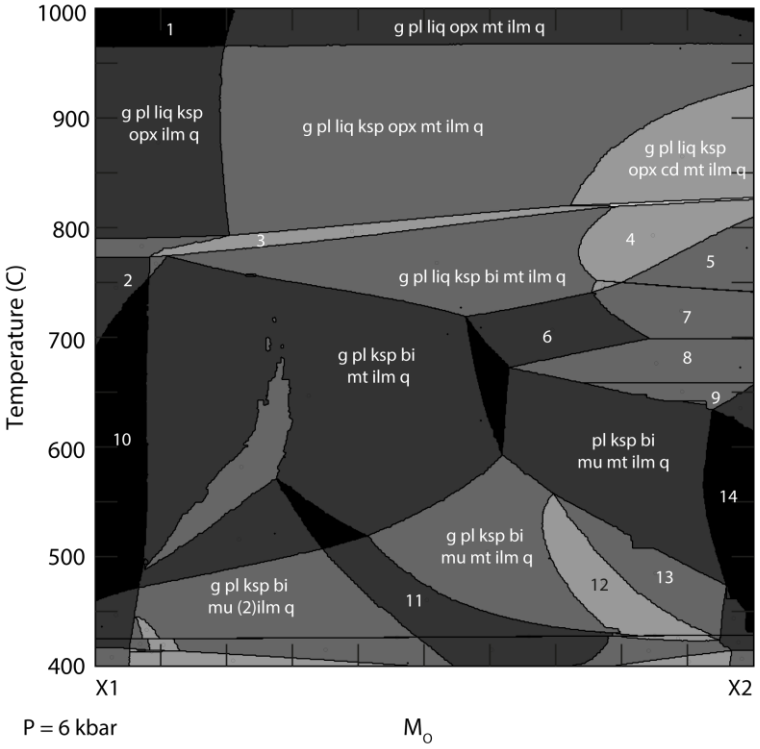

1. g pl liq opx ilm q
2. g pl ksp bi opx ilm q
3. g pl liq ksp bi opx mt ilm q
4. g pl liq ksp bi cd mt ilm q
5. pl liq ksp bi cd mt ilm q
6. pl liq ksp bi mt ilm q
7. pl liq ksp bi mt ilm sill q
8. pl liq ksp bi mu mt ilm q
9. pl ksp bi mu mt ilm q H2O
10. g pl ksp bi ilm q
11. g pl ksp bi mu ilm q
12. g pl ksp bi mu mt ilm ky q
13. pl ksp bi mu mt ilm ky q

RB2012-02

	H2O	SiO2	Al2O3	CaO	MgO	FeO	K2O	Na2O	TiO2	MnO	O
X1 =	0.01	76.41	7.89	2.32	2.86	6.10	2.08	2.69	0.67	0.10	1.13
X2 =	2.08	74.83	7.73	2.28	2.80	5.98	2.03	2.63	0.65	0.10	1.11

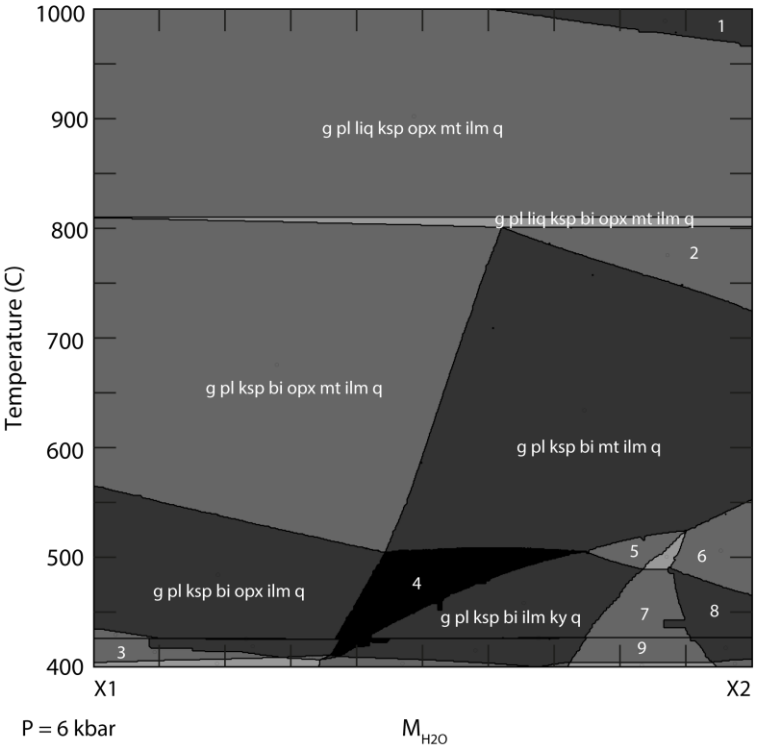

1. g pl liq opx mt ilm q
2. g pl liq ksp bi mt ilm q
3. g pl bi opx ilm ky mic q
4. g pl ksp bi ilm q
5. g pl ksp bi mt ilm ky q
6. g pl ksp bi mu mt ilm q
7. g pl ksp bi mu ilm ky q
8. g pl ksp bi mu ilm q
9. g pl bi mu ilm ky mic q

RB2012-03

	H2O	SiO2	Al2O3	CaO	MgO	FeO	K2O	Na2O	TiO2	MnO	O
X1 =	8.26	47.40	9.06	2.11	11.76	14.70	3.08	1.56	1.92	0.15	0.00
X2 =	8.70	49.97	9.55	2.23	12.40	15.50	3.25	1.65	2.03	0.16	5.42

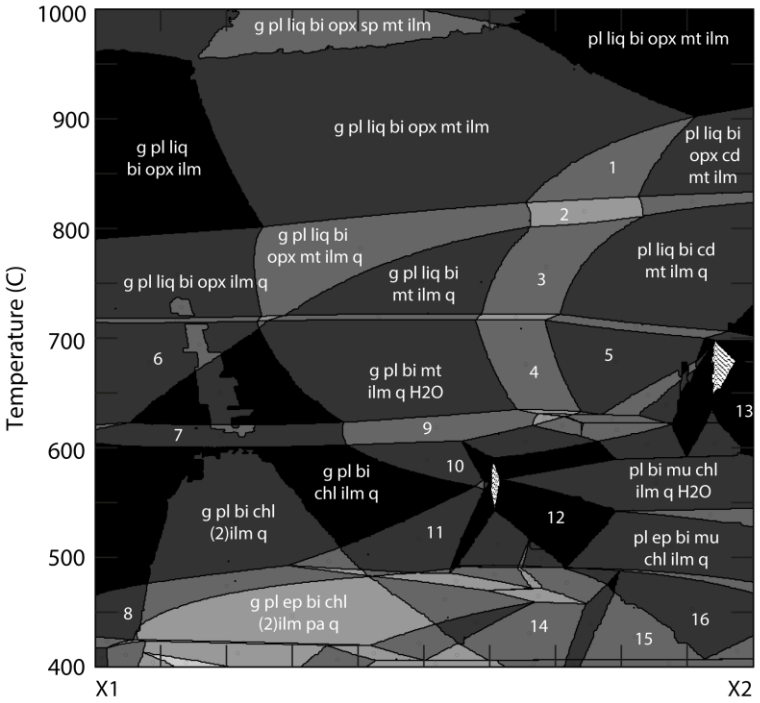

P = 6 kbar M_O

1. g pl liq bi opx cd mt ilm
2. g pl liq bi cd opx mt ilm q
3. g pl liq bi cd mt ilm q
4. g pl bi cd mt ilm q H2O
5. pl bi cd mt ilm q H2O
6. g pl bi opx ilm q H2O
7. g pl bi chl ilm q H2O
8. g pl bi chl ilm pa q
9. g pl bi chl sp ilm q H2O
10. g pl bi chl mt ilm q
11. g pl bi st chl ilm q
12. pl bi mu chl ilm q
13. pl bi mu ilm q H2O
14. g pl ep bi ilm ky pa q
15. pl ep bi mu ilm ky pa q
16. pl ep bi mu ilm pa q

RB2012-03

	H2O	SiO2	Al2O3	CaO	MgO	FeO	K2O	Na2O	TiO2	MnO	O
X1 =	0.01	52.49	10.03	2.34	13.03	16.28	3.41	1.73	2.13	0.16	1.61
X2 =	8.38	48.1	9.20	2.14	11.93	14.92	3.12	1.59	1.95	0.15	1.48

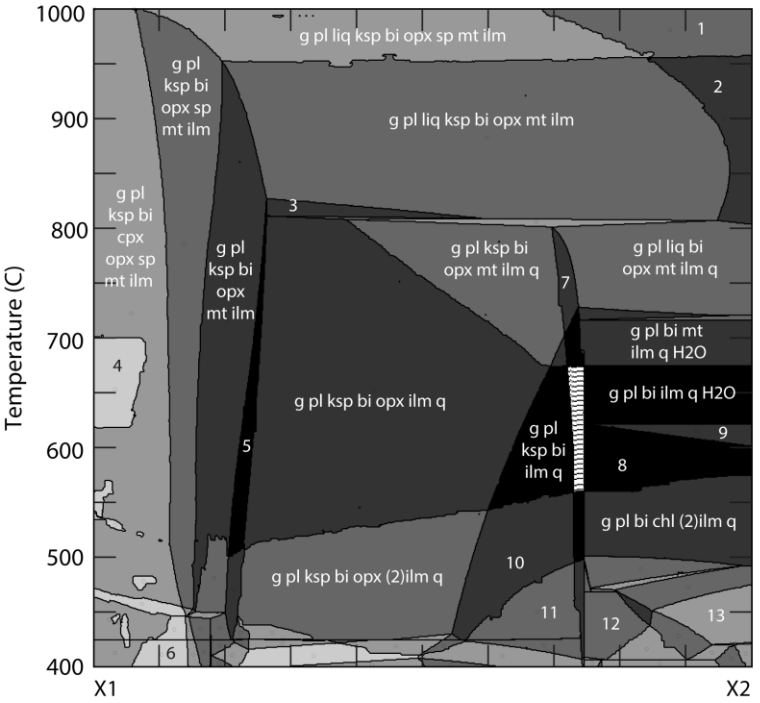

P = 6 kbar M_{H2O}

1. g pl liq bi opx sp mt ilm
2. g pl liq bi opx mt ilm
3. g pl liq ksp bi opx ilm
4. g pl ksp cpx opx (2)sp mt ilm
5. g pl ksp bi opx ilm
6. g bi cpx opx sp mt (2)ilm ab mic
7. g pl bi opx mt ilm q
8. g pl bi chl ilm q
9. g pl bi chl ilm q H2O
10. g pl ksp bi (2)ilm q
11. g pl ksp bi (2)ilm ky q
12. g pl bi (2)ilm ky pa q
13. g pl ep bi chl (2)ilm pa q

AAE907

	H2O	SiO2	Al2O3	CaO	MgO	FeO	K2O	Na2O	TiO2	MnO	O
X1 =	1.21	72.90	8.36	1.89	4.23	16.04	0.48	1.29	0.16	1.31	7.86
X2 =	1.12	67.58	7.75	1.75	3.92	14.87	0.45	1.20	0.15	1.21	0.00

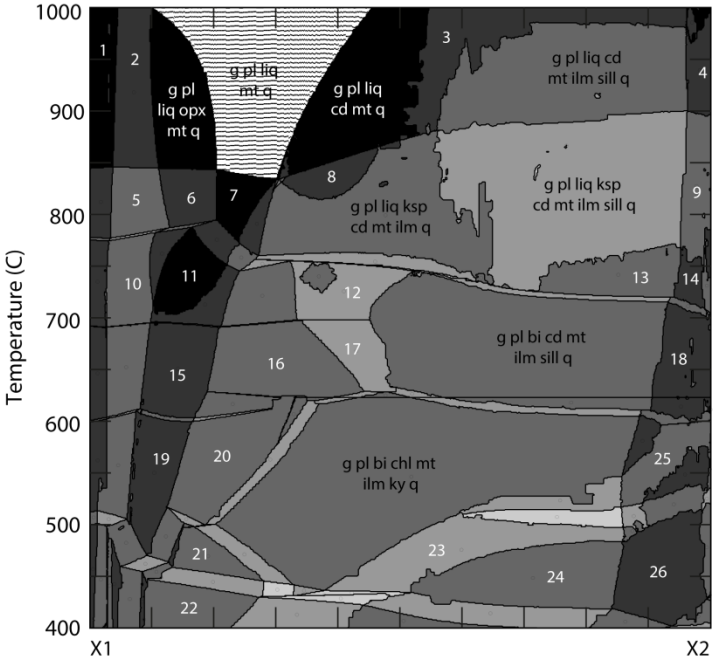

P = 6 kbar M_O

1. g pl liq opx ilm q
2. g pl liq opx mt ilm q
3. g pl liq cd mt ilm q
4. g pl liq cd ilm sill q
5. g pl liq ksp opx mt ilm q
6. g pl liq ksp opx mt q
7. g pl liq ksp mt q
8. g pl liq ksp cd mt q
9. g pl liq ksp cd ilm sill q
10. g pl liq bi opx mt ilm q
11. g pl liq bi mt q
12. g pl liq bi cd mt ilm sill q
13. g pl ksp cd mt ilm sill q
14. g pl ksp cd ilm sill q
15. g pl bi mt ilm q H2O
16. g pl bi mt ilm sill q H2O
17. g pl bi cd mt ilm sill q H2O
18. g pl bi cd ilm sill q
19. g pl bi chl mt ilm q
20. g pl bi st chl mt ilm q
21. g pl bi mt ilm ky pa q
22. g bi mt ilm pa ab ky q
23. g pl bi chl mt ilm parg ky q
24. g pl bi mt ilm parg ky q
25. g pl bi chl ilm ta ky q
26. g pl bi ilm parg ky q

AAE907

	H2O	SiO2	Al2O3	CaO	MgO	FeO	K2O	Na2O	TiO2	MnO	O
X1 =	0.01	72.14	8.27	1.87	4.19	15.87	0.48	1.28	0.16	1.29	5.55
X2 =	1.18	71.29	8.18	1.85	4.14	15.68	0.47	1.26	0.15	1.28	5.49

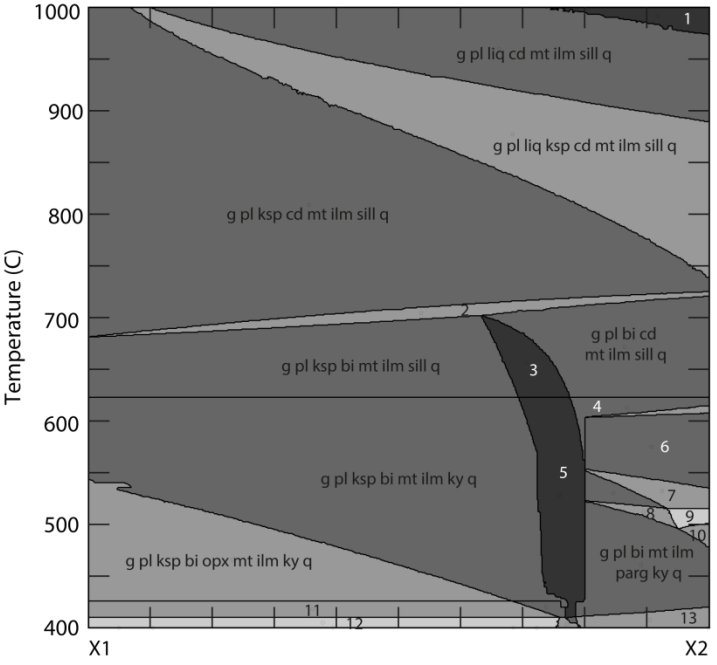

P = 6 kbar M_{H2O}

1. g pl liq cd mt ilm q
2. g pl ksp bi cd mt ilm sill q
3. g pl bi mt ilm sill q
4. g pl liq bi cd mt ilm ky q
5. g pl bi mt ilm ky q
6. g pl bi chl mt ilm ky q
7. g pl bi chl mt ilm ta ky q
8. g pl bi mt ilm parg ta ky q
9. g pl bi chl mt ilm parg ta ky q
10. g pl bi chl mt ilm parg ky q
11. g pl ksp bi opx mt ilm mic ky q
12. g pl ksp bi opx mt ilm ab mic ky q
13. g pl bi mt ilm parg ab ky q

AAE1233

	H2O	SiO2	Al2O3	CaO	MgO	FeO	K2O	Na2O	TiO2	MnO	O
X1 =	1.43	69.04	9.79	0.73	4.58	9.51	3.10	0.81	0.68	0.33	0.00
X2 =	1.47	71.42	0.12	0.75	4.73	9.84	3.21	0.84	0.71	0.35	3.44

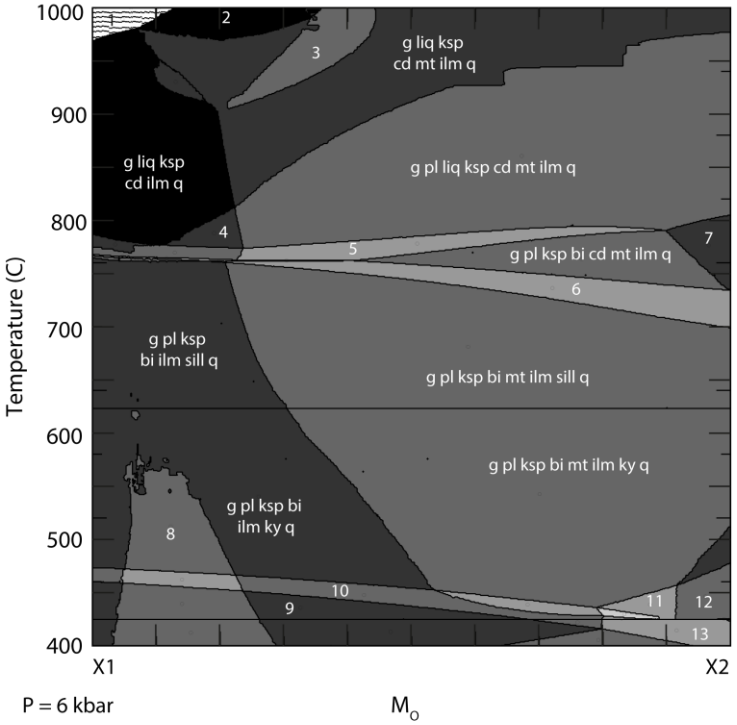

1. g liq ksp ilm q
2. g liq ksp mt ilm q
3. g liq ksp cd sp mt ilm q
4. g pl liq ksp cd ilm q
5. g pl liq ksp bi cd mt ilm q
6. g pl ksp bi cd mt ilm sill q
7. g pl liq cd mt ilm q
8. g pl ksp bi (2)ilm ky q
9. g pl bi ilm ky ab q
10. g pl ksp bi ilm ky ab q
11. g pl ksp bi opx mt ilm ky q
12. g pl ksp bi opx ilm ky q
13. g pl bi opx ilm ky ab mic q

P = 6 kbar M_O

AAE1233

	H2O	SiO2	Al2O3	CaO	MgO	FeO	K2O	Na2O	TiO2	MnO	O
X1 =	0.01	70.37	9.98	0.74	4.66	9.69	3.16	0.82	0.70	0.34	0.48
X2 =	1.43	69.37	9.83	0.73	4.60	9.56	3.12	0.81	0.69	0.34	0.48

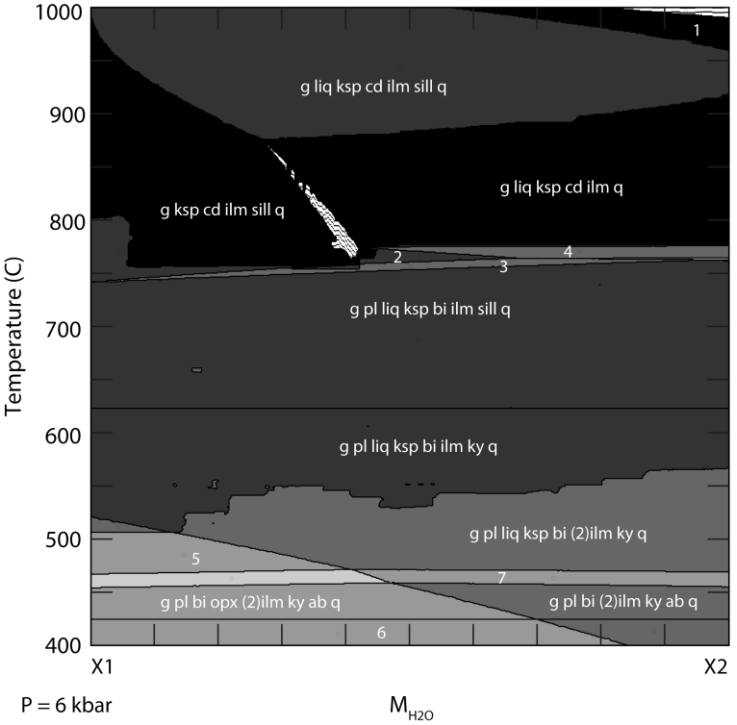

1. g liq ksp cd ilm q
2. g pl ksp bi cd ilm q
3. g pl ksp bi cd ilm sill q
4. g pl liq ksp bi cd ilm q
5. g pl ksp bi opx (2)ilm ky q
6. g bi opx (2)ilm ky ab mic q
7. g pl ksp bi (2ilm) ky ab q

P = 6 kbar M_{H2O}

APPENDIX D: LA–ICP–MS MONAZITE U–PB GEOCHRONOLOGY SAMPLE ANALYSES

Set	Analysis	207Pb/ 206Pb	1σ	206Pb/ 238U	1σ	207Pb/ 235U	1σ	% Conc.	207Pb/ 206Pb age (Ma)	1σ	206Pb/ 238U age (Ma)	1σ	207Pb/ 235U age (Ma)	1σ	204Pb/ 206Pb (%)	Rho (ρ)	Reason for omission
757	757-01	0.144	0.0017	0.425	0.006	8.409	0.119	101	2271	20.06	2282.8	25.67	2276.1	12.87	0.000	0.6401	
757	757-02	0.151	0.0018	0.428	0.006	8.907	0.128	98	2356.3	20.24	2298.1	25.93	2328.6	13.13	0.000	0.6339	
757	757-03	0.145	0.0021	0.394	0.005	7.887	0.126	93	2291.5	24.4	2140.1	25.01	2218.2	14.39	0.011	0.5446	conc. <95%
757	757-04	0.150	0.0025	0.405	0.006	8.403	0.151	93	2351.3	28.2	2192.5	26.73	2275.5	16.32	0.041	0.4876	conc. <95%
757	757-05	0.147	0.0019	0.414	0.006	8.404	0.127	96	2316.3	21.9	2231.9	25.9	2275.7	13.75	0.034	0.6059	
784-1	784-01	0.160	0.0017	0.482	0.007	10.594	0.164	103	2450.6	17.81	2535.6	32.06	2488.2	14.34	0.001	0.7626	
784-1	784-02	0.156	0.0017	0.448	0.007	9.650	0.149	99	2415.5	18.05	2387.1	30.46	2401.9	14.24	0.001	0.7583	
784-1	784-03	0.156	0.0016	0.456	0.007	9.796	0.151	100	2413.4	17.78	2419.8	30.9	2415.8	14.23	0.001	0.7668	
784-1	784-04	0.158	0.0017	0.469	0.007	10.209	0.159	102	2435	17.99	2478	31.57	2453.9	14.38	0.001	0.7604	
784-1	784-05	0.159	0.0017	0.457	0.007	9.984	0.156	99	2439.9	17.99	2426.4	31.12	2433.3	14.38	0.000	0.7629	
784-1	784-06	0.150	0.0017	0.440	0.007	9.071	0.143	100	2340.9	18.9	2351	30.28	2345.2	14.47	0.000	0.7469	
784-2	784-07	0.154	0.0020	0.444	0.006	9.419	0.143	99	2388.9	21.76	2369.7	27.77	2379.7	13.89	0.017	0.6121	
784-2	784-08	0.154	0.0022	0.419	0.006	8.883	0.138	94	2388.8	23.64	2256	26.49	2326.1	14.2	0.000	0.5551	conc. <95%
784-2	784-09	0.157	0.0016	0.444	0.006	9.598	0.130	98	2422.4	17.29	2368.2	27.02	2396.9	12.47	0.006	0.7151	
784-2	784-10	0.154	0.0016	0.474	0.007	10.092	0.138	104	2395.7	17.5	2501.9	28.44	2443.2	12.61	0.004	0.7131	
784-2	784-11	0.154	0.0016	0.495	0.007	10.514	0.143	108	2393.3	17.41	2591	29.29	2481.2	12.58	0.003	0.7147	conc. >105%
784-2	784-12	0.153	0.0018	0.506	0.007	10.661	0.150	111	2378.9	19.44	2638.7	29.5	2494.1	13.07	0.001	0.6554	conc. >105%
784-2	784-13	0.150	0.0017	0.444	0.006	9.188	0.127	101	2348.1	18.72	2368	26.9	2356.9	12.68	0.005	0.6795	
784-2	784-14	0.154	0.0017	0.435	0.006	9.208	0.130	98	2386.5	18.8	2328.3	26.9	2358.9	12.96	0.011	0.6822	
784-2	784-15	0.153	0.0016	0.496	0.007	10.419	0.144	109	2375.1	17.85	2594.7	29.58	2472.8	12.84	0.000	0.7098	conc. >105%
784-2	784-16	0.158	0.0017	0.447	0.006	9.740	0.134	98	2436.5	17.65	2381.1	27.25	2410.5	12.66	0.000	0.7078	
784-3	784-17	0.157	0.0016	0.477	0.006	10.326	0.138	104	2426	17.39	2512.2	28.03	2464.4	12.4	0.000	0.7057	
784-3	784-18	0.155	0.0018	0.450	0.006	9.626	0.139	100	2403.5	19.7	2396.4	27.6	2399.6	13.25	0.016	0.6584	
784-4	784-19	0.154	0.0018	0.475	0.007	10.081	0.144	105	2391.1	19.17	2505.1	28.75	2442.2	13.18	0.032	0.6738	
784-4	784-20	0.154	0.0017	0.503	0.007	10.660	0.150	110	2389.6	18.83	2625.2	29.72	2493.9	13.08	0.028	0.6825	conc. >105%
Set	Analysis	207Pb/ 206Pb	1σ	206Pb/ 238U	1σ	207Pb/ 235U	1σ	% Conc.	207Pb/ 206Pb age (Ma)	1σ	206Pb/ 238U age (Ma)	1σ	207Pb/ 235U age (Ma)	1σ	204Pb/ 206Pb (%)	Rho (ρ)	Reason for omission

784-4	784-21	0.155	0.0022	0.454	0.007	9.705	0.158	100	2403.3	24.01	2413.3	29.1	2407.2	14.94	0.078	0.5741	
784-4	784-22	0.158	0.0017	0.460	0.006	10.035	0.137	100	2439.1	17.52	2437.6	27.55	2438	12.57	0.000	0.7066	
784-4	784-23	0.159	0.0017	0.455	0.006	9.941	0.136	99	2441.8	17.7	2415.3	27.41	2429.3	12.65	0.002	0.7031	
784-4	784-24	0.154	0.0018	0.447	0.006	9.481	0.134	100	2391.6	19.19	2380.3	27.09	2385.7	12.97	0.003	0.6652	
784-4	784-25	0.157	0.0017	0.455	0.006	9.832	0.137	100	2423.2	18.37	2415.5	27.42	2419.2	12.86	0.000	0.6880	
784-4	784-26	0.157	0.0016	0.455	0.006	9.843	0.134	100	2421.9	17.62	2419.2	27.27	2420.2	12.53	0.000	0.7027	
784-4	784-27	0.155	0.0018	0.460	0.006	9.831	0.138	102	2402.6	19.01	2439.9	27.61	2419.1	12.94	0.037	0.6665	
784-4	784-28	0.157	0.0016	0.493	0.007	10.667	0.144	106	2425.4	17.25	2581.5	28.83	2494.6	12.53	0.000	0.7134	conc. >105%
784-5	784-29	0.156	0.0016	0.484	0.007	10.395	0.138	106	2410.4	16.99	2545.6	28.42	2470.6	12.27	0.000	0.7163	conc. >105%
784-5	784-30	0.159	0.0016	0.498	0.007	10.895	0.146	107	2441	17.02	2607	29.1	2514.2	12.44	0.001	0.7198	conc. >105%
784-5	784-31	0.156	0.0020	0.461	0.007	9.918	0.150	101	2414.7	21.28	2442.9	28.71	2427.2	13.98	0.044	0.6311	
784-5	784-32	0.162	0.0021	0.475	0.007	10.576	0.163	101	2472.6	21.54	2504.5	29.44	2486.6	14.28	0.017	0.6241	
784-5	980-01	0.157	0.0019	0.390	0.005	8.430	0.122	88	2422.3	19.9	2122.5	25.19	2278.4	13.18	0.092	0.6570	conc. <95%
784-5	980-02	0.154	0.0018	0.479	0.007	10.166	0.146	105	2391.4	19.58	2522.4	29.02	2450	13.31	0.000	0.6672	conc. >105%
784-5	980-03	0.154	0.0017	0.507	0.007	10.730	0.154	111	2386.4	18.71	2643.5	30.38	2500	13.29	0.000	0.6945	conc. >105%
784-5	980-04	0.144	0.0018	0.414	0.006	8.188	0.125	98	2271.8	21.07	2231.2	27.07	2252	13.81	0.000	0.6556	
784-5	980-05	0.153	0.0019	0.451	0.006	9.478	0.145	101	2374.6	21.56	2399.1	28.46	2385.4	14.06	0.000	0.6306	
784-5	980-06	0.157	0.0017	0.504	0.007	10.880	0.151	109	2420.4	18.11	2630.4	29.62	2513	12.88	0.002	0.6975	conc. >105%
980	980-07	0.156	0.0016	0.457	0.007	9.807	0.150	101	2409.6	17.23	2426.4	31.17	2416.9	14.08	0.000	0.7789	
980	980-08	0.159	0.0016	0.469	0.007	10.254	0.157	102	2441	17.26	2479.4	31.72	2457.9	14.18	0.001	0.7766	
980	980-09	0.158	0.0016	0.459	0.007	10.024	0.154	100	2437.7	17.35	2437.1	31.34	2437	14.2	0.001	0.7770	
980	980-10	0.159	0.0016	0.462	0.007	10.124	0.156	100	2443.5	17.37	2450.3	31.47	2446.1	14.22	0.000	0.7756	
980	980-11	0.159	0.0017	0.474	0.007	10.392	0.161	102	2447.7	17.82	2498.9	32.02	2470.4	14.37	0.003	0.7652	
980	980-12	0.157	0.0016	0.458	0.007	9.915	0.153	100	2423.2	17.64	2432.4	31.26	2426.9	14.24	0.000	0.7708	
980	980-13	0.158	0.0016	0.447	0.007	9.752	0.151	98	2438.9	17.46	2380.3	30.77	2411.6	14.22	0.002	0.7754	

Set	Analysis	207Pb/ 206Pb	1σ	206Pb/ 238U	1σ	207Pb/ 235U	1σ	% Conc.	207Pb/ 206Pb age (Ma)	1σ	206Pb/ 238U age (Ma)	1σ	207Pb/ 235U age (Ma)	1σ	204Pb/ 206Pb (%)	Rho (ρ)	Reason for omission
980	980-14	0.152	0.0016	0.439	0.007	9.174	0.142	99	2363.7	17.67	2346.9	30.36	2355.5	14.14	0.001	0.7721	
980	980-15	0.159	0.0017	0.470	0.007	10.326	0.160	101	2449.5	17.6	2483.4	31.79	2464.4	14.31	0.001	0.7699	
980	980-16	0.158	0.0017	0.455	0.007	9.932	0.155	99	2438.6	17.92	2417.3	31.14	2428.5	14.38	0.001	0.7637	
980-2	980-17	0.156	0.0016	0.481	0.007	10.314	0.143	105	2409.7	17.51	2530	28.85	2463.4	12.8	0.000	0.7163	
980-2	980-18	0.157	0.0017	0.487	0.007	10.570	0.151	105	2428.9	18.46	2557.7	29.28	2486.1	13.21	0.003	0.6951	conc. >105%
980-2	980-19	0.158	0.0021	0.455	0.007	9.908	0.155	99	2433.4	22.05	2418.9	29.13	2426.3	14.46	0.099	0.6240	
980-2	980-20	0.160	0.0017	0.503	0.007	11.109	0.155	107	2459.8	17.38	2624.9	29.95	2532.3	12.98	0.000	0.7233	conc. >105%
980-2	980-21	0.113	0.0013	0.349	0.005	5.427	0.081	105	1843.3	21.25	1931.9	23.58	1889.1	12.8	0.000	0.6715	
980-2	980-22	0.156	0.0016	0.496	0.007	10.664	0.150	108	2413.2	17.74	2596.4	29.58	2494.3	13.01	0.000	0.7153	conc. >105%
980-2	980-23	0.159	0.0017	0.494	0.007	10.822	0.152	106	2443.7	17.5	2589.1	29.72	2507.9	13.05	0.000	0.7244	conc. >105%
RB02-1	RB02-01	0.104	0.0012	0.319	0.004	4.597	0.062	105	1704.6	21.74	1786.7	19.11	1748.7	11.17	0.015	0.5744	
RB02-1	RB02-02	0.104	0.0015	0.301	0.004	4.301	0.066	100	1694.7	26.1	1693.8	18.93	1693.6	12.58	0.017	0.4940	
RB02-1	RB02-03	0.103	0.0014	0.302	0.004	4.297	0.063	101	1685.5	24.67	1699.6	18.94	1692.7	12.14	0.000	0.5272	
RB02-1	RB02-04	0.104	0.0014	0.298	0.004	4.270	0.064	99	1694.7	25.41	1682.7	18.82	1687.6	12.36	0.000	0.5108	
RB02-1	RB02-05	0.104	0.0013	0.300	0.004	4.323	0.061	99	1704.5	23.19	1693.2	18.41	1697.7	11.61	0.004	0.5421	
RB02-2	RB02-06	0.104	0.0011	0.295	0.004	4.228	0.057	98	1697.2	19.76	1666.1	19.54	1679.5	11.15	0.000	0.6791	
RB02-2	RB02-07	0.105	0.0017	0.303	0.004	4.369	0.079	100	1708.4	30.28	1705.7	21.75	1706.4	14.89	0.000	0.4955	
RB02-2	RB02-08	0.104	0.0011	0.296	0.004	4.242	0.058	99	1694.2	19.36	1673.5	20.01	1682.2	11.28	0.000	0.6989	
RB02-2	RB02-09	0.105	0.0015	0.304	0.004	4.401	0.070	100	1714.7	25.55	1711.4	20.97	1712.4	13.22	0.000	0.5698	
RB02-2	RB02-10	0.105	0.0013	0.289	0.004	4.171	0.060	96	1711.2	21.91	1635.1	19.59	1668.3	11.84	0.000	0.6339	
RB02-2	RB02-11	0.103	0.0013	0.285	0.004	4.049	0.060	96	1681.8	22.84	1615.7	19.44	1644.2	12.02	0.000	0.6134	
RB02-2	RB02-12	0.105	0.0012	0.304	0.004	4.387	0.061	100	1711.5	20.78	1709.4	20.08	1709.9	11.54	0.016	0.6558	
RB02-2	RB02-13	0.105	0.0013	0.304	0.004	4.408	0.066	100	1717	23.2	1712.2	20.54	1713.9	12.39	0.000	0.6073	
RB02-2	RB02-14	0.104	0.0015	0.298	0.004	4.278	0.068	99	1700.7	25.55	1680.7	20.54	1689.1	13.08	0.000	0.5641	
RB02-2	RB02-15	0.103	0.0012	0.291	0.004	4.142	0.057	97	1686.8	20.55	1644.3	19.32	1662.6	11.3	0.016	0.6589	

Set	Analysis	207Pb/ 206Pb	1σ	206Pb/ 238U	1σ	207Pb/ 235U	1σ	% Conc.	207Pb/ 206Pb age (Ma)	1σ	206Pb/ 238U age (Ma)	1σ	207Pb/ 235U age (Ma)	1σ	204Pb/ 206Pb (%)	Rho (ρ)	Reason for omission
526	526-01	0.111	0.0018	0.318	0.004	4.883	0.085	98	1819.7	28.96	1781.4	21.81	1799.3	14.72	0.079	0.4954	
526	526-02	0.105	0.0012	0.309	0.004	4.458	0.063	102	1709.3	21.7	1735.6	19.84	1723.2	11.69	0.000	0.6218	
526	526-03	0.105	0.0012	0.301	0.004	4.368	0.061	99	1717.4	21.26	1698.1	19.42	1706.3	11.53	0.013	0.6257	
526	526-04	0.104	0.0012	0.294	0.004	4.228	0.060	97	1705.2	21.77	1659.7	19.11	1679.4	11.64	0.007	0.6225	
526	100-01	0.105	0.0014	0.310	0.004	4.467	0.069	102	1707.5	24.59	1739.9	20.47	1724.8	12.77	0.007	0.5696	
526	100-02	0.106	0.0014	0.300	0.004	4.371	0.066	98	1727.2	24.02	1691.3	19.87	1706.9	12.57	0.030	0.5834	
526	100-03	0.105	0.0013	0.307	0.004	4.468	0.065	100	1722.7	22.5	1727.8	20.04	1725	12.11	0.000	0.6110	
526	100-04	0.106	0.0014	0.309	0.004	4.512	0.070	100	1733.8	24.67	1733.6	20.43	1733.1	12.91	0.000	0.5694	
526	100-05	0.104	0.0013	0.303	0.004	4.363	0.064	100	1705.4	22.51	1706.1	20.05	1705.3	12.12	0.000	0.6156	
612-1	612-01	0.155	0.0018	0.518	0.007	11.041	0.162	112	2397.6	19.88	2691.3	30.46	2526.6	13.65	0.000	0.6601	conc. >105%
612-1	612-02	0.105	0.0012	0.310	0.004	4.502	0.065	101	1718.4	20.87	1743	20.9	1731.4	12	0.006	0.6727	
612-1	612-03	0.105	0.0012	0.307	0.004	4.426	0.064	101	1707.1	20.96	1726.2	20.74	1717.1	12	0.000	0.6702	
612-1	612-04	0.105	0.0014	0.333	0.005	4.823	0.076	108	1713.8	23.95	1855.1	22.45	1789	13.24	0.000	0.6133	conc. >105%
612-1	612-05	0.104	0.0012	0.312	0.004	4.488	0.065	103	1701	21.01	1752.7	21.06	1728.8	12.06	0.000	0.6691	
612-1	612-06	0.155	0.0018	0.511	0.007	10.924	0.161	111	2404.4	19.88	2659.3	30.13	2516.7	13.7	0.000	0.6608	conc. >105%
612-2	612-07	0.104	0.0012	0.320	0.004	4.602	0.062	105	1703.8	21.36	1789.2	19.2	1749.7	11.15	0.000	0.5879	conc. >105%
612-2	612-08	0.106	0.0013	0.307	0.004	4.477	0.062	100	1726.4	22.21	1727.6	18.73	1726.6	11.42	0.007	0.5678	
612-2	612-09	0.104	0.0013	0.314	0.004	4.497	0.063	104	1697.8	22.62	1758.3	19.07	1730.4	11.58	0.000	0.5615	
612-3	612-10	0.104	0.0012	0.308	0.004	4.420	0.059	102	1701	20.26	1729.1	19.54	1716	11.12	0.002	0.6487	
612-3	612-11	0.156	0.0021	0.470	0.006	10.103	0.152	103	2413.7	22.58	2482.1	27.47	2444.2	13.92	0.000	0.5612	
612-3	612-12	0.105	0.0012	0.320	0.004	4.620	0.062	105	1709.4	20.2	1790.4	20.11	1752.9	11.23	0.004	0.6465	
612-3	612-13	0.104	0.0012	0.311	0.004	4.474	0.062	103	1703.1	21.31	1746.1	19.66	1726.2	11.48	0.000	0.6185	
612-3	612-14	0.105	0.0012	0.306	0.004	4.427	0.062	100	1716.1	21.47	1719.4	19.56	1717.5	11.57	0.000	0.6183	
612-3	612-15	0.104	0.0012	0.310	0.004	4.429	0.060	103	1693.7	20.56	1738.5	19.65	1717.8	11.26	0.001	0.6390	
612-3	612-16	0.104	0.0012	0.301	0.004	4.335	0.061	100	1705	21.67	1696.7	19.37	1700	11.6	0.000	0.6174	

Set	Analysis	207Pb/ 206Pb	1σ	206Pb/ 238U	1σ	207Pb/ 235U	1σ	% Conc.	207Pb/ 206Pb age (Ma)	1σ	206Pb/ 238U age (Ma)	1σ	207Pb/ 235U age (Ma)	1σ	204Pb/ 206Pb (%)	Rho (ρ)	Reason for omission
612-3	612-17	0.105	0.0013	0.306	0.004	4.445	0.063	100	1720.6	21.79	1721.7	19.71	1720.8	11.75	0.011	0.6166	
612-3	612-18	0.105	0.0013	0.300	0.004	4.352	0.061	98	1720.6	21.64	1690.1	19.32	1703.3	11.63	0.001	0.6190	
612-3	612-19	0.104	0.0012	0.299	0.004	4.301	0.060	99	1703.7	21.25	1686.1	19.23	1693.5	11.47	0.000	0.6297	
612-4	612-20	0.104	0.0012	0.304	0.004	4.345	0.058	101	1692.7	20.79	1710	19.02	1701.9	11.07	0.008	0.6211	
612-4	612-21	0.104	0.0012	0.301	0.004	4.321	0.059	100	1700.8	21.4	1695.3	18.88	1697.4	11.25	0.000	0.6062	
612-4	612-22	0.153	0.0022	0.464	0.006	9.760	0.152	103	2376.8	24.29	2455.7	27.34	2412.4	14.37	0.000	0.5197	
612-4	612-23	0.154	0.0024	0.463	0.006	9.835	0.160	103	2391.7	25.72	2453.6	27.72	2419.4	15.02	0.000	0.4909	
612-4	612-24	0.152	0.0021	0.465	0.006	9.761	0.147	104	2372.4	23.1	2461.4	26.65	2412.5	13.83	0.031	0.5339	
612-4	612-25	0.154	0.0022	0.462	0.006	9.822	0.150	102	2394.7	23.59	2447.4	26.64	2418.3	14.04	0.012	0.5203	
612-4	612-26	0.155	0.0020	0.451	0.006	9.606	0.136	100	2398.2	21.33	2398.1	25.54	2397.7	13.05	0.004	0.5669	
612-4	612-27	0.154	0.0020	0.443	0.006	9.432	0.135	99	2395.5	21.78	2364.7	25.33	2380.9	13.18	0.000	0.5545	
801	801-01	0.104	0.0012	0.315	0.005	4.511	0.079	104	1694.1	21.76	1766.1	26.1	1733	14.57	0.011	0.7640	
801	801-02	0.107	0.0013	0.299	0.005	4.412	0.079	97	1748.2	22.29	1687.8	25.23	1714.5	14.74	0.000	0.7492	
801	801-03	0.105	0.0011	0.299	0.005	4.306	0.073	99	1706.7	19.36	1685.3	25.15	1694.5	13.99	0.000	0.8044	
801	801-04	0.104	0.0012	0.300	0.005	4.303	0.075	99	1700.2	21.13	1689.7	25.18	1694	14.37	0.002	0.7762	
801	801-05	0.100	0.0014	0.312	0.005	4.303	0.081	107	1627.9	25.82	1748.5	26.27	1693.9	15.53	0.000	0.7027	conc. >105%
801	162A-01	0.101	0.0013	0.312	0.005	4.344	0.079	107	1643.1	23.06	1750.5	26.22	1701.8	14.93	0.001	0.7464	conc. >105%
801	162A-02	0.102	0.0012	0.297	0.005	4.167	0.073	101	1655.8	21.49	1677.6	25.06	1667.5	14.37	0.003	0.7706	
801	162A-03	0.102	0.0012	0.308	0.005	4.326	0.076	104	1660.4	21.69	1729.8	25.83	1698.3	14.58	0.000	0.7706	
801	162A-04	0.103	0.0014	0.285	0.005	4.033	0.075	97	1671.6	24.53	1617.9	24.45	1640.9	15.08	0.008	0.7221	
813-2	526A-01	0.105	0.0011	0.305	0.005	4.394	0.070	100	1707.8	19.92	1714.7	23.57	1711.3	13.21	0.000	0.7627	
813-2	526A-02	0.103	0.0011	0.296	0.005	4.219	0.068	99	1686.7	20.25	1671.4	23.09	1677.8	13.2	0.000	0.7595	
813-2	526A-03	0.104	0.0011	0.293	0.005	4.191	0.067	98	1690.9	19.91	1658.2	22.99	1672.2	13.13	0.001	0.7641	
813-2	526A-04	0.103	0.0012	0.297	0.005	4.232	0.069	100	1683.6	20.46	1678.3	23.24	1680.3	13.3	0.001	0.7570	
813-2	526A-05	0.104	0.0011	0.289	0.005	4.165	0.067	96	1705.4	19.85	1637.9	22.8	1667.2	13.13	0.000	0.7689	

Set	Analysis	207Pb/ 206Pb	1σ	206Pb/ 238U	1σ	207Pb/ 235U	1σ	% Conc.	207Pb/ 206Pb age (Ma)	1σ	206Pb/ 238U age (Ma)	1σ	207Pb/ 235U age (Ma)	1σ	204Pb/ 206Pb (%)	Rho (ρ)	Reason for omission
813-2	813-01	0.103	0.0012	0.304	0.005	4.330	0.070	101	1686.1	20.3	1710.6	23.75	1699.2	13.37	0.002	0.7586	
813-2	813-02	0.104	0.0012	0.301	0.005	4.324	0.071	100	1702.6	20.59	1694.8	23.57	1697.9	13.46	0.003	0.7571	
813-2	813-03	0.103	0.0011	0.297	0.005	4.200	0.068	100	1670.4	20.48	1677.6	23.4	1674	13.35	0.003	0.7607	
813-2	813-04	0.104	0.0012	0.291	0.005	4.171	0.068	97	1698.4	20.71	1645.1	23.05	1668.3	13.43	0.000	0.7535	
907	1233-01	0.116	0.0016	0.332	0.004	5.316	0.082	97	1900.6	24	1845.7	21.28	1871.4	13.13	0.098	0.5632	
907	1233-02	0.104	0.0012	0.309	0.004	4.417	0.062	103	1689.5	21.24	1737.7	19.81	1715.5	11.56	0.004	0.6329	
907	1233-03	0.097	0.0013	0.280	0.004	3.740	0.058	102	1563.2	25.25	1593.5	18.72	1579.9	12.43	0.000	0.5671	
907	1233-04	0.101	0.0012	0.291	0.004	4.046	0.057	100	1641.4	21.61	1646	18.96	1643.6	11.46	0.011	0.6313	
907	1233-05	0.102	0.0014	0.298	0.004	4.187	0.065	102	1657.9	25.01	1683.4	19.84	1671.4	12.78	0.000	0.5658	
907	907-01	0.103	0.0012	0.311	0.004	4.431	0.063	104	1682.9	21.86	1748	20	1718.1	11.79	0.001	0.6217	
907	907-02	0.103	0.0013	0.302	0.004	4.300	0.065	101	1684.9	23.64	1701.6	19.76	1693.5	12.37	0.006	0.5905	
907	907-03	0.101	0.0021	0.312	0.005	4.343	0.094	107	1639.8	38.23	1753	22.12	1701.6	17.8	0.012	0.3849	conc. >105%
907	907-04	0.102	0.0013	0.310	0.004	4.376	0.064	105	1666.9	22.79	1742.1	20.01	1707.8	12.06	0.004	0.6034	
907	907-05	0.102	0.0012	0.317	0.004	4.467	0.063	106	1666.8	21.3	1773.7	20.52	1724.8	11.73	0.000	0.6408	conc. >105%
907-2	907-06	0.104	0.0012	0.311	0.004	4.439	0.062	103	1688	21.86	1746.6	19.77	1719.7	11.67	0.000	0.6091	
907-2	907-07	0.102	0.0012	0.310	0.004	4.371	0.061	104	1668.2	21.42	1739.3	19.71	1706.9	11.48	0.000	0.6265	
907-2	907-08	0.101	0.0013	0.300	0.004	4.197	0.063	103	1650.7	23.92	1692.1	19.52	1673.4	12.23	0.005	0.5758	
907-2	907-09	0.101	0.0029	0.291	0.005	4.052	0.112	100	1644.3	51.64	1645.7	23.8	1644.7	22.55	0.008	0.2592	
907-2	907-10	0.104	0.0012	0.305	0.004	4.350	0.062	101	1690	21.98	1714.3	19.51	1703	11.69	0.000	0.6137	
907-2	907-11	0.101	0.0026	0.323	0.005	4.504	0.112	109	1647	46.23	1803.4	24.13	1731.7	20.74	0.002	0.2860	conc. >105%
907-2	907-12	0.103	0.0013	0.317	0.004	4.489	0.064	106	1675.1	22.4	1774.6	20.15	1728.9	11.87	0.003	0.6001	conc. >105%
907-2	907-13	0.102	0.0014	0.314	0.004	4.429	0.068	106	1665.4	24.95	1761.7	20.39	1717.7	12.74	0.000	0.5576	conc. >105%
907-2	907-15	0.103	0.0013	0.307	0.004	4.372	0.063	102	1686.6	22.33	1724.5	19.67	1707	11.82	0.000	0.6056	
907-3	907-16	0.102	0.0012	0.316	0.004	4.431	0.061	107	1658.2	21.79	1768.7	19.69	1718.1	11.43	0.000	0.6017	conc. >105%
907-3	907-17	0.102	0.0012	0.306	0.004	4.302	0.058	104	1658.5	20.9	1723.4	19.3	1693.8	11.14	0.000	0.6259	

Set	Analysis	207Pb/ 206Pb	1σ	206Pb/ 238U	1σ	207Pb/ 235U	1σ	% Conc.	207Pb/ 206Pb age (Ma)	1σ	206Pb/ 238U age (Ma)	1σ	207Pb/ 235U age (Ma)	1σ	204Pb/ 206Pb (%)	Rho (ρ)	Reason for omission
907-3	907-18	0.103	0.0013	0.308	0.004	4.372	0.063	103	1678.4	23.46	1731.8	19.56	1707.1	11.99	0.001	0.5674	
907-3	907-19	0.102	0.0013	0.323	0.004	4.563	0.065	108	1668.3	22.81	1806.2	20.11	1742.5	11.8	0.008	0.5805	conc. >105%
907-3	907-20	0.103	0.0012	0.300	0.004	4.251	0.057	101	1677.3	20.45	1690.4	18.97	1684	10.99	0.000	0.6355	
907-3	907-21	0.102	0.0012	0.306	0.004	4.309	0.059	103	1664.6	21.7	1720.8	19.35	1695	11.38	0.000	0.6066	
907-3	907-22	0.118	0.0041	0.358	0.006	5.799	0.194	103	1919.3	60.6	1975	29.9	1946.3	29.04	0.161	0.2042	High 204Pb
907-3	907-23	0.100	0.0013	0.315	0.004	4.342	0.063	109	1622.1	23.61	1767.6	19.76	1701.3	11.91	0.005	0.5619	conc. >105%
907-3	907-24	0.102	0.0013	0.319	0.004	4.474	0.063	108	1655.9	22.81	1785.9	19.84	1726.2	11.74	0.001	0.5793	conc. >105%
907-3	907-25	0.102	0.0012	0.311	0.004	4.374	0.060	105	1664.1	21.27	1744	19.49	1707.5	11.29	0.001	0.6194	

APPENDIX E: BULK-ROCK GEOCHEMISTRY

	AAE 100	AAE 100A	AAE 155	AAE 162A	AAE 526	AAE 526A	AAE 612	AAE 754
Major elements (wt%)								
SiO_2	49.97	44.98	57.20	62.44	53.37	51.94	45.36	68.53
TiO_2	0.26	0.52	0.71	0.70	0.91	1.73	0.39	0.38
Al_2O_3	31.60	29.20	13.75	17.65	21.18	14.28	23.85	16.53
Fe_2O_3T	2.63	6.28	16.63	9.86	13.82	16.62	8.07	3.60
MnO	0.06	0.08	1.55	0.29	0.18	0.38	0.08	0.04
MgO	10.06	14.64	2.77	2.75	4.38	8.93	18.33	1.49
CaO	0.44	0.12	1.53	0.72	0.39	0.87	0.29	3.35
Na_2O	2.08	0.72	1.57	0.97	0.57	0.47	0.98	4.64
K_2O	2.69	3.18	4.03	4.32	5.03	4.58	2.30	1.33
P_2O_5	0.11	0.09	0.22	0.18	0.06	0.20	0.23	0.06
LOI	1.91	3.15	0.19	0.21	0.18	0.91	5.73	0.71
Total	**101.81**	**102.96**	**100.15**	**100.09**	**100.07**	**100.91**	**105.61**	**100.66**
Trace elements (ppm)								
Rb	127.4	89.8	160.6	258.7	221.7	196.2	59.1	17.3
Sr	54	14	173	106	90	13	20	637
Y	16.9	35.2	26.8	21.4	53.1	44.6	43.1	6.0
Zr	215	128	44	125	152	150	82	91
V	100	261	87	95	145	265	274	52
Ni	98	11	35	44	73	85	23	19
Cr	22	35	117	35	133	50	10	46
Nb	5.2	12.1	10.6	15.3	14.5	11.0	4.4	1.7
Ga	42.2	71.8	16.7	26.7	28.6	21.8	58.9	26.6
Cu	12	19	18	25	24	243	16	16
Zn	37	59	142	116	148	203	68	67
Co	9	23	36	22	37	76	36	5
Ba	359	676	1216	778	620	196	415	643
La	115	79	37	33	33	10	49	35
Ce	365	284	99	81	75	29	208	59
U	2.9	7.3	<0.5	<0.5	<0.5	9.0	6.1	<0.5
Th	30.4	57.6	17.2	21.2	25.7	15.1	39.6	<0.5
Sc	29	7	10	15	19	17	9	3
Pb	16	5	14	16	12	9	<1	16

Fe_2O_3T, total iron (Fe_2O_3 + FeO); LOI, Loss on Ignition

	AAE 757	AAE 767	AAE 784	AAE 801	AAE 811	AAE 813	AAE 907	AAE 935
Major elements (wt%)								
SiO_2	71.06	48.82	59.55	35.66	65.75	62.06	62.42	43.57
TiO_2	0.48	2.29	0.68	0.80	0.52	0.61	0.18	3.71
Al_2O_3	15.49	12.49	18.81	9.28	18.07	17.68	12.15	13.91
Fe_2O_3T	2.28	18.51	8.83	46.67	8.22	10.98	18.25	20.82
MnO	0.04	0.25	0.16	0.89	0.32	0.13	1.32	0.25
MgO	0.76	5.01	3.98	2.93	3.19	2.89	2.43	5.49
CaO	1.42	9.17	0.16	0.67	0.16	0.39	1.51	7.77
Na_2O	3.45	2.18	3.98	0.36	0.23	0.56	1.14	2.59
K_2O	4.61	0.85	4.46	1.90	3.26	4.50	0.65	1.05
P_2O_5	0.10	0.24	0.10	0.35	0.08	0.11	0.28	0.54
LOI	0.39	-0.10	0.43	-0.55	0.96	0.80	0.31	-0.23
Total	**100.08**	**99.71**	**101.14**	**98.96**	**100.76**	**100.71**	**100.64**	**99.47**
Trace elements (ppm)								
Rb	70.4	19.1	125.7	57.4	271.7	282.3	28.6	16.7
Sr	337	141	242	39	59	69	55	178
Y	12.9	46.2	40.4	41.4	32.4	23.9	44.6	49.3
Zr	279	145	163	74	268	137	67	194
V	41	421	155	134	65	94	57	305
Ni	19	28	97	22	35	45	14	63
Cr	16	31	187	113	65	97	79	93
Nb	1.0	11.9	7.7	7.6	19.0	13.3	<0.5	15.8
Ga	20.7	18.3	23.7	16.5	30.8	24.2	13.0	20.4
Cu	9	74	72	31	14	17	46	64
Zn	28	151	122	159	84	101	78	188
Co	1	64	33	52	20	27	27	76
Ba	2025	208	1193	<3	721	403	185	282
La	54	16	36	41	52	30	36	10
Ce	116	27	79	157	123	69	73	14
U	<0.5	<0.5	<0.5	<0.5	<0.5	<0.5	<0.5	<0.5
Th	6.1	5.0	20.4	30.5	36.3	21.0	13.6	9.9
Sc	2	47	16	21	8	14	8	30
Pb	24	5	16	1	<1	11	3	<1

Fe_2O_3T, total iron (Fe_2O_3 + FeO); LOI, Loss on Ignition

	AAE 953	AAE 975	AAE 976	AAE 977	AAE 978	AAE 980	AAE 1233
Major elements (wt%)							
SiO_2	48.91	48.03	48.15	48.74	48.83	45.95	62.98
TiO_2	2.69	2.54	2.51	2.57	2.67	0.97	0.83
Al_2O_3	13.03	13.09	13.17	13.11	12.95	21.92	15.15
Fe_2O_3T	19.30	19.05	19.24	18.87	19.33	17.02	11.53
MnO	0.27	0.26	0.28	0.25	0.26	0.34	0.36
MgO	4.61	5.08	5.07	4.91	4.74	5.61	2.80
CaO	8.72	9.15	9.09	8.97	8.69	3.31	0.62
Na_2O	0.81	1.22	1.26	0.96	0.85	2.83	0.76
K_2O	1.25	1.12	1.06	1.31	1.31	1.83	4.44
P_2O_5	0.27	0.25	0.23	0.25	0.26	0.10	0.19
LOI	0.25	0.28	0.19	0.26	-0.01	1.36	0.39
Total	**100.11**	**100.07**	**100.25**	**100.20**	**99.88**	**101.24**	**100.05**
Trace elements (ppm)							
Rb	18.6	12.8	11.8	17.7	18.9	62.0	284.9
Sr	83	84	96	102	88	239	122
Y	52.3	53.2	51.6	51.1	51.8	163.4	16.7
Zr	176	161	154	162	169	150	178
V	347	346	350	345	346	225	98
Ni	56	50	49	49	55	176	58
Cr	101	120	116	119	97	388	116
Nb	12.1	11.4	11.1	10.6	12.8	10.3	14.7
Ga	18.4	19.5	18.9	19.2	18.6	22.3	23.5
Cu	122	77	75	95	114	93	23
Zn	158	149	144	153	159	126	113
Co	68	64	61	66	66	56	28
Ba	236	211	214	229	258	397	840
La	15	14	15	15	14	44	33
Ce	28	25	31	33	29	113	82
U	<0.5	1.5	<0.5	<0.5	<0.5	<0.5	<0.5
Th	5.3	6.7	5.0	3.9	4.8	31.3	26.0
Sc	43	45	45	44	43	41	13
Pb	<1	2	<1	1	<1	<1	10

Fe_2O_3T, total iron (Fe_2O_3 + FeO); LOI, Loss on Ignition